

**T.R.  
SAKARYA UNIVERSITY  
GRADUATE SCHOOL OF NATURAL AND APPLIED SCIENCES**

**BREAST CANCER DETECTION AND TREATMENT USING  
ACTIVE SENSOR IMAGING AND MICROWAVE  
HYPEROTHERMIA**

**PhD THESIS**

**Fawzia ABDIEN ALI ABDULLA**

**Elektrik-Elektronik Mühendisliği Department**

**Elektronik Mühendisliği Program**

**JANUARY 2025**



**T.R.  
SAKARYA UNIVERSITY  
GRADUATE SCHOOL OF NATURAL AND APPLIED SCIENCES**

**BREAST CANCER DETECTION AND TREATMENT USING  
ACTIVE SENSOR IMAGING AND MICROWAVE  
HYPER THERMIA**

**PhD THESIS**

**Fawzia ABDIEN ALI ABDULLA**

**Elektrik-Elektronik Mühendisliği Department**

**Elektronik Mühendisliği Program**

**Thesis Advisor: Prof. Dr. Askin DEMIRKOL**

**JANUARY 2025**



The thesis work titled “Breast Cancer Detection and Treatment Using Active Sensor Imaging and Microwave Hyperthermia” prepared by Fawzia ABDIEN ALI ABDULLA was accepted by the following jury on 17/01/2025 by a majority of votes as a PhD THESIS in Sakarya University, Graduate School of Natural and Applied Sciences, Electrical and Electronics Engineering department, Electronics programe.

### Thesis Jury

**Head of Jury :**        **Prof. Dr. Askin DEMIRKOL**        .....

Sakarya University

**Jury Member :**        **Prof. Dr. Ali Fuat BOZ**        .....

Sakarya University of Applied Sciences

**Jury Member :**        **Prof. Dr. Ali TANGEL**        .....

Kocaeli University

**Jury Member :**        **Prof.Dr. Cenk YAVUZ**        .....

Sakarya University

**Jury Member :**        **Asst. Prof. Dr. Seckin ARI**        .....

Sakarya University



## **STATEMENT OF COMPLIANCE WITH THE ETHICAL PRINCIPLES AND RULES**

I declare that the thesis work titled "Breast Cancer Detection and Treatment Using Active Sensor Imaging and Microwave Hyperthermia", which I have prepared in accordance with Sakarya University Graduate School of Natural and Applied Sciences regulations and Higher Education Institutions Scientific Research and Publication Ethics Directive, belongs to me, is an original work, I have acted in accordance with the regulations and directives mentioned above at all stages of my study, I did not get the innovations and results contained in the thesis from anywhere else, I duly cited the references for the works I used in my thesis, I did not submit this thesis to another scientific committee for academic purposes and to obtain a title, in accordance with the articles 9/2 and 22/2 of the Sakarya University Graduate Education and Training Regulation published in the Official Gazette dated 20.04.2016, a report was received in accordance with the criteria determined by the graduate school using the plagiarism software program to which Sakarya University is a subscriber, I accept all kinds of legal responsibility that may arise in case of a situation contrary to this statement.

(...../01/2025)

Fawzia ABDIEN ALI ABDULLA



## **ACKNOWLEDGMENTS**

At the end of my thesis, I would like to express my deepest gratitude to all those who made this work possible and contributed to making this journey an unforgettable experience for me.

First and foremost, I am sincerely thankful to my supervisor, Prof. Dr. Askin Demirkol, for his continuous advice, encouragement, and invaluable guidance throughout the course of this thesis. His systematic approach and dedicated effort in training me in the scientific field have been pivotal to my growth.

I would also like to extend my heartfelt thanks to the Department of Electrical and Electronics Engineering at Sakarya University, along with the entire teaching staff, for providing me with a high-quality education. Special recognition goes to my instructors, Prof. Dr. Cenk Yavuz and Assist. Prof. Dr. Seckin Ari, whose constructive support during both the jury process and the natural course of my work was indispensable.

I am deeply grateful to the Turkish government and the Turkish scholarship program for granting me the opportunity to study in Turkey.

My sincere thanks go to my friends for their unwavering support, and generous care, and for making me feel at home whenever I needed it during my time in Turkey. To my family, words cannot fully express my gratitude. I am especially thankful to my mother, Najah, God bless her soul, who supported me every step of the way throughout this period and whose memory, which I hold dear after her passing five months ago, has been my greatest motivation in completing this work during such a difficult time. My father, brothers, sisters, and all my family members in Sudan, who, despite the challenges of war, continuously asked about my well-being, have been a constant source of strength. The unwavering support of my husband throughout these years, my unborn daughter who stays awake with me at night, and my loved ones have been the driving force behind the completion of this work.

Lastly, I would like to extend my gratitude to the Scientific and Technological Research Council of Turkey (TÜBİTAK) for providing the open-access funding that enabled the publication of my scientific paper.

Fawzia ABDIEN ALI ABDULLA



## TABLE OF CONTENTS

	<u>Page</u>
<b>ACKNOWLEDGMENTS</b> .....	vii
<b>TABLE OF CONTENTS</b> .....	ix
<b>ABBREVIATIONS</b> .....	xiii
<b>SYMBOLS</b> .....	xv
<b>LIST OF TABLES</b> .....	xvii
<b>LIST OF FIGURES</b> .....	xix
<b>SUMMARY</b> .....	xxi
<b>ÖZET</b> .....	xxv
<b>1. INTRODUCTION</b> .....	<b>1</b>
1.1. Introduction .....	1
1.2. Problem Statement .....	5
1.3. Research Objective.....	6
1.3.1. General objective .....	6
1.3.2. Specific objectives .....	6
1.4. Research Methodology .....	6
1.5. Organization of the Thesis .....	6
<b>2. BACKGROUND AND LITERATURE REVIEW</b> .....	<b>9</b>
2.1. Physiology of Breast .....	9
2.1.1. Anatomy of the breast .....	9
2.1.2. Breast cancer .....	10
2.1.3. Electrical properties .....	11
2.2. Current Breast Cancer Detection Methods.....	15
2.2.1. X-ray mammography .....	15
2.2.2. Ultrasound imaging.....	16
2.2.3. Magnetic resonance imaging (MRI) .....	17
2.3. Microwave Imaging Techniques .....	18
2.3.1. Passive microwave imaging .....	19
2.3.2. Hybrid microwave imaging .....	19
2.3.3. Active microwave imaging .....	20
2.3.3.1. Microwave tomography .....	20
2.3.3.2. UWB radar microwave imaging for breast cancer.....	22
2.4. Thermal Therapy .....	26
2.4.1. Heating principle .....	26
2.4.2. Electromagnetic interactions with biological systems .....	27
2.4.2.1. Specific absorption rate (SAR) .....	28
2.4.2.2. Bioheat equation.....	28
2.4.3. Applications in cancer therapy .....	29
2.4.4. Categories and methods of hyperthermia.....	30
2.4.4.1. Whole-body hyperthermia .....	30
2.4.4.2. Local or regional hyperthermia .....	31
2.4.5. External microwave hyperthermia .....	32

<b>3. UWB MICROSTRIP PATCH ANTENNA DESIGN .....</b>	<b>33</b>
3.1. Ultra-Wideband Technology .....	33
3.2. Antenna Theory .....	34
3.3. Microstrip Patch Antenna.....	34
3.3.1. Structure of microstrip patch antenna .....	35
3.3.1.1. Dielectric substrate .....	36
3.3.1.2. Conductor layers .....	37
3.3.2. Feeding techniques of microstrip antenna.....	38
3.3.2.1. Microstrip line feeding techniques .....	38
3.3.2.2. Coaxial probe feeding techniques .....	39
3.3.2.3. Proximity coupled feeding techniques .....	39
3.3.2.4. Aperture coupled feed .....	40
3.3.3. Microstrip antenna analysis methods .....	40
3.3.3.1. Transmission line analysis method .....	40
3.3.3.2. Cavity model .....	48
3.3.4. Fundamental parameters of antennas .....	48
3.3.4.1. Radiation pattern .....	48
3.3.4.2. Radiation power density .....	49
3.3.4.3. Radiation intensity.....	49
3.3.4.4. Beam width .....	50
3.3.4.5. Directivity.....	50
3.3.4.6. Gain .....	51
3.3.4.7. Bandwidth .....	51
3.3.4.8. Polarization.....	51
3.3.4.9. Input impedance .....	51
3.3.4.10. Return loss.....	52
3.3.4.11. Radiation efficiency .....	52
3.3.5. Microstrip patch antennas bandwidth enhancing.....	52
3.3.6. Numerical methods for computational electromagnetics.....	55
3.3.7. Microstrip Patch antennas for biomedical applications .....	57
3.3.8. Microstrip patch antennas for breast cancer diagnosis.....	58
3.3.9. Textile microstrip patch antennas .....	60
3.3.10. Antenna Array .....	61
<b>4. RESEARCH METHODOLOGY.....</b>	<b>65</b>
4.1. Methodology.....	65
4.2. Computer Simulation Technology CST .....	66
4.3. Single Microstrip Patch Antenna Design .....	67
4.3. Trust-Region Framework (TRF) for Ground Length Optimization .....	68
4.4. Breast Modeling and Assigning Material Properties.....	69
4.5. Testing the Single Antenna in a 3D Breast Imaging Model.....	70
4.6. Pending Antenna For Flexibility Test .....	72
4.7. Microstrip Patch Antenna Array Design For Hyperthermia .....	72
4.8. Testing the Array Antenna in 3D Breast Hyperthermia System .....	73
4.9. Testing the proposed antenna in a moving system.....	74
<b>5. RESULTS AND DISCUSSIONS .....</b>	<b>77</b>
5.1. Simulation Results.....	77
5.1.1. Results of S-parameters.....	77
5.1.2. VSWR Results.....	80
5.1.3. SAR Distribution.....	82
5.1.4. Results of a proposed antenna in a dynamic imaging system .....	84

5.1.5. Temperature distribution.....	86
5.2. Discussions.....	88
<b>6. CONCLUSIONS AND RECOMMENDATIONS.....</b>	<b>93</b>
6.1. Conclusions.....	93
6.2. Recommendations.....	94
<b>REFERENCES.....</b>	<b>97</b>
<b>CURRICULUM VITAE.....</b>	<b>109</b>



## **ABBREVIATIONS**

<b>ABUS</b>	: Automated breast ultrasound systems
<b>ACS</b>	: American Cancer Society
<b>AJCC</b>	: American Joint Committee on Cancer
<b>BCO</b>	: Breast Cancer Organization
<b>CEM</b>	: Computational electromagnetics
<b>CMI</b>	: Confocal microwave imaging
<b>CST</b>	: Computer Simulation Technology
<b>DCIS</b>	: Ductal carcinoma in situ
<b>DGS</b>	: Defective Ground Structures
<b>DORT</b>	: Decomposition of the time reversal operator
<b>EBG</b>	: Electromagnetic bandgap
<b>EMC</b>	: Electromagnetic compatibility
<b>ETRI</b>	: Electronics and Telecommunications Research Institute
<b>FCC</b>	: Federal Communications Commission
<b>FDTD</b>	: Finite Difference Time Domain
<b>FEM</b>	: Finite element method
<b>FFT</b>	: Fast Fourier Transform
<b>FNBW</b>	: First-Null Beam width
<b>GHz</b>	: Gigahertz
<b>HMI</b>	: Holographic microwave imaging technology
<b>HPBW</b>	: Half-Power Beam width
<b>IC-DAS</b>	: Iteratively corrected delay and sum
<b>IFFT</b>	: Inverse Fast Fourier Transform
<b>MHz</b>	: Megahertz
<b>MIST</b>	: Microwave imaging via space time
<b>MRI</b>	: Magnetic Resonance Imaging
<b>MRS-UWB</b>	: Multiple Ring Slot Ultra-Wideband
<b>MSA</b>	: Multi-static adaptive microwave imaging
<b>MWH</b>	: Microwave Hyperthermia Microwave hyperthermia
<b>PEC</b>	: Perfect electrical conductor

<b>PET</b>	: Positron emission tomography
<b>PMC</b>	: Perfect magnetic conductors
<b>PO2</b>	: Permeability, and elevate oxygen partial pressure
<b>RF</b>	: Radio Frequency
<b>RL</b>	: Return loss
<b>SAR</b>	: Specific absorption rate
<b>TNM</b>	: Tumor size, lymph node, distant metastases
<b>TRF</b>	: Trust Region Framework
<b>TR-MUSIC</b>	: Time reversal multiple signal classification
<b>TSAR</b>	: Tissue sensing adaptive radar
<b>US</b>	: Ultrasonic
<b>UWB</b>	: Ultra-wideband
<b>VNA</b>	: Vector network analyzer
<b>VSWR</b>	: Voltage standing wave ratio
<b>WHO</b>	: World Health Organization's

## SYMBOLS

<b>AF</b>	: Array Factor
<b>bw</b>	: Bandwidth
<b>c</b>	: The Specific Heat of the Tissue [J/kg/°C]
<b>c<sub>b</sub></b>	: Specific Heat of Blood [J/kg/°C]
<b>c<sub>o</sub></b>	: Speed of Light in free space
<b>D</b>	: Directivity
<b>E</b>	: Electric Field Amplitude [Volts per meter]
<b>f<sub>H</sub></b>	:The Highest Frequency [GHz]
<b>f<sub>L</sub></b>	: The Lowest Frequency [GHz]
<b>G</b>	: Conductance
<b>h</b>	: Substrate Hight
<b>H</b>	: Magnatic Field Amplitude
<b>N</b>	: Number of Elements in Array
<b>L</b>	: Transmission Line Length [meter]
<b>L<sub>eff</sub></b>	: Patch Effective Length [meter]
<b>T</b>	: Temperature elevation [°C]
<b>T<sub>a</sub></b>	: Arteries Average Temperature Elevation [°C]
<b>P<sub>rad</sub></b>	: Power Radiated
<b>Q<sub>m</sub></b>	: Metabolic Heat Source [W/m <sup>3</sup> ]
<b>R<sub>in</sub></b>	: Input Resistance
<b>RL</b>	: Return Loss
<b>W</b>	: Patch Width [Meter]
<b>w<sub>b</sub></b>	: Blood volumetric perfusion [kg/m <sup>3</sup> /s]
<b>w<sub>bc<sub>b</sub></sub></b>	: Perfusion Heat Loss [W/m <sup>3</sup> ]
<b>Y</b>	: Admittance
<b>Z<sub>c</sub></b>	: Characteristic Impedance [W/m <sup>3</sup> ]
<b>Z<sub>in</sub></b>	: Input Impedance [W/m <sup>3</sup> ]
<b>ρ</b>	: Tissue Density [Kilograms per cubic meter]
<b>ε*</b>	: The Complex Dielectric Constant
<b>ε<sub>s</sub></b>	: Static Dielectric Constant

$\epsilon_{\infty}$	: Infinite Dielectric Constant
$\epsilon_r$	: Dielectric Constant
$\epsilon_{\text{reff}}$	: Effective Dielectric Constant
$\sigma$	: Conductivity [Siemens per meter]
$k$	: Wave Number
$\theta$	: Elevation Angle
$\varphi$	: Azimuth Angle

## LIST OF TABLES

<b>Table 4.1.</b> Optimized Antenna Dimensions .....	68
<b>Table 4.2.</b> Breast phantom tissue dielectric properties.....	69
<b>Table 5.1.</b> Comparison between the proposed antenna and four works from literature .....	92



## LIST OF FIGURES

<b>Figure 2.1.</b> The anatomy of the breast.....	9
<b>Figure 2.2.</b> X-ray Mammography .....	16
<b>Figure 2.3.</b> Breast Ultrasound Imaging Device.....	17
<b>Figure 2.4.</b> MRI of the Breast .....	17
<b>Figure 2.5.</b> The behavior of electromagnetic waves (a) in the absence of a tumor (b) in the presence of a tumor. ....	18
<b>Figure 2.6.</b> Microwave Imaging Types .....	19
<b>Figure 2.7.</b> First breast microwave imaging prototype. ....	21
<b>Figure 2.8.</b> The microwave system of the McGill University group .....	25
<b>Figure 2.9.</b> Thermal therapy in the electromagnetic spectrum.....	26
<b>Figure 3.1.</b> Microstrip Patch Antenna and its coordinate system.....	35
<b>Figure 3.2.</b> Types of Microstrip Patch Antenna .....	36
<b>Figure 3.3.</b> Microstrip line feeding techniques .....	39
<b>Figure 3.4.</b> Coaxial probe feeding techniques.....	39
<b>Figure 3.5.</b> Proximity coupled feeding techniques.....	39
<b>Figure 3.6.</b> Aperture coupled feed.....	40
<b>Figure 3.7.</b> Patch antenna extended length due to fringing effects .....	42
<b>Figure 3.8.</b> Patch antenna and its equivalent transmission-line circuit .....	43
<b>Figure 3.9.</b> Inset internal feed.....	46
<b>Figure 3.10.</b> Antenna Coordinate system .....	49
<b>Figure 3.11.</b> Three and two-dimensional power patterns.....	50
<b>Figure 4.1.</b> Methodology flow chart.....	65
<b>Figure 4.2.</b> CST user interface .....	66
<b>Figure 4.3.</b> (a) Primary Rectangular patch antenna, (b) Optimized antenna.....	67
<b>Figure 4.4.</b> Proposed Breast Phantom .....	70
<b>Figure 4.5.</b> Single antenna with tumor-free breast (Model A) .....	70
<b>Figure 4.6.</b> Single antenna with one spherical tumor breast model (Model B).....	71
<b>Figure 4.7.</b> Single antenna with one cubic tumor breast model (Model C) .....	71
<b>Figure 4.8.</b> Single antenna with two tumors breast model (Model D) .....	71
<b>Figure 4.9.</b> Antenna Bending .....	72
<b>Figure 4.10.</b> Proposed 2x4 antenna array for hyperthermia.....	73
<b>Figure 4.11.</b> Antenna array with Model E including one tumor in the center .....	73
<b>Figure 4.12.</b> Antenna array with model F .....	74
<b>Figure 4.13.</b> Antenna array with model G.....	74
<b>Figure 5.1.</b> Antenna return loss (S11) in the free space. ....	78
<b>Figure 5.2.</b> Antenna return loss (S11) in the presence of human breast before optimization. ....	78
<b>Figure 5.3.</b> The effect of partial ground length and notches on the return loss.....	78
<b>Figure 5.4.</b> Antenna return loss (S11) in the presence of human breast after optimization (Model A).....	79
<b>Figure 5.5.</b> Antenna return loss (S11) in the presence of a 5 mm tumor (Model B). 79	
<b>Figure 5.6.</b> Antenna return loss (S11) in the presence of a 5 mm tumor (Model C). 79	
<b>Figure 5.7.</b> Antenna return loss (S11) in the presence of two tumors (Model D).....	80

<b>Figure 5.8.</b> Antenna return loss (S11) after bending and optimization .....	80
<b>Figure 5.9.</b> VSWR values for the proposed antenna in free space .....	80
<b>Figure 5.10.</b> VSWR value in the presence of human breast before optimization. ....	81
<b>Figure 5.11.</b> The effect of partial ground length on the VSWR .....	81
<b>Figure 5.12.</b> VSWR values for Model (A). .....	81
<b>Figure 5.13.</b> VSWR values for Model (B). .....	81
<b>Figure 5.14.</b> VSWR values for Model (C). .....	82
<b>Figure 5.15.</b> VSWR values for Model (D) .....	82
<b>Figure 5.16.</b> SAR distribution for Model (A).....	82
<b>Figure 5.17.</b> SAR distribution for Model (B).....	83
<b>Figure 5.18.</b> SAR distribution for Model (C).....	83
<b>Figure 5.19.</b> SAR distribution for Model (C).....	83
<b>Figure 5.28.</b> Temperature distribution for model E with one tumor (5 mm) radius in the center. ....	87
<b>Figure 5.29.</b> Temperature distribution for model H with one tumor (5 mm) radius. .	87
<b>Figure 5.30.</b> Temperature distribution for model G with two tumors (5 and 2 mm) radius. ....	87
<b>Figure 5.31.</b> Temperature distribution when using unsuitable phase and power .....	88

# **BREAST CANCER DETECTION AND TREATMENT USING ACTIVE SENSOR IMAGING AND MICROWAVE HYPERTHERMIA**

## **SUMMARY**

Breast cancer is a health challenge all over the world, and it is the second leading cause of death among women all over the world. Early detection and effective treatment of the disease are important to improve survival rates by up to about 97%. This thesis designs and simulates a textile-based ultra-wideband (UWB) patch antenna that is specifically intended to serve dual purposes: early breast cancer detection and treatment using microwave hyperthermia. The design of an antenna that can work in the field of breast imaging and breast thermal therapy at the same time is a real revolution and a major development in this field. Due to its excellent accuracy and absence of harmful radiation, wideband microwave (UWB) imaging is considered to be an effective method for early diagnosis of breast cancer. Microwave hyperthermia is also an effective method for treating cancer and a suitable alternative to the methods currently used because it raises the temperature of the malignant tumor tissue while preserving the surrounding healthy tissue. The primary objective of this research is to develop a safe, accurate, not expensive, flexible, lightweight, and fully textile wearable microstrip patch antenna capable of operating efficiently within the UWB frequency range of 2–11.6 GHz, able to detect breast cancer and help treat it. The textile-based antenna design ensures user comfort and safety, allowing for portable, non-invasive medical applications. Obtaining such a wide bandwidth using textile materials is a major challenge. The integration of UWB microwave technology with textile-based antenna design provides a novel approach to addressing the limitations of conventional diagnostic and therapeutic methods. Given the limited size of the breast and the need for efficient tumor detection, a wearable antenna designed for this purpose must exhibit a wide bandwidth, compact dimensions, low specific absorption rate values, and high flexibility. Previous research on wearable UWB antennas has highlighted challenges related to these factors. To address these limitations, microstrip patch antennas were used. This study presents a new solution to biocompatibility issues through the use of a full-fabric-based antenna, breaking away from traditional approaches that typically use fabric as the substrate and metal as the conductor. The proposed antenna includes a denim substrate with a dielectric constant ( $\epsilon_r$ ) of 1.7 and a thickness (h) of 0.7 mm. For the conductive patch and ground plane, a copper-nickel-silver-coated polyamide fabric, featuring a thickness of 0.11 mm, was used. The antenna was developed with dimensions of 31\*31 mm<sup>2</sup>. The characteristics of a patch antenna depend largely on its dimensions. To work in a specific frequency range, the length and width must be calculated and chosen accurately. The research methodology includes the systematic design and simulation of the antenna structure using Computer Simulation Technology (CST) Microwave Studio as an advanced electromagnetic simulation tool. Essential design factors, including return loss, impedance matching, bandwidth, specific absorption rate (SAR), Voltage standing wave ratio (VSWR), and temperature distribution, are optimized to ensure the antenna performs for therapeutic and diagnostic purposes. Patch antennas mainly operate in a narrow bandwidth, but

several methods can be used to increase the bandwidth. In this work, the bandwidth was increased by adding cutoffs in both the conductive patch and the ground layer, in addition to using a partial ground plane. The partial ground plane length was optimized using the Trust Region Framework algorithm to achieve the best return loss values in the desired frequency range. The UWB antenna's performance is validated through extensive simulations on breast tissue phantom models. Compared to several computerized breast models in previous research that reduced tumor shapes by assuming them to be spherical only, this research used more realistic models assuming different tumor shapes and sizes that might be encountered in real scenarios. The antenna was tested on four computerized breast models. The models varied and included a basic tumor-free model, two models containing spherical tumors with a diameter of 5 and 2 mm, in addition to a model containing two tumors, and a final model containing a cube-shaped tumor. These dimensions and shapes were varied and their position changed to evaluate the ability of the proposed antenna to identify tumors of different shapes, sizes, and locations. Simulation results show that the high-resolution imaging capabilities of the antenna allow for the detection of tumors as small as 5 and 2 millimeters, enhancing the chances of early intervention. And it demonstrates the antenna's ability to achieve accurate tumor localization. Simulation findings for a single antenna indicated that SAR values ranged from 0.397 to 1.64 which were less than 2 W/g (10 g SAR) and consistent with permissible limits for medical applications. The highest SAR values are precisely measured in tumor centers or their immediate vicinity, and that indicates the presence of a malignance tumor at that point. Throughout the frequency band used in all experiments, VSWR values remained consistently within the permissible range between 1 and 2. Antenna return losses for all models varied between -38 and -18.5 dB, depending on tumor size, shape, and location. To evaluate the flexibility of the antenna, it was subjected to a bending test. Results of the bendable design showed that the antenna fits complex breast shapes, providing consistent and accurate diagnostic results. The performance of the antenna was further assessed beyond its application as a wearable device by evaluating its functionality in a dynamic system. This involved positioning the antenna at 112 different locations above a breast phantom and processing the resulting signals using MATLAB to generate a two-dimensional (2D) image. The generated image demonstrated the capability of the proposed antenna to effectively detect tumors, even when employed in a dynamic imaging setup rather than a wearable configuration. This highlights the versatility and adaptability of the antenna for various imaging system applications. In addition, a 2x4 element antenna array was designed and tested to measure the ability of the proposed antenna to be integrated in array systems which is critical for both cancer imaging and hyperthermia. In addition to detection, the antenna is designed for breast microwave hyperthermia. The research solves important issues related to microwave hyperthermia, including ensuring uniform heat distribution, ensuring patient safety, and reducing hot spots. Antenna performance in hyperthermic applications was evaluated using CST MPHISICS STUDIO software. Simulation results demonstrated the antenna's ability to selectively raise the temperature of malignant cells to the therapeutic thermal range while being able to maintain the temperature of healthy tissues within an acceptable medical range. Beamforming techniques were utilized to adjust the phase of signals emitted from designated antennas, assuring optimal directionality of the electromagnetic wave towards the tumor, hence facilitating precise targeting of malignant cells, even when located deep into the breast. This work demonstrates the feasibility of textile-based UWB antennas to elevate the temperature of breast cancers to adequate therapeutic levels. Our antenna

shows the ability to increase tumor temperatures up to 42.3°C,45.6°C,43.3°C, and 42.4°C using different adjustments.

The results of this study demonstrate that the proposed UWB textile-based microstrip patch antenna is a viable tool for early breast cancer detection and microwave hyperthermia treatment. Its dual application in diagnostic and therapeutic areas, coupled with its wearability, makes it a great addition to the field of biomedical engineering. This thesis develops the next generation of medical devices by integrating UWB technology with textile-based antenna design. Its results demonstrate the potential of wearable, flexible, versatile, and fully textile-based microwave antennas to transform breast cancer management.



## AKTİF SENSÖR GÖRÜNTÜLEME VE MİKRODALGA HİPERTERMİ KULLANARAK MEME KANSERİ TESPİTİ VE TEDAVİSİ

### ÖZET

Meme kanseri küresel bir sağlık sorunudur ve dünya çapında bir çoğu kadınların ölüm nedenlerinden ikinci sırada gelmektedir. Erken teşhis ve etkili tedavi, sağkalım oranlarını %97'ye kadar iyileştirmek ve hastaların yaşam kalitesini artırmak için hayati öneme sahiptir. Bu tez, erken meme kanseri tespiti ve mikrodalga hipertermi tedavisi olmak üzere iki amaç için tasarlanmış bir Ultra Geniş Bant (UWB) tekstil tabanlı mikro şerit yama anteninin tasarımını, simülasyonunu ve uygulamasını araştırmaktadır. Aynı zamanda meme görüntüleme ve meme termal tedavisi alanında çalışma yeteneğine sahip bir antenin tasarımı gerçek bir devrim ve bu alanda büyük bir gelişmedir. Ultra Geniş Bant (UWB) teknolojisi, yüksek mekansal çözünürlüğü ve düşük radyasyon maruziyeti nedeniyle erken kanser tespiti için umut verici bir çözüm olarak ortaya çıkmıştır. Ek olarak, mikrodalga hipertermi, çevredeki sağlıklı dokulara zarar vermeden tümör dokularını seçici olarak ısıtarak kanseri tedavi etmek için etkili bir terapötik yöntem olarak kabul edilmiştir. Bu araştırmanın temel amacı, 2-11.6 GHz UWB frekans aralığında verimli bir şekilde çalışabilen ve meme kanserini tespit edip tedavisine yardımcı olabilen güvenli, doğru, pahalı olmayan, esnek, hafif ve tamamen tekstilden yapılmış giyilebilir bir mikroşerit yama anten geliştirmektir. UWB mikrodalga görüntüleme, sağlıklı ve kanserli meme dokuları arasındaki dielektrik kontrast nedeniyle yüksek mekansal çözünürlüklü görüntüleme ve tümörlerin hassas lokalizasyonu sağlama yeteneği nedeniyle seçilmiştir. Tekstil tabanlı tasarım, kullanıcı konforu ve uyarlanabilirliği sağlayarak invaziv olmayan ve taşınabilir tıbbi uygulamalara olanak tanır. UWB mikrodalga teknolojisinin tekstil tabanlı anten tasarımıyla entegrasyonu, geleneksel tanı ve tedavi yöntemlerinin sınırlamalarını ele almak için yeni bir yaklaşım sağlar. Önceki araştırmalarda, giyilebilir UWB antenleri çözünürlük, düşük bant genişliği, yüksek SAR değerleri ve daha büyük boyutlarda sınırlamalar göstermiştir. Tümörleri verimli bir şekilde tespit etmek için, meme tümörü tespiti için tasarlanmış giyilebilir bir antenin geniş bant genişliğine, düşük SAR'a, kompakt tasarıma ve yüksek derecede uyarlanabilirliğe sahip olması gerekir. Düşük profilli konformal tasarımları, düşük maliyetleri, basit üretim süreçleri ve uygulama açısından uyarlanabilirlikleri nedeniyle mikroşerit yama antenleri kullanılmaya başlanmıştır. Kumaşı genellikle alt tabaka ve metali iletken olarak kullanan geleneksel çalışmaların aksine, bu çalışma tamamen tekstil bazlı bir anten kullanarak biyouyumluluk endişelerini ele almaktadır. Anten, dielektrik  $\epsilon_r$ 'si 1,7 ve yüksekliği (h) 0,7 mm olan bir kot alt tabakası ile geliştirilmiştir. Bakır, gümüş ve nikel ile metalize edilmiş %100 poliamid bazlı bir kumaş, 0,11 mm kalınlığında yama ve toprak düzlemi için iletken malzeme olarak kullanılmıştır. Anten, genel olarak 31\*31 mm<sup>2</sup> boyutunda tasarlanmıştır. Bir yama anteninin boyutları, özelliklerini ve performansını belirlemede temel bir rol oynar. Yamanın uzunluğu ve genişliği antenin rezonans frekansını belirler. Genellikle, daha uzun bir yama daha düşük bir rezonans frekansına karşılık gelirken, daha geniş bir yama daha yüksek bir rezonans frekansına karşılık gelir. Uzunluğun ve genişliğin ayarlanması, antenin belirli bir frekansta veya

istenen bir frekans bandında çalışmasını sağlar. Araştırma metodolojisi, gelişmiş elektromanyetik simülasyon araçları olarak CST Microwave Studio kullanılarak anten yapısının sistematik tasarımı ve simülasyonunu içerir. Geri dönüş kaybı, empedans uyumu, bant genişliği, özgül emilim oranı (SAR), Gerilim duran dalga oranı (VSWR) ve sıcaklık dağılımı dahil olmak üzere temel tasarım parametreleri, antenin hem tanı hem de tedavi uygulamaları için işlevselliğini sağlamak üzere optimize edilmiştir. Yama antenleri genellikle dar bir frekans bandında çalışmak üzere tasarlanmıştır. Ancak, yama antenlerinin bant genişliğini artırmak için birkaç yöntem vardır, bu çalışmada bant genişliği, kısmi bir toprak düzlemi kullanılmasına ek olarak kesme çentikleri eklenerek artırılmıştır. UWB anteninin performansı, meme dokusu fantom modelleri üzerinde kapsamlı simülasyonlar yoluyla doğrulanmıştır. Tümör şekillerini küresel olduklarını varsayarak basitleştiren birçok mevcut modelin aksine, bu araştırma daha gerçekçi modeller kullanır ve klinik senaryolarda karşılaşılan tümör şekillerinin ve boyutlarının çeşitliliğini kabul eder. Tasarlanan anten dört dijital meme modeli üzerinde test edildi. Modeller, basit tümörsüz modellerden küçük tümörlü karmaşık modellere kadar uzanmaktadır. Tümör boyutu, yapısı ve konumu, önerilen antenin farklı şekil, boyut ve konumlardaki kanserleri tespit etme yeteneğini test etmek için değiştirildi. Erken meme kanseri tespiti için önerilen anten, anormallikleri belirlemek için dielektrik kontrastı kullanarak meme dokularıyla etkileşime giren elektromanyetik sinyaller iletir ve alır. Antenin yüksek çözünürlüklü görüntüleme yetenekleri, 5 ve 2 milimetre kadar küçük tümörlerin tespit edilmesini sağlayarak erken müdahale şansını artırır. Simülasyon sonuçları, antenin doğru tümör lokalizasyonuna ulaşma yeteneğini göstermektedir. Tek bir anten için simülasyon bulguları, SAR değerlerinin 0,397 ila 1,64 arasında değiştiğini, bunun 2 W/g'dan (10 g SAR) az olduğunu ve tıbbi uygulamalar için izin verilen sınırlarla tutarlı olduğunu göstermiştir. En yüksek SAR değerleri tümör merkezlerinde veya bunların yakın çevresinde hassas bir şekilde ölçülmüştür ve bu, o noktada bir kötü huylu tümörün varlığını gösterir. Ek olarak, VSWR 1 ila 2 arasında kabul edilebilir bir aralıkta kalmıştır. Tümörün boyutuna ve konumuna bağlı olarak, dört modelin anten dönüş kayıpları -38 ila -18,5 dB arasında değişmiştir. Esnek tasarım, antenin memenin karmaşık konturlarına uyum sağlamasını, tutarlı ve güvenilir tanı sonuçları sağlamasını garanti eder. Esnekliği belirlemek için bükülme etkisi test edildi. Antenin performansı, giyilebilir bir cihaz olarak kullanımının ötesine geçerek, dinamik bir sistem içinde değerlendirilerek daha kapsamlı bir şekilde analiz edilmiştir. Bu değerlendirme, antenin bir meme fantomu üzerinde 112 farklı konuma yerleştirilmesi ve bu konumlardan elde edilen sinyallerin MATLAB yazılımı kullanılarak iki boyutlu (2D) bir görüntü oluşturmak üzere işlenmesiyle gerçekleştirilmiştir. Elde edilen görüntüler, önerilen antenin, yalnızca giyilebilir konfigürasyonlarda değil, aynı zamanda dinamik bir görüntüleme sistemi içinde kullanıldığında da tümörleri etkin bir şekilde tespit edebildiğini ortaya koymuştur. Bu bulgular, antenin çeşitli görüntüleme sistemi uygulamaları için sahip olduğu çok yönlülüğü ve uyarlanabilirliği açıkça ortaya koymaktadır. Ayrıca, önerilen antenin hem kanser görüntüleme hem de hipertermi için kritik olan dizi sistemlerine entegre edilme yeteneğini ölçmek için 2x4 elemanlı bir anten dizisi tasarlanmış ve test edilmiştir. Tez, homojen ısı dağılımını sağlama, sıcak noktaları en aza indirme ve hasta güvenliğini sağlama gibi mikrodalga hipertermisi ile ilişkili kritik zorlukları ele almaktadır. Hipertermik uygulamalardaki anten performansı, CST MPMISICS STUDIO yazılımı kullanılarak değerlendirilmiştir. Simülasyon sonuçları, antenin kötü huylu hücrelerin sıcaklığını seçici olarak terapötik termal aralığa yükseltme yeteneğini ve sağlıklı dokuların sıcaklığını kabul edilebilir bir tıbbi aralıkta tutabilme yeteneğini göstermiştir.

Belirlenen antenlerden yayılan sinyallerin fazını ayarlamak için ışın oluşturma teknikleri kullanılmış, elektromanyetik dalganın tümöre doğru optimum yönelimi sağlanmış ve böylece kötü huylu hücrelerin, memenin derinliklerinde bulunsalar bile, hassas bir şekilde hedeflenmesi kolaylaştırılmıştır. Bu çalışma, tekstil tabanlı UWB antenlerinin meme kanserlerinin sıcaklığını yeterli terapötik seviyelere yükseltmesinin uygulanabilirliğini göstermektedir. Tasarlanan anten dizileri, farklı ayarlamalar kullanarak tümör sıcaklıklarını 42,3°C, 45,6°C, 43,3°C ve 42,4°C'ye kadar yükseltme yeteneğini göstermektedir. Bu çalışmanın sonuçları, önerilen UWB tekstil tabanlı mikro şerit yama anteninin hem erken meme kanseri tespiti hem de mikrodalga hipertermisi tedavisi için umut verici bir araç olduğunu göstermektedir. Tanı ve tedavi yeteneklerinin benzersiz kombinasyonu, giyilebilir tasarımıyla birlikte, onu biyomedikal mühendisliği alanında değerli bir yenilik olarak konumlandırıyor. Araştırma, doğru, invaziv olmayan ve uygun maliyetli tümör tespiti ve etkili lokalize tedavi elde etmede önemli ilerlemeler göstererek gelecekte kliniklerde bile uygulanabilmesi için yolu açmaktadır. Bu tez, UWB teknolojisini tekstil tabanlı anten tasarımıyla entegre ederek yeni nesil tıbbi cihazların geliştirilmesine katkıda bulunmaktadır. Bulgular, giyilebilir, esnek ve çok işlevli tamamen tekstil tabanlı antenlerin meme kanseri yönetiminde devrim yaratma potansiyelini vurgulamaktadır.



# 1. INTRODUCTION

## 1.1. Introduction

Breast cancer is characterized by the uncontrolled development and division of breast cells, leading to their invasion of nearby healthy cells or extending to other regions of the body through metastasis (Russo, 2021). In 2022, breast cancer was the second leading cause of death among women worldwide, resulting in approximately 670,000 fatalities. The World Health Organization's (WHO) data revealed that the global number of newly identified cases of female breast cancer surpassed 2.3 million (World Health Organization, 2024). Breast cancer can occur in both men and women, but it's far more common in women. In 2024, projections by the American Cancer Society (ACS) estimate that 310,720 women in the United States will be diagnosed with invasive breast cancer, alongside 56,500 cases of ductal carcinoma in situ (DCIS) (American Cancer Society, 2024). Additionally, approximately 2,790 cases of breast cancer are expected to be diagnosed in men. The anticipated mortality from breast cancer includes roughly 42,250 women and 530 men (American Cancer Society, 2024).

Reliable diagnosis of breast cancer in its early stages is a critical factor in treatment. Early detection and treatment of breast cancer can result in survival rates as high as 97%, highlighting the critical need for a reliable and efficient method for early diagnosis (Redig & Mcallister, 2013). Early detection of localized cancer results in a 5-year survival rate of 97%, according to the American Cancer Society's statistics from 1996-2003 (Coleman, 2017). The 5-year survival rate decreases to 83.5% if cancer has metastasized to adjacent tissue at the time of diagnosis. The survival rate decreases to 26.7% when cancer metastasizes to distant tissues. The data demonstrates the advantages of early detection: smaller and more localized malignant tumors at the time of detection correlate with higher treatment success rates.

In the realm of medical diagnostics, imaging modalities hold a significant position in the context of cancer identification and therapeutic interventions. These modalities are

instrumental in revealing concealed information and rendering internal anatomical visuals (Koundal et al., 2020). Within the domain of breast cancer diagnostics, a range of imaging techniques, including ultrasonic (US), mammography, positron emission tomography (PET), and magnetic resonance imaging, are widely employed in the identification of breast tumors (Lima et al., 2019; Ronckers et al., 2005). X-ray mammography uses low-energy Rontgen rays to produce breast images (Nicosia et al., 2023a). Although it has significant disadvantages, including using ionized radiation and the high false-negative rates, especially in individuals with dense tissue, it is the standard approach for diagnosing breast cancer at an early stage (Hoheisel, 2006). Ultrasound utilizes sound waves with frequencies exceeding 20 kHz to observe the inside structures of the body (Carovac et al., 2011). A probe placed on the skin emits ultrasound signals, and these signals are reflected from different tissues, forming ultrasound images. This method is free from radiation and comparatively uncomplicated. Despite offering effective contrast for soft tissues, ultrasound encounters challenges with bone and air detection, depends on the operator's proficiency, results in limited resolution, and fails to differentiate between cancerous and benign tumors (Moore, 2010). MRI is valuable for the examination of various organs and the identification of specific diseases. It relies on radio waves and powerful magnetic fields to produce detailed internal body images. While MRI is frequently utilized for additional assessment in cases of uncertain results, its application for early detection is limited because of its elevated cost (Morrow et al., 2011). PET is another imaging technique that involves injecting a radioactive substance attached to an active biomolecule into the patient's body (Flanagan et al., 1998). Cancer cells, which are more metabolically active, absorb radioactive substances, which emit positrons. PET detects these Positrons to create an image. Compared with other modalities, it excels at early cancer detection but has a lower resolution.

The limitations of existing breast imaging methods have spurred researchers to explore and develop new microwave-based techniques. Microwave imaging stands out because of its nonionizing radiation and noninvasive nature, making it a promising domain in breast cancer detection (Kwon & Lee, 2013, 2016). The predominant techniques that subject the body to microwaves and evaluate the sent and received signals are microwave tomography and ultra-wideband radar imaging (Conceição et al., 2016). In any imaging system, the antenna is the most important system component

for transmitting and receiving microwave signals that are used to create accurate images of tissues. The antenna must be designed to emit microwaves with a high enough resolution to distinguish between different types of tissue, such as healthy and cancerous cells, in any breast imaging system. Antenna design for medical imaging is a challenge. The human body is made up of cells whose electrical properties greatly influence the characteristics of the antenna designed for use in the free space. In addition, the antenna must penetrate deep enough to image internal structures without losing too much signal, especially in dense breast tissue. High resolution is critical to detecting small abnormalities, but this must be balanced against the risk of noise and interference from surrounding tissue or external sources. The antenna must also be safe, comfortable, and non-invasive for the patient. These challenges underscore the need for innovative antenna designs that address technical performance and patient comfort in breast imaging. Recently, there has been an increasing interest in developing flexible, textile-based, wearable microwave antennas. The sensitivity of tumor identification is contingent upon the distance between the antenna and the breast; reducing this distance enhances detection sensitivity(Hamza et al., 2024). Additionally, wearable prototypes are more cost-effective and compact than table-based systems. The flexibility and wearer comfort of textile substrates make them increasingly popular as the basic materials for wearable biomedical antennas (Giftsy et al., 2023).

On the other hand, breast cancer treatment remains a significant challenge due to the often debilitating side effects of conventional therapies(Chandraprasad et al., 2022). The most widely used approaches include surgical interventions such as mastectomy, which involves the complete removal of the breast, and lumpectomy, where only the affected portion is excised(Timmerman et al., 2009). Additionally, ablative therapies like radiation and chemotherapy, which inflict cellular damage to eradicate cancerous tissues, are commonly employed but can also harm healthy tissues.

An alternative, thermal therapy presents a promising avenue by raising the temperature of cancerous tissue to induce cell death while potentially minimizing side effects(R. W. Y. Habash et al., 2007). This technique has garnered attention for its ability to provide noninvasive treatment options with lower patient burden. Among thermal methods, microwave hyperthermia is particularly noteworthy. It leverages focused microwave energy to selectively heat tumor tissues to a controlled temperature range

of 41°C to 45°C, sparing surrounding healthy tissue(Chu & Dupuy, 2014). Achieving this requires precise energy delivery, which can be accomplished using advanced focusing techniques and antenna arrays(Pfannenstiel, 2020). Microwave hyperthermia offers a compelling balance between penetration depth and energy concentration, making it a viable candidate for advancing cancer treatment strategies. Continued development and refinement of this technique hold great promise for improving patient outcomes while reducing the adverse effects associated with traditional therapies(Bevacqua et al., 2023).

Conversely, Recent worldwide health concerns, including the COVID-19 pandemic that originated in 2019, have highlighted the necessity of exploring alternatives to traditional breast imaging and cancer treatment technologies. The impact of the pandemic has led to the realization that finding alternative methods for breast screening is imperative. According to the Breast Cancer Organization, many healthcare facilities have had to postpone or halt nonessential procedures, including imaging and elective surgeries, to minimize potential exposure to the virus for patients(Siegel et al., 2023).

Many studies used microstrip patch antennas in breast microwave imaging. The main objective of recent research is to create a novel, fully textile UWB microstrip patch antenna with a compact size and uncomplicated design with a dual ability to detect tumors of varying shapes and sizes in different areas within the breast, and at the same time can be integrated into hyperthermia system to raise the temperature of the detected breast tumors into a therapy range of 41 to 45. Most researchers assume that the tumor has a spherical shape, which is not always true. This study fills this gap in the literature by using different tumor shapes, sizes, and locations. This research also focuses on overcoming challenges specific to wearable antennas, including signal detuning caused by body proximity, material losses, and environmental factors. Innovative design solutions, such as the use of conductive textile materials, are implemented to mitigate these issues. Various factors, such as the specific absorption rate (SAR), return losses, voltage standing wave ratio (VSWR), and temperature distributions were computed. This thesis aims to develop the next generation of medical devices by integrating UWB technology with textile-based antenna design for breast cancer detection and treatment.

## 1.2. Problem Statement

- The available breast cancer imaging techniques have their own set of downfalls (low resolution, unsafe, painful, high cost, and inaccurate results). This highlights the necessity for enhanced methodologies for the early diagnosis of breast cancer.
- Conversely, the methods now employed for breast cancer treatment frequently result in significant adverse effects. A noninvasive and comfortable treatment technique with low side effects is required.
- Owing to pandemic-related restrictions, many healthcare facilities have postponed nonurgent operations and imaging procedures, causing delays in cancer detection and treatment. Therefore, the need for innovative, portable, and wearable imaging systems to avoid potential diagnostic delays that could adversely affect patients' lives in the long term becomes evident.
- Most of the research in the literature developed antennas from materials that are not skin-friendly for microwave and hyperthermia imaging; some experiments concentrated on enhancing contrast, while others aimed at augmenting penetration. However, there isn't a complete imaging model made entirely of textile-based materials that can achieve both high resolution and deep penetration, making it a safe and comfortable way to do breast imaging and hyperthermia. This highlights the need to manufacture wearable antennas from harmless, skin-friendly, and bendable materials such as fabric for use in the medical field.
- Moreover, none of the currently known antenna designs can operate in both imaging and hyperthermia systems, despite this combination yielding cost-effective imaging and therapy methods.
- Additionally, the majority of researchers assumed that the tumor had a spherical morphology, a presumption that is not universally accurate. This necessitates the evaluation of systems that utilize various tumor forms.

### **1.3. Research Objective**

#### **1.3.1. General objective**

To design a safe, accurate, not expensive, and comfortable textile-based imaging and hyperthermia system able to detect breast cancer and help to treat it.

#### **1.3.2. Specific objectives**

- To design an effective textile-based microstrip patch antenna for breast cancer imaging.
- To design a 3d breast phantom.
- To examine the designed imaging system in the designed 3d breast model.
- To design an effective antenna array for breast microwave hyperthermia.
- To examine the designed antenna array system in a 3d breast model.

### **1.4. Research Methodology**

The antennas in the microwave breast cancer detection device emit a pulse that penetrates the breast tissue. The scattered signals emanating from different layers of breast tissue are collected and analyzed. The fluctuation in S parameters and SAR values is analyzed to detect malignant tissue in the breast, as the water content in tumors influences these factors distinctively compared to other breast tissues. On the other hand, the designed antenna was integrated into an array, and beamforming theories were applied to modify the phase and power of each element to steer the radiation beam directly to the tumor position and raise the tumor temperature to the range of (41°C – 45°C). The proposed microstrip antenna was initially built using computer simulation technology, specifically microwave studio and Mphysics studio, to operate in free space and later optimized for use with a breast phantom.

### **1.5. Organization of the Thesis**

Chapter 1 provides an overview of the research, outlines the problems and objectives of the study, and research methodology, and concludes with research outlines. Chapter 2 provides a theoretical background on the main concepts of the research, along with a review of relevant literature. Chapter 3 presents the background of the UWB microstrip patch antenna design, and its use in the medical field and breast cancer

imaging, as well as the history of using textile materials in microstrip antennae for breast imaging. In Chapter 4, the proposed antenna design and its representation in various scenarios along with a constructed breast phantom that features four different versions, an array design, and hyperthermia system scenarios are provided. Chapter 5 outlines and discusses the results gained, while Chapter 6 summarizes the whole research and offers recommendations for future studies.



## 2. BACKGROUND AND LITERATURE REVIEW

### 2.1. Physiology of Breast

#### 2.1.1. Anatomy of the breast

The breast is highly complicated. It undergoes more transformations than any other organ of the human body—from birth, puberty, pregnancy, and lactation to menopause(Alex et al., 2020). Breast tissue spans from the collarbone to the lower ribs, sternum, and axilla(Kalimuthu et al., 2015). Each breast comprises 15-20 glands known as lobes, which are responsible for milk production in mothers who are breastfeeding(Vorherr, 2012). Figure 2.1 illustrates a depiction of breast anatomy, including the chest wall, adipose tissue, nipple, ducts, and lobules(Hipwell et al., 2016). Embedded within the adipose breast tissue are lymph nodes, tiny structures that harbor white blood cells. A network of vessels connects the breast's lymph nodes to the body's lymphatic system. Lymph nodes are significant as they play a crucial role in the immune system and frequently serve as a pathway for the dissemination of malignant tumors from the breast to other areas of the body.

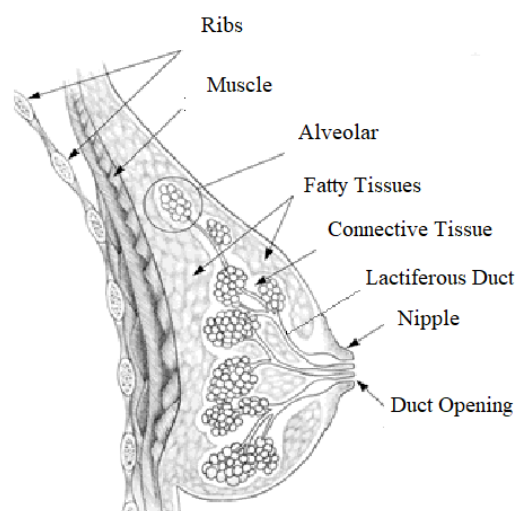


**Figure 2.1.**The anatomy of the breast

### **2.1.2. Breast cancer**

Breast cancer represents an international health crisis and is the second strongest cause of mortality among women worldwide. The breast, like any other physiological part, comprises billions of tiny cells. These cells typically replicate in an organized manner, with new healthy cells consistently dividing to replace those that have expired (Feng et al., 2018). Nonetheless, cells may occasionally develop abnormalities (mutations). This transpires when the genes responsible for ensuring accurate cellular replication fail to identify mutations. In such instances, atypical cells persist in dividing and proliferating, occasionally at an accelerated rate. At that point, the growth may not be malignant. It may be a "non-invasive tumor" that remains localized within the duct or lobe. A tumor is considered malignant when it is capable of invading adjacent tissue. These malignancies necessitate therapy, as their continued growth and spreading could pose a life-threatening risk. Breast cancer typically originates in the ducts that transport milk to the nipple or within the smaller components of the lobes(Akram et al., 2017). A limited percentage of malignancies originate in other breast tissues; these are known as sarcomas and lymphomas. While numerous factors may induce a breast lump, not all are responsible.

Breast cancer may metastasize when cells separate from the original tumor and then spread to other regions of the body(Nathanson et al., 2022). This may occur through the lymphatic system or the circulatory system. Lymphatic vessels, which resemble little veins, transport a transparent fluid known as lymph away from the breast. Lymph comprises tissue fluid, waste materials, and immune system cells. Breast cancer cells can infiltrate neighboring lymphatic arteries and multiply within lymph nodes. Lymphatic veins transport lymph fluid from the body and direct it toward the chest, where it ultimately enters the bloodstream. The dissemination of cancer cells to one or more lymph nodes increases the likelihood of metastasis to other locations in the body(Nathanson et al., 2018). A surgical biopsy is typically required to excise one or more lymph nodes to ascertain the presence of malignancy.

There are about 200 different types of cancer. The majority of cancers originate from genetic alterations that occur throughout an individual's life. Cancers may infrequently arise from inherited defective genes transmitted within families(Talseth-Palmer & Scott, 2011). Currently, the precise etiology of cancer remains unclear; nonetheless, some variables may elevate cancer risk, including tobacco use, obesity, physical

inactivity, alcohol use, infections, and genetic and molecular processes(Anand et al., 2008). The most prevalent kinds of cancer include lung cancer, skin cancer, breast cancer, prostate cancer, liver cancer, and colorectal cancer (Sung et al., 2021). Breast cancer progresses through many stages throughout time(Edge, 2010). In the localized stage, cancer appears as a tumor inside the breast tissue that grows. Subsequently, the cancer cells disseminate via the lymphatic system to the lymph nodes, spreading the malignancy to the regional stage. In the advanced stage, cancer cells communicate via the bloodstream into faraway organs, such as the bones, lungs, brain, or liver(Breast Cancer Grade, n.d.; Edge, 2010; Feng et al., 2018). This is a rudimentary explanation that does not apply to all malignancies.

Physicians at the clinics employ a far more comprehensive staging approach for selecting suitable treatment. The TNM classification is used for standard anatomic staging. In this classification, T stands for tumor size, N for lymph node metastases, and M for distant metastases. The three classifiers receive individual scores, which are aggregated to establish a comprehensive breast cancer stage ranging from 0 to IV(Cong et al., 2018).

In the most recent (8th) tumor staging guidelines, the American Joint Committee on Cancer (AJCC) endorses the implementation of prognostic stages, categorizing breast tumors based on anticipated survival durations, whereby a higher stage indicates a poorer prognosis(Edge, 2010). By using criteria like grade, hormone receptor-positive status (ER/PR/HER2), and multigene panels, this staging method makes it easier to see how different diseases are. In Norway, the anatomic stage-specific 5-year relative survival rates for cases identified from 1995 to 2007 were 100% for Stage I, 92% for Stage II, 76% for Stage III, and 26% for Stage IV (Coleman BM BCh et al., 2011).

### **2.1.3. Electrical properties**

Understanding the dielectric properties of breast tissue is essential in various medical and technological applications, especially in the fields of medical imaging, cancer detection, and therapeutic techniques(Hesabgar et al., 2017). Dielectric properties refer to how a material interacts with an electric field, encompassing permittivity, conductivity, and loss factors. These parameters provide crucial insights into the tissue's behavior when subjected to electromagnetic fields and play a significant role in the development of microwave imaging, electromagnetic therapy, and cancer

detection technologies(S. Gabriel et al., 1996). Dielectric properties of biological tissues vary depending on their water content, ion concentration, and structural composition. In general, tissues with high water content have high permittivity and conductivity because water is polar and easily interacts with electromagnetic fields(C. Gabriel et al., 1996). Breast tissue, comprising adipose (fat), glandular, and fibrous tissues, demonstrates unique dielectric characteristics based on its composition. For example, adipose tissue, which has low water content, tends to have lower permittivity compared to fibrous or glandular tissues, which have higher water content and thus higher dielectric constants(Pollacco et al., 2018). These differences are particularly significant in breast tissue, where the ratio of fat to glandular tissue can vary significantly from one individual to another. This variation plays a key role in applications such as microwave imaging for breast cancer detection. One of the most critical areas where the dielectric properties of breast tissue come into play is in distinguishing between healthy and cancerous tissues(Fornes-Leal et al., 2016). Tumor tissues generally exhibit higher water content and cellularity, leading to significantly different dielectric properties compared to healthy tissues(Sha et al., 2002). Cancerous tissues tend to have higher permittivity and conductivity due to their higher concentration of cells, water, and ionic components. This creates a dielectric contrast between malignant and normal tissues, which can be leveraged in cancer detection techniques such as microwave imaging and electromagnetic tomography. Microwave imaging, for instance, exploits the dielectric contrast between malignant and normal tissues(Nikolova, 2011). This non-invasive technique uses low-power microwaves to create images based on how different tissues scatter and absorb these waves. The distinct dielectric properties of cancerous tissues cause them to interact differently with the microwaves, allowing for the detection of tumors with high sensitivity.

The Cole-Cole and Debye models are frequently utilized to analyze the dielectric characteristics of biological tissues, offering insights into how these tissues interact with electromagnetic fields(Cruciani et al., 2012). These models are essential for advancing applications in fields such as medical imaging and electromagnetic therapy. The intricate behavior of tissue dielectric properties across a frequency range is described by the Cole-Cole model (Kang et al., 2007). It takes into consideration the distribution of relaxation times, capturing the heterogeneous nature of tissues, as shown in equation (2.1) below:

$$\varepsilon^*(w) = \varepsilon_\infty + \frac{\varepsilon_s + \varepsilon_\infty}{1 + (jw\tau)^{1-\alpha}} \quad (2.1)$$

Where  $\varepsilon^*$  is the complex dielectric constant,  $\varepsilon_s$  and  $\varepsilon_\infty$  are the "static" and "infinite frequency" dielectric constants,  $w$  is the angular frequency and  $\tau$  is a dielectric relaxation time constant.

On the other hand, the Debye model provides a simplified representation of tissue dielectric properties (Lazebnik, Okoniewski, et al., 2007). It involves a single relaxation time equation (2.2), which reflects the average behavior of the tissue at a specific frequency.

$$\varepsilon_r = \varepsilon_\infty + \frac{\varepsilon_s + \varepsilon_\infty}{1 + (jw\tau)} - j \frac{\sigma}{w\varepsilon_0} \quad (2.2)$$

where  $\varepsilon_r$  is the dielectric constant and  $\sigma$  is the conductivity.

Previous studies have demonstrated that there is a significant dielectric differential between healthy and cancerous breast tissue to distinguish between the two. For example, Chaudhary et al. (Chaudhary et al., 1984) demonstrated that cancerous breast tissues at 12 GHz exhibit properties 35 times greater than those of normal tissues. In their study, Surowiec et al. (Surowiec et al., 1988) used an end-of-the-line capacitive sensor and a network analyzer on samples from three different locations (the tumor's center, the surrounding tissue, and the healthy tissue two cm from the tumor) and observed important differences in the dielectric properties of the breast. The experiments were conducted at a frequency range of 20 kHz--100 MHz with 28 samples from 7 different patients. The physical features of breast tissue fluctuate under various physiological situations, according to Sabouni et al. (Sabouni et al., 2013). Ex vivo breast tissue samples that had been surgically removed were analyzed to determine how physiologic circumstances affect the dielectric characteristics. Campbell et al. (Margaret Campbell & John, 1990) utilized a resonant cavity technique at 3.2 GHz on samples from 37 patients to measure the dielectric properties of cancerous, benign, and normal breast tissue. While they observed differences in the resonant frequency, they noted that in vivo approaches may not reliably differentiate between cancer and benign cells because of the similarity of the dielectric characteristics acquired in the tests. Joines et al. (WT Joines et al., 1994), on the basis of 12 measurements of healthy and malignant breast tissues at 50–900 MHz and 23–

25°C, reported notable variations in conductivity and permittivity between malignant and normal breast tissues, with differences of 233% and 577%, respectively. Gabriel et al. (Camelia, 1996; S Gabriel et al., 1996) published significant results on the description of biological tissues in the 0.01 GHz–20 GHz frequency domain.

Because of their higher water content and increased activity, malignant tissues typically have dielectric characteristics that are around ten times higher than those of noncancerous breast tissues (Barnes & Greenebaum, n.d.).

However, more recent studies (Barnes & Greenebaum, n.d.; Cheng & Fu, 2018) have revealed heterogeneity in the dielectric characteristics of healthy breast tissue, indicating differences between patients and different tissue types. The dielectric characteristics of normal, cancerous, and benign breast tissues in the 0.5–20 GHz UWB microwave frequency range were investigated by a joint team of researchers from the Universities of California in Canada and the University of Wisconsin in America (Lazebnik, McCartney, et al., 2007; Lazebnik, Popovic, et al., 2007). They analyzed 319 samples from 196 patients obtained during reduction and cancer surgeries. The experiments highlighted a significant difference in the microwave dielectric characteristics between cancerous breast tissues and adipose-dominant normal breast tissues, with up to a 10-fold difference. However, the difference between the dielectric characteristics of cancerous and healthy fibroconnective/glandular breast tissues was smaller, approximately 10%. Another study carried out by researchers from the University of Electronic Science and Technology of China involved 98 patients and 509 samples collected during surgical operations at Sichuan Provincial People's Hospital (Cheng & Fu, 2018). This research examined cancerous, benign, and healthy breast tissues. The S-parameters of the samples were tested across a frequency band of 0.5--8 GHz, with intervals of 0.0375 GHz. The study revealed that cancerous breast tissues exhibited significantly greater effective relative permittivity and effective conductivity at all frequencies than benign tumors. Additionally, benign tumors presented higher levels than normal tissues did. The study also revealed that at approximately 2.5 GHz, normal and cancerous breast tissues presented the smallest standard deviations.

## **2.2. Current Breast Cancer Detection Methods**

Imaging technologies are integral to clinical procedures for cancer and represent the initial step in disease diagnosis (Gerami et al., 2022). These techniques offer several advantages, including real-time monitoring without compromising tissue integrity, suitability for extended applications, and minimally invasive procedures. Early detection of breast cancer is facilitated by various imaging modalities, although the sensitivity and specificity of these methods differ (Pulumati et al., 2023).

### **2.2.1. X-ray mammography**

Mammography, a widely utilized imaging technique for breast cancer screening, employs low-energy X-rays (approximately 30 kVp) to identify small tumors by detecting masses or microcalcifications as shown in Figure 2.2 (Nicosia et al., 2023b). To perform a mammogram, the breast is carefully placed on a flat support plate and gently compressed with a parallel paddle to spread the tissue evenly and reduce movement, ensuring a clearer image. The X-ray machine then emits a short burst of low-dose X-rays, which pass through the breast tissue. On the other side, a detector captures these X-rays. This detector can be either a photographic film plate that produces an image on film, or a modern solid-state detector that converts the X-rays into electronic signals. These signals are processed by a computer to create a high-resolution digital image. These images, called mammograms, are essential for detecting abnormalities, including early signs of breast cancer (EGAN, 1966). However, its diagnostic accuracy diminishes in women with dense breast tissue, as both dense tissue and tumors exhibit similar radiographic characteristics, appearing white on the mammogram, leading to overtreatment, unnecessary follow-up exams, and psychological distress. Several variables influence the effectiveness of mammography, including patient-specific factors such as age, weight, breast density, hormonal sensitivity, menstrual cycle timing, and tumor-specific factors like size and location (White et al., 1998). Breast compression is an essential aspect of the procedure, aiding in the reduction of structural overlap and radiation exposure while enhancing image clarity (Holland et al., 2017). The mammographic image's quality and the radiologist's expertise further impact its accuracy.

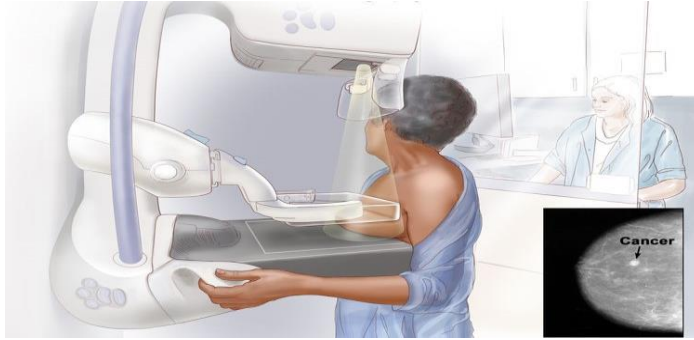


**Figure 2.2.** X-ray Mammography

While mammography offers significant diagnostic advantages, it has limitations. False-positive results occur in approximately 10% of screenings, often necessitating additional tests, such as biopsies, which carry inherent risks (Heywang-Köbrunner et al., 2011). Additionally, false-negative results, where cancer remains undetected, occur in about 20% of cases, potentially delaying diagnosis and treatment.

### **2.2.2. Ultrasound imaging**

Ultrasonography is a widely utilized imaging modality for breast cancer diagnosis, relying on acoustic wave reflections to analyze breast tissue. Figure 2.3 shows the breast Ultrasound imaging system (Moore, 2010). It is a safe, well-tolerated procedure and is frequently used in conjunction with physical examinations and mammography to evaluate breast masses (Duck, 2008). This technique effectively differentiates between cystic and solid masses and aids in distinguishing benign from malignant solid lesions. However, the traditional hand-held ultrasound is highly operator-dependent, resulting in variability in diagnostic outcomes. Automated breast ultrasound systems (ABUS) provide enhanced consistency and objectivity (Philadelpho et al., 2021). When combined with mammography, ultrasonography significantly improves cancer detection rates, particularly in women with dense breast tissue, identifying up to four additional cases per 1,000 women screened (Hadadi et al., 2021).

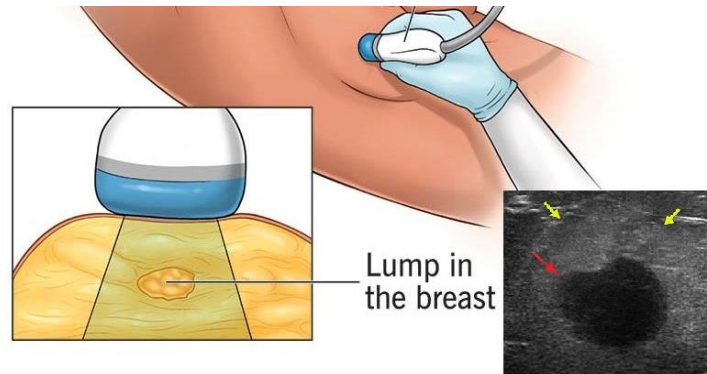


**Figure 2.3.** Breast Ultrasound Imaging Device.

### 2.2.3. Magnetic resonance imaging (MRI)

Protons in the body are aligned by a powerful magnetic field generated by MRI, which employs powerful magnets. The protons are perturbed, and their spins deviate from their intended orientation when a radiofrequency pulse is administered. Once the pulse is turned off, the MRI sensors detect the energy released as the protons realign with the magnetic field. The rate and amount of energy released depend on the tissue's environment and chemical composition, allowing physicians to differentiate between tissue types (Morrow et al., 2011). During an MRI, the patient must remain still as shown in Figure 2.4 to avoid blurring the image.

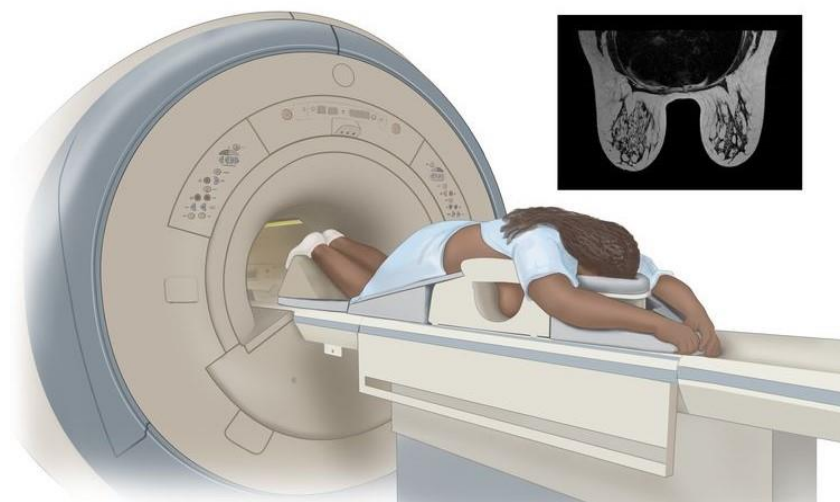


**Figure 2.4.** MRI of the Breast

Gadolinium-containing contrast agents may be administered to improve image clarity by expediting proton realignment (Heywang-K6brunner et al., 1997). MRI does not involve X-rays, thus avoiding radiation exposure. Despite its higher sensitivity than mammography, MRI is not commonly used for breast cancer screening due to its high

cost and the potential for false positives. However, it is useful for screening women with dense breast tissue(Gao et al., 2021).

Integrating these imaging modalities can enhance breast cancer detection and prove particularly beneficial in imaging dense breast tissue.

### 2.3. Microwave Imaging Techniques

One type of medical imaging approach is the microwave imaging technique. It is the process of exposing an item to low-power electromagnetic fields at microwave frequencies, which are between 300 MHz and 300 GHz, to observe its internal structure. The strong contrast between the permittivity and conductivity of healthy and cancerous breast tissue is the basic idea behind microwave breast imaging. Figure 2.5 shows the behavior of microwave signals in both situations.

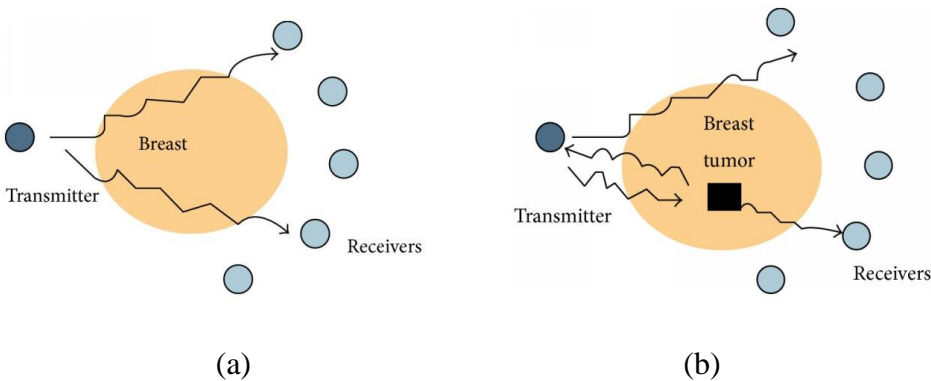


**Figure 2.5.** The behavior of electromagnetic waves (a) in the absence of a tumor (b) in the presence of a tumor.

In general, there are three types of microwave imaging techniques: active, passive, and hybrid.

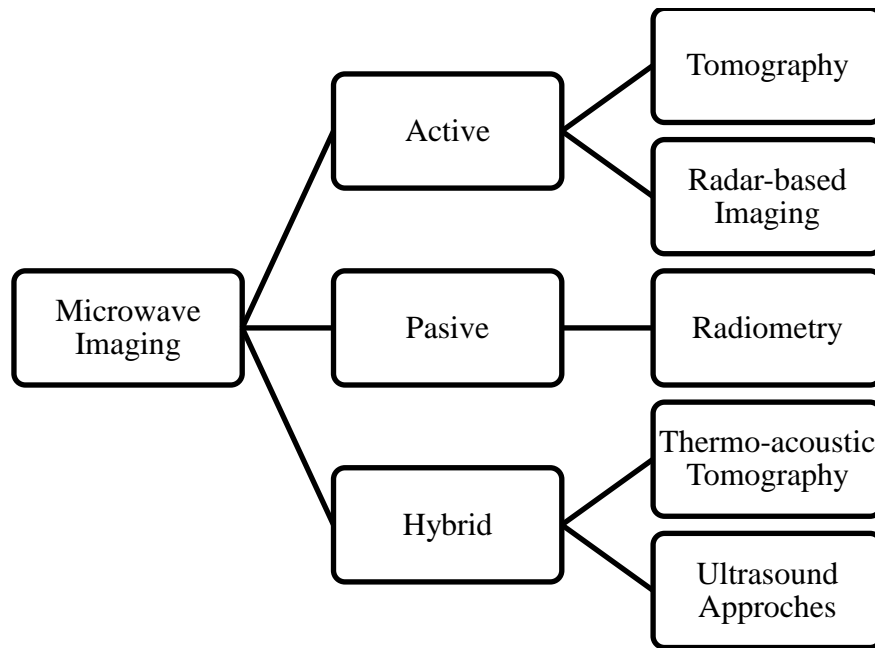


**Figure 2.6.** Microwave Imaging Types

### 2.3.1. Passive microwave imaging

Passive approaches utilize a microwave signal to stimulate biological tissue, while thermal fluctuations are observed by radiometry (Groumpas et al., 2022). The highly vascularized tumor region absorbs a significant amount of energy, leading to an elevated temperature in the tumor compared to surrounding healthy tissue. The primary constraint of this method is the low-power radiation emitted by these tumors, resulting in technical challenges (Karanasiou et al., 2004). Another disadvantage is its inability to distinguish between a cool substance on the body's surface and a hot tumor situated deep within.

### 2.3.2. Hybrid microwave imaging

Hybrid approaches combine microwave imaging with another method, like the thermo-acoustic method, to improve the resolution, sensitivity, and specificity of the imaging (Ku & Wang, 2000; Matloubian et al., 1999; Xu et al., 2002). The variability in breast morphology and the near closeness of the skin to the transducer present major challenges to this technique. The skin tissue exhibits greater conductivity than the tumor, resulting in stronger reflections.

### **2.3.3. Active microwave imaging**

Active microwave imaging utilizes electromagnetic scattering that arises from the dielectric contrast between the various objects under examination. Numerous transducers (microwave antennas) operate at microwave frequencies, typically ranging from 300 MHz to 20 GHz, illuminating the breast. Various receiving antennas collect the scattered electromagnetic radiation and process it to create an image (Kwon & Lee, 2016). Recently, researchers have developed several active microwave breast imaging systems and performed experimental validation on breast phantoms and people in clinical trials. Two common techniques in breast imaging research rely on the use of microwaves. These methods involve directing microwaves at the breast and analyzing the signals that are transmitted or reflected from the tissue. These methods known as microwave tomography and radar-based imaging are particularly effective for this process (Wang, 2023).

#### **2.3.3.1. Microwave tomography**

Microwave tomography refers to techniques that utilize measurable disturbances of an electromagnetic field, induced by a specific object, to extract information regarding the object's geometry and electromagnetic properties (Semenov, 2009). The application of microwave tomography for breast cancer screening garnered significant attention in the late 1990s and early 2000s (Wang, 2023).

The goal of microwave tomography is to find out how the object being scanned's electromagnetic properties are distributed within an imaging domain by using measurements taken with several antennas that are placed outside the imaging domain. A challenge associated with this approach is inverse scattering. The heterogeneity of the breast's form causes numerous undesirable reflections of the transmitted microwaves, leading to inverse scattering. Inverse scattering employs scattering signals, encompassing diffraction from objects. It generates a map of permittivity and conductivity by inverting those signals. Nonetheless, the inverse problem requires considerable time due to the complexity of the calculating method. A nonlinear inverse scattering problem must be addressed, necessitating iterative image reconstruction procedures to derive a solution. Most of the time, these ill-posed inverse scattering methods are not unique and need to be regularized in order to get to a significant solution (Lui et al., 2012).

Several studies have investigated the application of microwave tomography for breast cancer imaging. The breast cancer microwave imaging prototype system created by Paul et al. (Meaney et al., 2000) comprises 16 monopole antennas that work in either transmitting or receiving mode within the 300–1000 MHz frequency spectrum. The system exams were performed on five women with the patient placed prone on an examination table, as shown in Figure 2.7, and it took 10–15 minutes per single breast. This system represents the first study of successful near-field breast microwave imaging, and it is the initial attempt to employ model-based image reconstruction from in-vivo tissue information to convert observed microwave signals into a dielectric properties map.

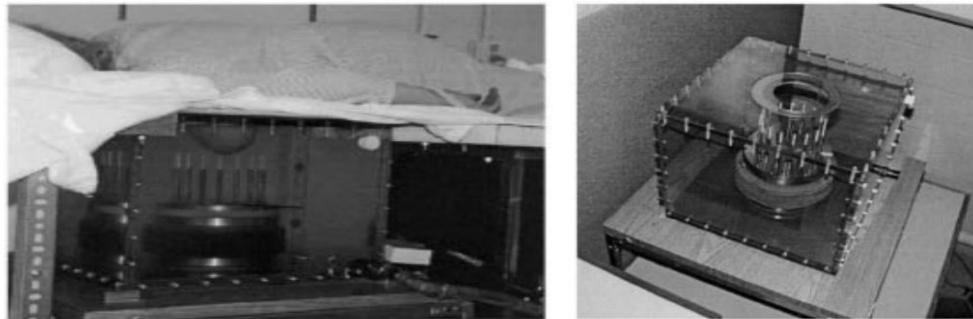


**Figure 2.7.** First breast microwave imaging prototype.

Despite being preliminary and necessitating further experiments, the obtained results are promising and have revealed intriguing findings. Specifically, there seems to be a potential correlation between the relative permittivity of the breast and the classification of breast radiological density. Moreover, the relative permittivity values obtained through this study appear to be significantly higher than those reported in previous studies based on ex vivo tissue samples.

The Dartmouth University group subsequently introduced a groundbreaking 3D microwave tomographic imaging system that boasts an examination time of less than 2 minutes, providing 3D images in less than 20 minutes (Grzegorzczuk et al., 2012). The system uses a circular array of 16 monopole antennas to transmit electromagnetic waves sequentially, whereas the remaining 15 antennas collect measurements. Both simulated data and real clinical data from patients were incorporated into the study. The results demonstrate the system's ability to distinguish between malignant and benign tumors with a diameter of 1 cm or larger.

The Electronics and Telecommunications Research Institute (ETRI) research team (Son et al., 2010) designed a preclinical prototype of microwave tomography to detect breast cancer. This system is valuable for conducting patient trials and phantom measurements within the 0.5-3 GHz frequency spectrum.

Additionally, Epstein and colleagues developed a third-generation microwave imaging system for clinical breast examination, which has a more compact and portable design (Epstein et al., 2014).

### **2.3.3.2. UWB radar microwave imaging for breast cancer**

This approach was originally developed by the military for ground penetration and subsequently adapted for use on the human body. Hagness from the University of Wisconsin and Benjamin from the University of Bristol invented this method in the late 1990s for use in breast cancer detection (Hagness et al., 1997).

The microwave radar imaging technique reconstructs images through the use of the reflected waves from objects. The dielectric disparity between healthy and malignant tissue at the microwave band produces scattered radar signals when a tumor is present. An imaging beamformer analyzes these dispersed signals to detect the presence and location of any notable scattered signals within the breast. Unlike microwave tomography, which aims to reconstruct images, UWB radar-based imaging focuses solely on detecting and identifying big, widespread obstacles such as malignant tumors. This is a simpler computational problem that can be solved more quickly.

Five main groups categorize radar-based microwave imaging methodologies: microwave imaging via space-time (MIST), confocal microwave imaging (CMI), multi-static adaptive microwave imaging (MSA), holographic microwave imaging technology (HMI), and tissue sensing adaptive radar (TSAR).

Hagness et al. (Hagness et al., 1998, 1999) created a CMI system. In their studies, they positioned a configuration of 17 monopole transceivers along the surface of a breast model, uniformly spacing all antennas over a distance of 8 cm. This approach can generate better-resolution images and possesses a strong interference rejection capability, but it has a limited capacity to differentiate between artifacts and noise.

Fear et al. (Fear et al., 2002) created a prototype system for TSAR. During data collection, the patient was positioned prone on the testing table with her breast

protruding via the designated opening while the antennas were collecting data surrounding the breast. To minimize the noise, the image was generated from reflected signals excluding skin effects. Clinical findings indicated that the TSAR can detect and locate lesions over 4 mm in diameter. The primary constraints of TSAR are the significant reflections produced by the skin and the costly electronics required for real-time imaging. A Bayesian predictor was utilized to improve the image being reconstructed.

A MIST beamforming technique was devised by Bond et al. (Bond et al., 2003; Li et al., 2005). A configuration of 16 horn antennas was positioned adjacent to the breast model's surface, and a UWB signal was delivered in succession from each antenna. The numerical findings indicated that a small tumor (2 mm in diameter) implanted in heterogeneous breast tissue could be effectively recognized, even in the presence of denser breast tissue. MIST provides a substantial enhancement in performance compared to UWB MI methods that utilize more basic focusing techniques. Nonetheless, the method produced artifacts on the breast skin in the preceding image. The study team enhanced the imaging method to address the difficulties of identifying, localizing, and resolving several or multifocal lesions (Bond et al., 2006). The experimental findings indicated that tumors measuring 4 mm in diameter may be imaged.

For the first time, the University of Bristol team conducted an experimental and clinical experiment utilizing the UWB microwave radar imaging procedure (Klemm et al., 2008). A vector network analyzer (VNA) is employed for measuring scattered signals in the frequency domain. The pair of antennae is changed during the signal measurement process by a switch matrix that is linked to the antenna input. The inverse Fast Fourier Transform (FFT) method is employed to convert the frequency-domain signals that were obtained into time-domain signals. The time-domain signals were used by a focusing algorithm to reconstruct the image.

The University of Calgary has created a prototype of a radar-based breast imaging system known as tissue TSAR (Bourqui et al., 2012). The patient assumes a prone position on the table for scanning and submerges the breast in a tank containing immersion fluid. Their technology differed from that of Bristol University, employing a monostatic approach and screening the skin's reflection. A limited group of

participants was examined with their prototypes. The outcomes were satisfactory as numerous recovered images had responses equivalent to laboratory findings.

Hossain et al.(Hossain et al., 2013) introduced a coherent beam-space maximum-likelihood approach for time-reversal microwave imaging, which was specifically designed for identifying and localizing numerous tumors in extremely dense breasts. They also extended coherent beam-space array processing to the standard decomposition of the time reversal operator (DORT) and time reversal multiple signal classification (TR-MUSIC) techniques. Additionally, they proposed a new combination method that combines arrival time and entropy to efficiently eliminate items early on and estimate the green function of the similar virtual medium needed for the time-reversal process. Researchers have obtained backscattered signals via 3D simulated breast phantoms and finite-difference time-domain calculations. The findings highlight the exceptional effectiveness of the developed C-B-TR-ML microwave imaging method in identifying and locating many tumors implanted in an extremely dense breast phantom.

Smith et al. (Smith et al., 2014) have introduced a near-field indirect HMI technique that entails capturing the holographic intensity pattern and recreating the image by Fourier processing the recorded pattern. In comparison to TSAR, indirect HMI can generate real-time images at a markedly reduced cost. Nevertheless, additional validation efforts are necessary for the theory and proof of concept regarding medical uses.

Time-domain measuring microwave imaging systems for the diagnosis of breast cancer are being developed by a top research group at McGill University in Canada. Their experimental setup, a 16-element antenna array for breast cancer detection, is shown in Figure 2.8 (Bahrami et al., 2014a). The same group has also conducted an early clinical trial utilizing time-domain microwave radar to monitor breast health. For eight months, they gathered 342 breast scans from 13 healthy volunteers who were scanned monthly. The researchers set out to examine the effect of monthly monitoring on a variety of human variables that are impossible to eliminate. They have also created a prototype of a bra that can be worn and uses microwaves to track breast health(Porter et al., 2016).

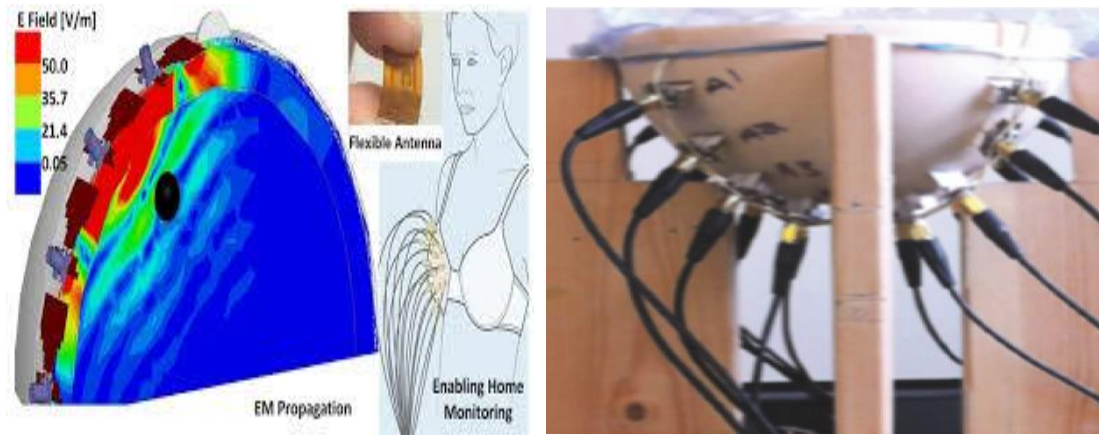


**Figure 2.8.** The microwave system of the McGill University group

In their work, Islam et al. (Islam et al., 2019) designed a portable microwave system with a directional Vivaldi antenna to detect breast tumors in real-time. The system contains nine antennas placed on a circular ABS container. Among the antennas, one serves as the transmitter, while the other eight function as receivers. The system operates by moving the antennas around the breast phantom, covering a range from  $0$  to  $2\pi$ , via the motor. At each  $7.2^\circ$  rotation, the backscattered signals are recorded, resulting in 50 data points covering the complete  $360^\circ$  rotation. To process the data, they employed a novel iteratively corrected delay and sum (IC-DAS) image reconstruction approach. The results from their system demonstrate an enhancement in antenna performance and a reduction in antenna size. Moreover, the experiments confirmed the system's ability to detect multiple cancerous tumors in the same location. Also, a substantial amount of research has been conducted focusing on the design and manufacture of microwave antennas made entirely from fabric materials specifically for breast cancer imaging applications (Abdulla & Demirkol, 2024; Elsheakh et al., 2023; X. Lin et al., 2020; Srinivasan & Gopalakrishnan, 2019a). These fabric-based antennas are being explored due to their unique properties, such as flexibility, comfort, and adaptability, which make them highly suitable for wearable medical devices. By incorporating these antennas into garments or wearable patches, researchers aim to improve patient comfort and provide a non-invasive, efficient, and potentially low-cost approach to breast cancer detection. Studies examine various textile materials and fabrication techniques to enhance the sensitivity, resolution, and overall effectiveness of these antennas, aiming to provide more accessible and accurate imaging solutions in the early detection and monitoring of breast cancer.

## 2.4. Thermal Therapy

The application of heat as a therapeutic intervention is not a novel concept. Medical practitioners commonly employ thermotherapy as a treatment for conditions like rheumatism and muscular disorders. These instances have utilized electromagnetic waves, infrared rays, ultrasonic waves, and warm water as sources of thermal energy (Rosen et al., 2004). These heating techniques rarely differ from those already employed in thermotherapy. Therapies employing physical energy are acknowledged as a form of physiotherapy (Vander Vorst et al., 2006). Therapies employing electromagnetic waves with wavelengths ranging from several hundred to several tens of meters are referred to as diathermy. They are referred to as short-wave or microwave diathermy, ultrasound diathermy, etc., based on variations in radiation type or wavelength. Figure 2.9 illustrates the employment of various thermotherapies across multiple frequency ranges of the electromagnetic spectrum.

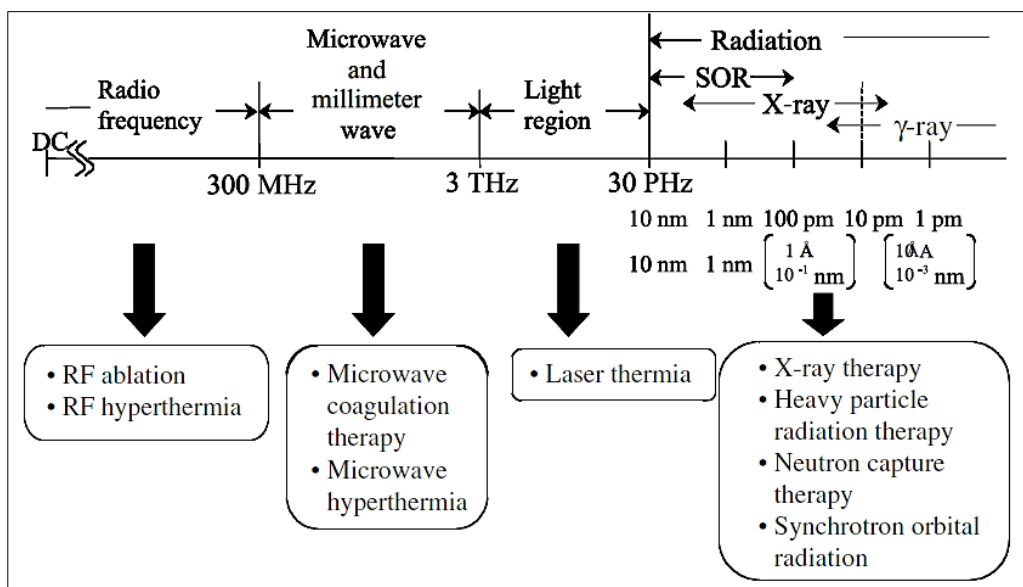


**Figure 2.9.** Thermal therapy in the electromagnetic spectrum

### 2.4.1. Heating principle

In medical terminology, applicators refer to devices that utilize radiative energy, such as electromagnetic waves or ultrasound waves. The applicators that emit electromagnetic waves are categorized into two groups according to their heating principles: dielectric heating applicators and inductive heating applicators (Vander Vorst et al., 2006).

The initial applicator operates on the same principle as a microwave oven. To our knowledge, most organisms consist of water molecules, and according to the theory of electronic polarization, the permanent dipole makes a significant contribution to heat generation. In the microwave band, the permanent dipole is unable to respond to the rapid fluctuations of a high-frequency electric field, resulting in significant loss. In this instance, the power loss produces heat(Vander Vorst et al., 2006). An inductive heating applicator employs an alternating magnetic field. The principle behind it relies on the generation of Joule's heat by the flow of electric currents in a resistor. Hyperthermia treatment uses this heating(Vander Vorst et al., 2006).

#### **2.4.2. Electromagnetic interactions with biological systems**

Three different phenomena can be identified that explain the interactions that occur between Radio Frequency (RF) and microwaves with body tissues:

1. The penetration of electromagnetic radiation into living systems and their transmission within these systems.
2. Waves primarily interact with biological tissues.
3. The possibility of secondary effects resulting from the main interaction (Vander Vorst et al., 2006).

The term interaction emphasizes that outcomes depend on both field actions and living system responses. Living systems can significantly mitigate the effects of external sources, particularly electromagnetic ones. This aspect is frequently overlooked, yet it is a primary reason why conclusions drawn from models must be approached with caution. Physiological compensation signifies the complete displacement of stress from external variables, enabling organisms to function normally. In contrast, pathological compensation indicates that the applied stress changes the organism's functions, potentially leading to structural alterations(Vander Vorst et al., 2006).

To apply hyperthermia, the radiation system must consist of a source that produces electromagnetic energy. The biological system absorbs and converts a portion of the incoming energy. The principles of electromagnetic field theory, reflection, diffraction, dispersion, interference, optics, and quantum effects must be utilized to examine and elucidate the observed occurrences. This holds universally for the entire spectrum of electromagnetic radiation(Vander Vorst et al., 2006).

Microwave exposure is being documented to influence reproduction, development, and immunological responses through various combinations of exposure frequency, duration, and power density. Variations in capacity may result from modifications in behavior, physiology, or morphology(J. Lin, 2012).

#### **2.4.2.1. Specific absorption rate (SAR)**

The Specific Absorption Rate (SAR) is the most reliable metric for assessing the effects of electromagnetic radiation exposure in the near field of a radio frequency source. It quantifies the rate at which energy is absorbed by body tissues when exposed to electromagnetic fields. Measured in watts per kilogram (W/kg), SAR is calculated using a specific formula (equation 2.3) that considers factors such as electromagnetic field strength, tissue conductivity, and density. It can be used at any location within human tissue.

$$SAR = \frac{\sigma E^2}{2 \rho} \quad (2.3)$$

Where E represents the electric field amplitude in volts per meter (V/m),  $\rho$  indicates the density of the tissue in kilograms per cubic meter (kg/m<sup>3</sup>), and  $\sigma$  represents the conductivity of the tissue in siemens per meter (S/m)(El Dein & Amr, 2010).

#### **2.4.2.2. Bioheat equation**

The elevation in temperature inside an organism is dependent upon the spatial arrangement of the electromagnetic fields, the theory of thermodynamics, and the thermally constitutive properties of the biological system. Understanding heat transmission in biological organisms has numerous therapeutic applications that include either increasing or decreasing temperature, frequently necessitating meticulous monitoring of the distribution of thermal histories generated throughout a treatment program(R. Habash, 2007). From a macroscopic perspective, thermal effects resulting from the absorption of electromagnetic radiation in biological tissues can be represented by the bioheat equation (Vander Vorst et al., 2006).

Pennes published a seminal work on bioheat transfer modeling over fifty years ago(Pennes, 1948). He created a cylindrical replica of a human limb, initially simulating the human forearm, which he eventually modified to encompass any limb. Pennes' model encompassed all critical parameters for conduction, thermal storage,

and environmental interaction in tissue, with a particular focus on blood characteristics within the circulation system. Pennes' model suggests that the temperature differential between arterial blood entering the tissue and venous blood exiting the tissue equals the total heat transmission from blood to tissue. The product of the volumetric perfusion rates and the temperature differential between arterial blood and nearby tissues directly determines the amount of heat transfer between blood and tissue (R. Habash, 2007).

The thermal energy equilibrium for perfused tissues, as proposed by Pennes, is represented in the equation:

$$\rho c \frac{\partial T}{\partial t} = k \frac{\partial^2 T}{\partial x^2} + k \frac{\partial^2 T}{\partial y^2} + k \frac{\partial^2 T}{\partial z^2} + w_b c_b (T_a - T) + Q_m + Q_r(x, y, z, t) \quad (2.4)$$

Where  $T = T(x, y, z, t)$  represents the temperature elevation ( $^{\circ}\text{C}$ ),  $c$  signifies the specific heat of the tissue ( $\text{J/kg}^{\circ}\text{C}$ ),  $k$  indicates the thermal conductivity of the tissue ( $\text{W/m}^{\circ}\text{C}$ ),  $w_b$  refers to the blood volumetric perfusion rate ( $\text{kg/m}^3/\text{s}$ ),  $c_b$  is the specific heat of blood ( $\text{J/kg}^{\circ}\text{C}$ ), and  $T_a = T_a(x, y, z, t)$  denotes the average temperature elevation of the arteries ( $^{\circ}\text{C}$ ).  $Q_m$  is the metabolic heat source ( $\text{W/m}^3$ ), while  $Q_r$  denotes the additional heat sources activated by the irradiation ( $\text{W/m}^3$ ). The phrase  $w_b c_b (T_a - T)$ , representing perfusion heat loss ( $\text{W/m}^3$ ), is consistently regarded in tissues with a high level of perfusion. Generally,  $w_b$  is presumed to be uniform across the tissue. Nonetheless, its value may be augmented with heating time due to vasodilation and capillary recruitment (R. Habash, 2007).

### 2.4.3. Applications in cancer therapy

Hyperthermia often denotes either an excessively elevated body temperature or the therapeutic approach of inducing fever for disease therapy, either through heat application or through the injection of foreign substances. Hyperthermia is known for its longstanding history as a cancer treatment modality. Numerous Greek and Roman physicians believed that regulating body temperature might treat any disease (R. Habash, 2007).

Hyperthermia is defined as the elevation of the temperature of a specific body part or the whole body over the usual range for a specified duration. The temperature increase

is several degrees over the typical range (41–45°C). The impact of hyperthermia is contingent upon temperature and duration of exposure(Sardari & Verga, 2011).

The application of microwaves is among the most potential hyperthermia methods. Microwave therapy relies on the principle that tumor tissues exhibit greater sensitivity to heat compared to surrounding normal tissues, enabling the controlled application of microwave heat to tumor tissues(Guan, 2015). Tumor tissues exhibit reduced blood flow and altered extracellular pH compared to normal tissues. Microwave irradiation causes a tumor to stagnate blood flow in its localized region due to the resultant heat. Once the temperature in cancerous tissue reaches 42-45°C, blood flow ceases, tumor cells turn anoxic, and mitochondrial vacuolation occurs, leading to the stop of molecular respiration, apoptosis, heat fixing, and cell death (Guan, 2015).

#### **2.4.4. Categories and methods of hyperthermia**

Researchers identify various types of hyperthermia procedures based on the organ containing the malignant tissue, the degree of cancer progression, and the energy delivery mechanism to the patient's tissues. The categories proposed by multiple researchers include whole-body hyperthermia and local or regional hyperthermia, categorized by heating range(Pang, 2015).

##### **2.4.4.1. Whole-body hyperthermia**

It is a technique that elevates the human body's temperature to a therapeutic level using different techniques for a specified duration. Whole-body hyperthermia may be utilized independently for cancer treatment or in conjunction with chemotherapy and radiotherapy to enhance therapeutic efficacy, referred to as thermal radiotherapy and thermal chemotherapy (Pang, 2015).

No precise standard exists for the temperature range used for whole-body hyperthermia. Currently, the body temperature for cancer hyperthermia is primarily maintained between 39.5°C and 41°C, not exceeding 41.8°C, referred to as whole-body mid-to-high thermal hyperthermia. Another form of whole-body hyperthermia maintains the body temperature between 38°C and 40°C, referred to as whole-body mid-to-low thermal hyperthermia(Pang, 2015).

#### **2.4.4.2. Local or regional hyperthermia**

It is a form of hyperthermia characterized by localized heating, with no significant increase in overall body temperature. The heat sources are microwave, radio frequency, ultrasonic waves, and others(Pang, 2015).

There are four classes based on therapeutic temperature:

- A. Mid- to low-temperature hyperthermia: Elevation of local malignant tissue temperature to 39°C–42°C for 60–90 minutes. The objective of this form of hyperthermia is to enhance the body's blood circulation, alleviate blood stasis in cancerous tissue, increase blood vessel permeability, and elevate oxygen partial pressure (PO<sub>2</sub>). Moreover, it boosts metabolic activity in heated areas, improves drug absorption, and increases the body's susceptibility to radiation and chemotherapy(Pang, 2015).
- B. Conventional hyperthermia: This technique is employed for localized hyperthermia, wherein the cancerous tissue is elevated to temperatures between 42°C and 45°C for a duration of 45 to 90 minutes. It is referred to as mid-to-high temperature hyperthermia when applied for whole-body hyperthermia, indicating that the body is elevated to temperatures between 39.5°C and 41.8°C for a duration of 180 to 240 minutes. It may also enhance the susceptibility of cancerous tissues to radiotherapy and chemotherapy(Pang, 2015).
- C. High-temperature hyperthermia: the application of heat to cancerous tissues at temperatures between 45°C and 60°C for a duration of 30 to 60 minutes. This type exhibits a more pronounced lethal effect on both cancerous and normal cells within the temperature range, leading to the destruction and coagulation of cells and tissues(Pang, 2015).
- D. Thermoablation: This technique directly destroys cancerous tissues with the application of heat, with temperatures ranging from 60°C to 90°C, sustained for a duration of 5 to 10 minutes. This therapy exerts a more pronounced destructive effect on both cancerous and healthy cells, leading to extensive coagulation and potential carbonization or gasification of the cancerous tissues (Pang, 2015).

#### **2.4.5. External microwave hyperthermia**

Microwave hyperthermia (MWH) is a type of hyperthermia treatment that uses microwave energy to eradicate cancerous cells through heat. The radiation radiated by the microwave antenna generates heat in the adjacent malignant cells without harming the surrounding tissue. External microwave hyperthermia is a treatment method that uses microwave energy to heat cancerous tissue from outside the body. It works by placing a microwave device on or near the skin, which emits radiation that penetrates the skin to heat the targeted tissue. The selection of microwave power level and heating period is based on the tumor's shape and size. A thermal lesion of anticipated volume is generated by the application of microwave heat to encompass the entire tumor. This raises the temperature of the tumor, which can either damage or destroy cancer cells. The purpose is to make the tumor more sensitive to other treatments like radiation or chemotherapy or to directly kill cancer cells by creating thermal stress. Before the completion of the clinical process, imaging devices may be employed to ascertain the dimensions and morphology of the lesion, with the ultimate objective of hyperthermia technology being the destruction of the breast tumor while efficiently conserving healthy tissue (Suleman & Riaz, 2020). Unlike interstitial microwave hyperthermia, which involves inserting microwave probes directly into the tumor, external microwave hyperthermia does not require any skin penetration, making it a more convenient option for treating certain types of cancer.

### 3. UWB MICROSTRIP PATCH ANTENNA DESIGN

#### 3.1. Ultra-Wideband Technology

Ultra-wideband technologies have been widely used in radar, military, and wireless communications for a long time. Unlike other systems, UWB radars use electromagnetic pulses instead of short-duration waves, resulting in a broad spectrum (O'Hara et al., 2002). The Federal Communications Commission (FCC) has defined an ultra-wideband transmitting antenna as “an intentional radiator that, at any moment, either has a fractional bandwidth of 0.20 or greater or a UWB bandwidth of at least 500 MHz, regardless of its fractional bandwidth” (O'Hara et al., 2002). According to this definition, the UWB bandwidth ( $bw$ ) can be calculated using equation (3.1).

$$bw = 2 \frac{f_H - f_L}{f_H + f_L} \geq 0.2 \quad (3.1)$$

Where  $f_H$  and  $f_L$  represent the highest and the lowest frequencies in the band, respectively.

In general, before 2001, the use of UWB was mainly limited to military areas. But since 2002, the FCC has allowed commercial use of these bands. The FCC has set the permissible UWB frequency in America in a range from 3.1 GHz to 10.6 GHz, while in Europe, the permissible frequencies include two parts: from 3.4 GHz to 4.8 GHz and from 6 GHz to 8.5 GHz. Typically, the UWB frequency range contains low and high frequencies. Low frequencies provide high penetration ability to detect relatively deeply buried tumors, while high frequencies lack the ability to penetrate, but provide high accuracy that enables them to detect relatively small tumors. Therefore, this feature is suitable for radar-based breast cancer detection. Radar-based microwave imaging aims to ascertain tumor location by generating images from back-scattered signals emitted by the tumor. Radar-based imaging prototype systems are categorized as multi-static and mono-static radar systems. The multi-static radar system employs an antenna array and a switch network controller. The antenna array often comprises many antennas to gather an extensive array of transmission coefficients, facilitating

the acquisition of high-resolution pictures. Conversely, the mono-static radar system (Sill & Fear, 2005) employs a singular antenna to examine the breast.

### **3.2. Antenna Theory**

An antenna is a metallic apparatus (such as a rod or wire) utilized for the transmission or reception of radio waves (Balanis, 2015). Antennas operate across a broad spectrum of frequencies, ranging from low to high. Microwaves represent a transitional spectrum between conventional radio waves and optical waves, hence microwave technology employs methodologies from both domains (Carr, 2001).

An antenna serves as a transducer amongst electrical pulses or guided waves and a traveling electromagnetic field in free space. Furthermore, it serves as an impedance-matching device that matches the transmission line impedance and the impedance of free space. Antennas are similarly effective in signal reception and transmission (Carr, 2001).

### **3.3. Microstrip Patch Antenna**

The origin of the microstrip antenna concept can be traced back to 1952 when researchers such as Deschamps theorized its potential as a microwave antenna (Deschamps, 1953). However, its practical implementation did not emerge until approximately two decades later. Since the 1970s, micro-strip antennas have been utilized, particularly in space technologies (Munson, 1974). Howell and Munson are widely recognized as the pioneering figures in the development and engineering of microstrip antenna technology. In recent years, the micro-strip patch antenna has become a subject of rigorous research due to its numerous advantages and promising prospects.

The microwave imaging system comprises antennas for signal transmission and reception; therefore, antenna selection is crucial. Various antenna types exist, including dipole and horn antennas; however, the microstrip patch antenna offers advantages due to its lightweight design and compact structure, featuring an electrically conducting plane on the top of a substrate with a plane of ground on the opposite side (Balanis, 2011). The microstrip patch antenna is a crucial component of the microwave imaging system, utilized for the transmission and reception of

microwaves. Microstrip patch antennas might be categorized as flexible and unflexible types according to the substrate employed. Currently, textile substrates are increasingly preferred for wearable biomedical antennas because of their user comfort and flexibility.

### 3.3.1. Structure of microstrip patch antenna

A microstrip patch antenna comprises a metallic patch, which can take various shapes, mounted on a dielectric substrate with a grounded base on the opposite side, as seen in Figure 3.2 (Balanis, 2005). The substrate's thickness typically ranges between  $0.03\lambda$  and  $0.05\lambda$ . The thickness of the substrate typically ranges between  $0.03\lambda$  and  $0.05\lambda$ . The dimensions of the metallic patch generally fall within the range of  $\lambda/3$  to  $\lambda/2$ .

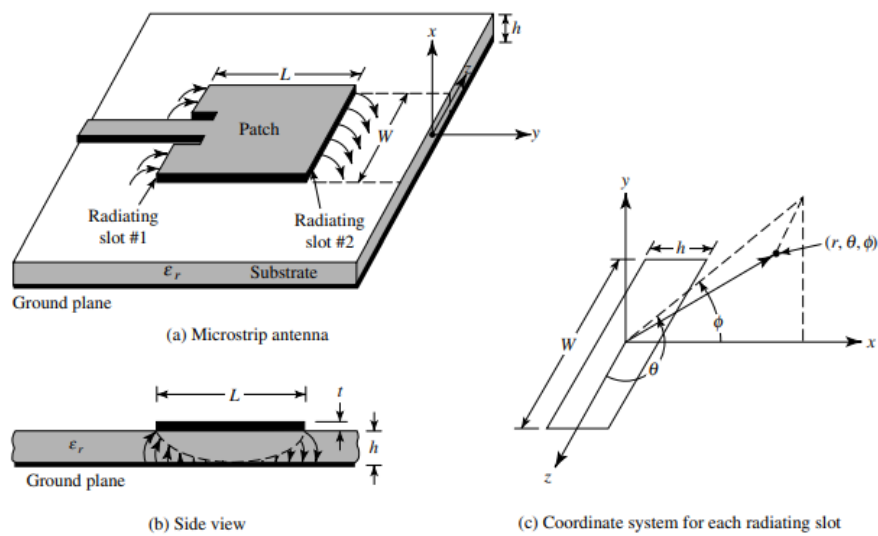


**Figure 3.1.** Microstrip Patch Antenna and its coordinate system

As illustrated in Figure 3.2, different types of microstrip patch antennas are designed for various applications. When a current is introduced via a feed line to the conductive strip of the antenna, it generates electromagnetic waves. These waves emanating from the patch create a distinct radiation pattern as they propagate from the edges of the patch.

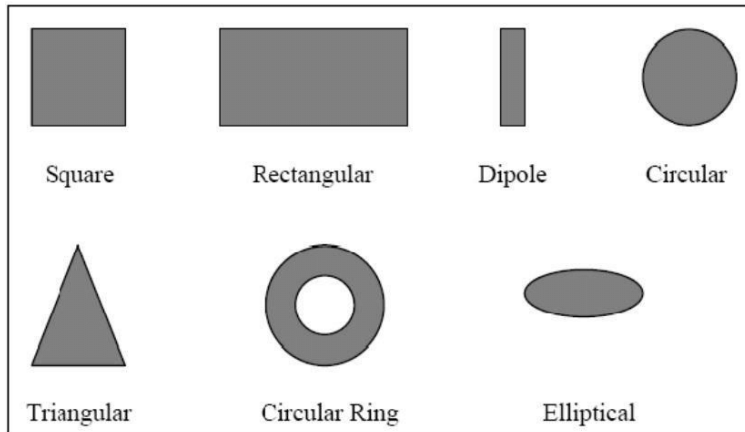


**Figure 3.2.**Types of Microstrip Patch Antenna

The characteristics of the radiated waves are influenced by the substrate thickness. Due to the relatively small thickness of the substrate, some of the waves are reflected at the edges. Additionally, the continuous structure of the conductive strip inhibits radiation emission. Radiation resumes at points of discontinuity, where transmission begins anew from the opposite side of the patch.

### 3.3.1.1. Dielectric substrate

The dielectric substrate serves as the structural foundation of the microstrip circuit, offering substantial support to the conductor sheets and patches that constitute the transmission lines, and resonators. It guarantees precise positioning and secure attachment of the embedded components, analogous to the role played by substrates in printed electronic circuits operating at low frequencies. Furthermore, the substrate performs a critical electrical role by focusing electromagnetic fields and mitigating undesirable radiation within the circuit. As an essential element of connecting transmission lines, the substrate's permittivity and thickness directly influence the antenna's properties. Substrate materials must have minimal insertion loss, with a loss tangent below 0.005, especially for extensive array applications. These materials are generally classified into three categories based on their relative dielectric constant ( $\epsilon_r$ ):

- Low  $\epsilon_r$  (1.0–2.0): Examples include air and polystyrene foam.
- Moderate  $\epsilon_r$  (2.0–4.0): Primarily composed of fiberglass-reinforced Teflon.
- High  $\epsilon_r$  (4.0–10.0): Made from materials such as ceramic, quartz, or alumina.

### 3.3.1.2. Conductor layers

Of the three basic layers of a microstrip patch antenna, the radiated patch and ground plane are the main conductor layers that govern the antenna's efficiency, gain, and bandwidth. Understanding the conductor layers in microstrip patch antennas is essential to improving their design and performance. The radiant patch usually consists of a thin metal layer, such as copper or aluminum, deposited on an insulating substrate. Its shape can vary according to design requirements. The dimensions of the patch are crucial because they determine the antenna's resonant frequency. Basic considerations for any patch include:

- Shape and size: This affects the antenna's radiation pattern and impedance matching.
- Surface Roughness: A smoother surface improves performance by reducing resistance losses.
- Material selection: It is preferable to use highly conductive metals such as copper to reduce ohmic losses.

The radiating patch not only emits signals but also determines the polarization of the radiated waves, which can be linear or circular, depending on its design and feeding method.

The ground plane is another important conductive layer in microstrip patch antennas. They are usually continuous metal sheets, similar in physical composition to the radiating patch. Its primary role is to provide a stable reference point for electromagnetic fields and prevent signal interference from below the substrate. Ground layer characteristics include:

- Material: Conductivity is crucial to ensure efficient signal reflection and minimize power dissipation.
- Size: Although the ground plane is often larger than the patch, its dimensions can be optimized to improve performance, especially in compact designs.
- Positioning: Uniform separation between the ground plane and the radiating patch is maintained by the insulating substrate.

An inappropriate ground plane can lead to undesirable effects such as increased back radiation and decreased gain, affecting antenna performance. Recent advances in

materials science and manufacturing techniques have improved the performance of conductive layers in microstrip patch antennas. Such as:

- **Hybrid Materials:** Combining unconventional materials in conductor layers to achieve specific performance goals, such as high bandwidth or reduced losses.
- **Conductive inks:** Used in flexible electronics, they enable antennas to be printed on non-traditional substrates such as textiles and polymers.
- **Graphene and nanomaterials:** These materials have emerged as alternatives to traditional metals, providing superior conductivity and flexibility.

Made of highly conductive materials, the radiant patch and ground plane must be precisely designed to ensure optimal performance. Advances in materials and manufacturing methods continue to push the limits of what these antennas can achieve, making them indispensable in modern communications systems. By understanding the principles and innovations in conductor layer design, engineers can develop more efficient and versatile antennas for a rapidly evolving technology landscape.

### **3.3.2. Feeding techniques of microstrip antenna**

There are several techniques for energizing patch antennas. The methods of feeding are categorized into two types:

- In the contacting category, the feeding technique is facilitated through a connecting component, such as a microstrip line, into the radiating patch.
- Transmission of power across the microstrip line and the emitting device occurs by electromagnetic field coupling in the absence of a contact category.

The predominant feeding mechanisms utilized in microstrip patch antennas include the coaxial probe, microstrip line feeding, and aperture or proximity coupling approaches.

#### **3.3.2.1. Microstrip line feeding techniques**

In this feeding technique (Figure. 3.3), the circumference of the microstrip patch is linked to a conductive sheet. This feeding approach allows for the conducting line to be inscribed on the same substrate as the patch antenna, resulting in a planar configuration. The width of the feed line is narrower than that of the patch part. This feeding method is widely employed because of its simplicity in design and analysis, as well as its ease of fabrication. It is extensively used in both single-patch antennas and array antennas.

### 3.3.2.2. Coaxial probe feeding techniques

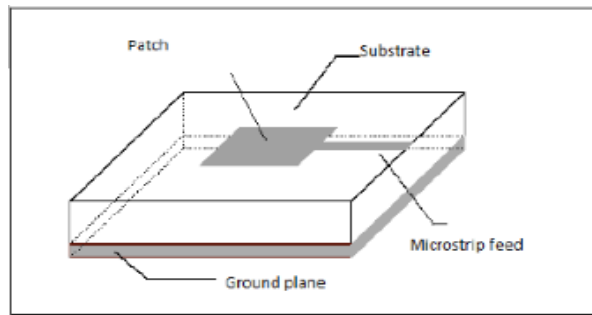


**Figure 3.3.** Microstrip line feeding techniques

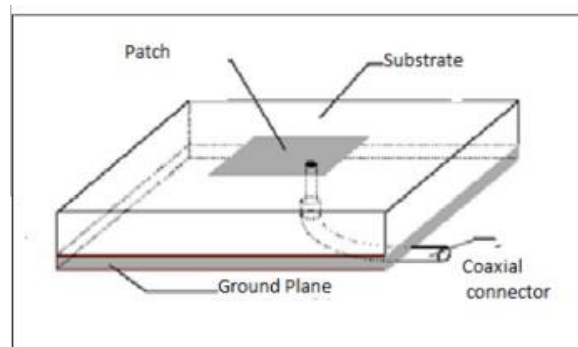


**Figure 3.4.** Coaxial probe feeding techniques

The external conductor of a coaxial probe is affixed to the ground plane, whereas the internal conductor penetrates through the dielectric and is soldered to the radiating part of the antenna. Nonetheless, the drawback of this method is the challenge of modeling and producing an extremely limited bandwidth. Figure 3.4 illustrates this specific approach.

### 3.3.2.3. Proximity coupled feeding techniques

This feeding method (Figure 3.5) employed dual substrates, with the feed line located between them, and the patch element positioned on the top substrate.

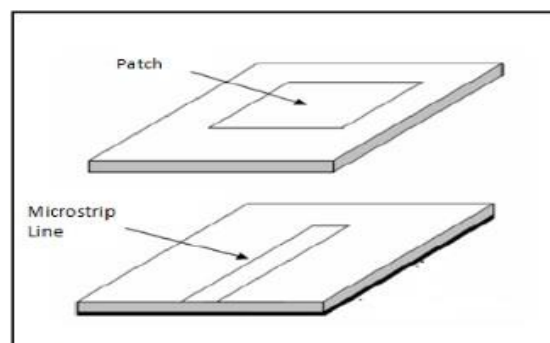


**Figure 3.5.** Proximity coupled feeding techniques

#### 3.3.2.4. Aperture coupled feed

In this feeding approach (Figure 3.5), the feed line is isolated from the radiating patch by the ground plane. The feed line and the patch are interconnected via a cut or slot in the ground layer. The coupling modifications will be contingent upon the slot's width and length to enhance the simulation outcomes for bandwidths and return losses. The slot is often positioned centrally below the radiating element.

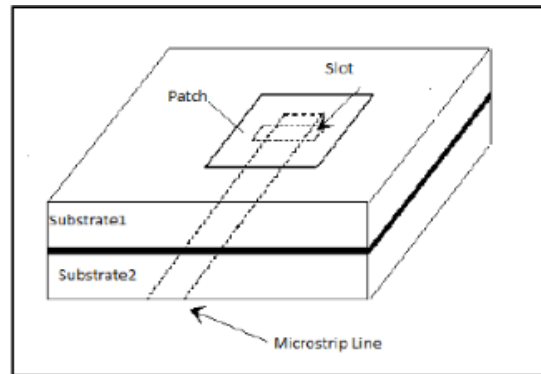


**Figure 3.6.** Aperture coupled feed

#### 3.3.3. Microstrip antenna analysis methods

Numerous analytical methods exist for patch antennas. The predominant models are the transmission line, cavity, and full-wave models. The transmission-line model is considered the simplest, providing valuable physical understanding; yet, it is less precise and more challenging to represent coupling. The cavity model in comparison to the transmission line is more precise while simultaneously more intricate. Nevertheless, it provides valuable physical knowledge and presents considerable challenges in modeling coupling. When used correctly, full-wave models exhibit high accuracy, adaptability, and capability to address individual components, arrays, stacked elements, irregularly shaped elements, and coupling. Nevertheless, they represent the most intricate models and typically provide diminished physical information. The simplest method for analyzing microstrip antennas is the transmission line method, which views the patch as either a transmission line or a segment of it.

##### 3.3.3.1. Transmission line analysis method

The transmission line method is one of the most direct ways to analyze microstrip antennas. This model envisions the microstrip antenna as two radiating

slots separated by a low-impedance transmission line with characteristic impedance  $Z_c$  and length  $L$ . The patch's limited dimensions in length and width ( $W$ ) lead to the observation of fringing fields at its edges. The patch size and substrate height determine fringing. The ratio of patch length to substrate height ( $L/h$ ) and the substrate dielectric constant influence the fringing effect of the E-plane. Although fringing is less impactful in microstrip antennas with a patch length to substrate height ratio far below one, its impact on the antenna's resonance frequency is permanent. Likewise, fringing alters the effective width of a microstrip line, causing it to seem electrically larger than its actual dimensions. The effective dielectric constant ( $\epsilon_{reff}$ ) accounts for the influences of fringing and wave propagation, as electromagnetic waves traverse both the substrate and the air.

For a transmission line having air above the substrate, the  $\epsilon_{reff}$  lies within the range of  $1 < \epsilon_{reff} < \epsilon_r$ , where  $\epsilon_r$  represents the substrate dielectric constant. In the applications where the substrate's dielectric constant is significantly higher than unity ( $\epsilon_r \gg 1$ ), the  $\epsilon_{reff}$  tends to approach the actual value of  $\epsilon_r$ . Notably,  $\epsilon_{reff}$  is frequency dependent. At higher operating frequencies, a greater proportion of the electric field lines become confined to the substrate, causing the effective dielectric constant to be more closely aligned with  $\epsilon_r$ . Conversely, at lower frequencies, the effective dielectric constant assumes its static value, which can be calculated using Equation 3.1 (Balanis, 2012).

$$\frac{W}{h} > 1 \tag{3.1}$$

$$\epsilon_{reff} = \frac{\epsilon_r + 1}{2} + \frac{\epsilon_r - 1}{2} \left[ 1 + 12 \frac{h}{W} \right]^{-1/2}$$

Due to the fringing effects, the microstrip antenna's patch appears electrically larger compared to its actual size. In the XY-plane, this phenomenon is illustrated in Figure 3.7, in which the patch's effective length is increased on the ends by an amount of  $\Delta L$ . This extension depends on the effective dielectric constant ( $\epsilon_{reff}$ ) and the ratio of the patch width to the substrate height ( $W/h$ ). An approximate practical expression for the normalized length extension is provided in equation 3.2 (Balanis, 2012), offering a convenient means of accounting for this effect in design calculations.

$$\frac{\Delta L}{h} = 0.412 \frac{(\epsilon_{reff} + 0.3) \left(\frac{W}{h} + 0.264\right)}{(\epsilon_{reff} - 0.3) \left(\frac{W}{h} + 0.8\right)} \quad (3.2)$$

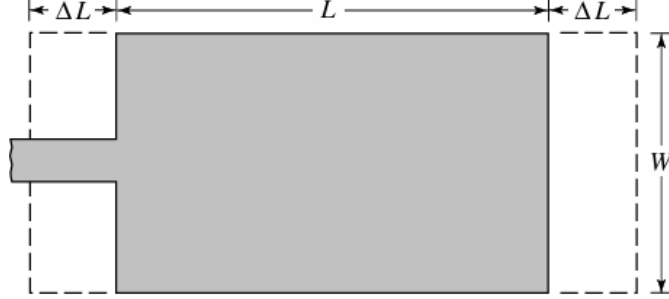


**Figure 3.7.** Patch antenna extended length due to fringing effects

As a result of the extension on  $\Delta L$  on both sides, the patch effective length ( $L_{eff}$ ) increases. The updated effective patch length is now be expressed as:

$$L_{eff} = L + 2\Delta L \quad (3.3)$$

The resonance frequency ( $f_r$ ) of a patch antenna depends on its length and is expressed as:

$$(f_r)_{010} = \frac{1}{2L\sqrt{\epsilon_r}\sqrt{\mu_0\epsilon_0}} = \frac{c_0}{2L\sqrt{\epsilon_r}} \quad (3.4)$$

Here,  $c_0$  denotes the speed of light in free space. As equation (3.4) does not consider the impact of fringing effects, it needs to be revised to incorporate edge effects. The adjusted resonance frequency ( $f_{rc}$ ) is determined through the following equation:

$$(f_{rc})_{010} = \frac{1}{2L_{reff}\sqrt{\epsilon_{reff}}\sqrt{\mu_0\epsilon_0}} = \frac{1}{2(L + 2\Delta L)\sqrt{\epsilon_{reff}}\sqrt{\mu_0\epsilon_0}} \quad (3.5a)$$

$$= q \frac{1}{2L\sqrt{\epsilon_r}\sqrt{\mu_0\epsilon_0}} = q \frac{c_0}{2L\sqrt{\epsilon_r}} \quad (3.5b)$$

Where

$$q = \frac{(f_{rc})_{010}}{(f_r)_{010}} \quad (3.6)$$

The q-factor, also known as the fringe factor or length reduction factor, accounts for the effects of fringing in microstrip antennas. An increase in substrate height enhances fringing, resulting in greater separation among the radiating ends and a reduction in the resonance frequency.

To ensure efficient radiation, a practical width that achieves favorable radiation efficiency is recommended, and is ascertained using equation (3.7)

$$W = \frac{1}{2f_r \sqrt{\mu_0 \epsilon_0}} \sqrt{\frac{2}{\epsilon_r + 1}} = \frac{\lambda c_0}{2f_r} \sqrt{\frac{2}{\epsilon_r + 1}} \quad (3.7)$$

The physical length of the patch is calculated by rearranging and solving equation (3.5) for L.

$$L = \frac{1}{2f_r \sqrt{\epsilon_{reff}} \sqrt{\mu_0 \epsilon_0}} - 2\Delta L \quad (3.8)$$

Every radiated slot is modeled using a parallel equivalent admittance Y, comprising a conductance G and a susceptance B. This representation is illustrated in figure 3.8.

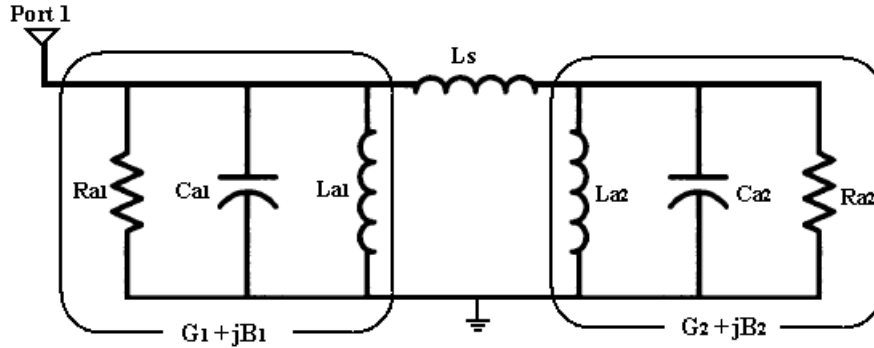


**Figure 3.8.** Patch antenna's equivalent transmission-line circuit

The equivalent admittance for slot 1 ( $Y_1$ ), as described in (Balanis, 2005), is given by:

$$Y_1 = G_1 + jB_1 \quad (3.9)$$

wherein a given slot of limited width W

$$G_1 = \frac{W}{120 \lambda_0} \left[ 1 - \frac{1}{24} (k_0 h)^2 \right] \quad \frac{h}{\lambda_0} < \frac{1}{10} \quad (3.10)$$

$$B_1 = \frac{W}{120 \lambda_0} [1 - 0.636 \ln(k_0 h)] \quad \frac{h}{\lambda_0} < \frac{1}{10} \quad (3.11)$$

As slot 2 is parallel to slot 1, its corresponding admittance ( $Y_2$ ) is the same and can be expressed as:

$$Y_2 = Y_1 \quad G_2 = G_1 \quad B_2 = B_1 \quad (3.12)$$

Conductance is generally described as the real part of the admittance, representing the capacity of the antenna to dissipate power. It is given by:

$$Y_1 = \frac{2P_{rad}}{|V_0|^2} \quad (3.13)$$

The power radiated  $P_{rad}$  is described as the sum of the power emitted by the antenna, represented as:

$$P_{rad} = \frac{|V_0|^2}{2\pi\eta_0} \int_0^\pi \left[ \frac{\sin \frac{k_0 W}{2} \cos \theta}{\cos \theta} \right]^2 \sin^3 \theta d\theta \quad (3.14)$$

Therefore, the conductance  $G_1$  in equation (3.10) can be written as:

$$G_1 = \frac{I_1}{120\pi^2} \quad (3.15)$$

Where

$$I_1 = \int_0^\pi \left[ \frac{\sin \frac{k_0 W}{2} \cos \theta}{\cos \theta} \right]^2 \sin^3 \theta d\theta \quad (3.16a)$$

$$= -2 + \cos(X) + X S_i(X) + \frac{\sin X}{X} \quad (3.16b)$$

$$X = k_0 W \quad (3.17)$$

The asymptotic values of equations (3.15) and (3.16a) are:

$$G_1 = \begin{cases} \frac{1}{90} \left(\frac{W}{k_0}\right)^2 & W \ll \lambda_0 \\ \frac{1}{120} \left(\frac{W}{k_0}\right) & W \gg \lambda_0 \end{cases} \quad (3.18)$$

The overall input admittance is ascertained by relocating the admittance of slot 2 from its terminals for output to the terminals for input by applying the principle of the transmission line admittance transformation algorithm. If possible, the two slots need to be distanced by  $\lambda/2$ . Nonetheless, due to fringing effects, the electrical length exceeds the physical length slightly. Consequently, the actual distance between the two slots is marginally less than  $\lambda/2$ . If the length reductions are suitably chosen, generally within the interval  $0.48 \lambda < L < 0.49 \lambda$ , the modified admittance of slot 2 is represented as:

$$\tilde{Y}_2 = \tilde{G}_2 + j\tilde{B}_2 = G_1 - jB_1 \quad (3.19)$$

Consequently, the overall resonant input admittance ( $Y_{in}$ ) is entirely real and may be expressed as:

$$Y_{in} = Y_1 + \tilde{Y}_2 = 2G_1 \quad (3.20)$$

If the overall input admittance is real, the resonance input impedance  $Z_{in}$  must likewise be real.

$$Z_{in} = \frac{1}{Y_{in}} = R_{in} = \frac{1}{2G_1} \quad (3.21)$$

The resonant input resistance, as described by equation (3.21), fails to include the mutual coupling effects. To incorporate these mutual effects, equation (3.21) can be adjusted as outlined in (Balanis, 2005):

$$R_{in} = \frac{1}{2(G_1 \pm G_{12})} \quad (3.22)$$

The positive (+) symbol denotes modes with an odd (antisymmetric) resonant voltage distribution under the patch and among the slots, whereas the negative (−) sign

indicates modes with an even (symmetric) resonant voltage distribution. The mutual conductance, articulated in relation to far-field radiation, is defined as:

$$G_{12} = \frac{1}{|V_0|^2} \text{Re} \iint_s E_1 \times H_1^* \cdot ds \quad (3.23)$$

Let  $E_1$  denote the electric field emitted by slot 1,  $H_2$  the magnetic field emitted by slot 2, and  $V_0$  represent the voltage over the slot. The integration is carried out across a spherical surface of a suitable radius. It has been demonstrated that  $G_{12}$  could be determined utilizing the methods described in (Derneryd, 1978; Lo & Lee, 2013).

$$G_{12} = \frac{1}{120\pi^2} \int_0^\pi \left[ \frac{\sin\left(\frac{k_0 W}{2} \cos \theta\right)}{\cos \theta} \right]^2 J_0(k_0 L \sin \theta) \sin^3 \theta d\theta \quad (3.24)$$

$J_0$  denotes the Bessel function of the first type of zero level. For conventional patch antennas, the mutual coupling derived from (3.24) is negligible compared to  $G_1$  as shown in (3.10) or (3.15). As shown in (3.10) and (3.22), the input resistance shows minimal dependence on the substrate height. For sufficiently small values of  $h$ , where  $k_0 h$  is less than 1, the input resistance is independent of  $h$ . It is clear from (3.10) and (3.22) that the  $R_{in}$  may be reduced by increasing the patch width  $W$ . This is permissible if the ratio  $W/L$  does not exceed 2, since the overall efficiency of a single patch decreases when  $W/L$  exceeds this limit. The input resistance can be altered by employing an internal feed, displaced from slot 1 by  $y_0$ , as seen in figure 3.9 (Balanis, 2005).

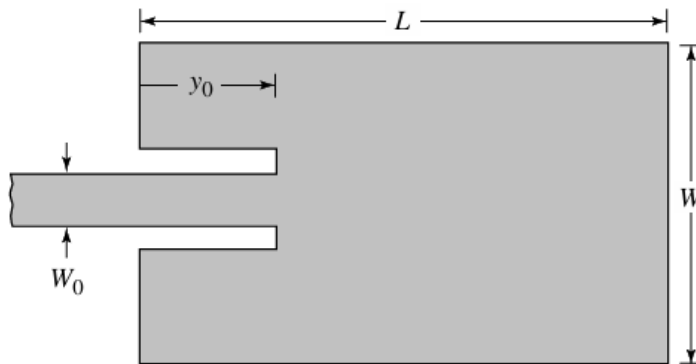


**Figure 3.9.** Inset internal feed

This method has been successfully employed for matching the antenna with a microstrip-line feed with a characteristic impedance specified by (Balanis, 2012).

$$Z_c = \begin{cases} \frac{60}{\sqrt{\epsilon_{reff}}} \ln \left[ \frac{8h}{W_0} + \frac{W_0}{4h} \right] & \frac{W_0}{h} \leq 1 \\ \frac{120\pi}{\sqrt{\epsilon_{reff}} \left[ \frac{W_0}{4h} + 0.667 \left( \frac{W_0}{h} + 1.444 \right) \right]} & \frac{W_0}{h} > 1 \end{cases} \quad (3.25)$$

$W_0$  represents the microstrip line width, as illustrated in figure 3.8. The input resistance for the inset feed is approximately determined via modal expansion analysis as referenced in (Balanis, 2012; Carver & Mink, 1981; Derneryd, 1978).

$$R_{in}(y = y_0) = \frac{1}{2(G_1 \pm G_{12})} \left[ \cos^2 \left( \frac{\pi}{L} y_0 \right) + \frac{G_1^2 + B_1^2}{Y_c^2} \sin^2 \left( \frac{\pi}{L} y_0 \right) - \frac{B_1}{Y_c} \sin \left( \frac{2\pi}{L} y_0 \right) \right] \quad (3.26)$$

Where  $Y_c$  equals 1 divided by  $Z_c$ . Given that for the majority of conventional microstrips  $G_1/Y_c \ll 1$  and  $B_1/Y_c \ll 1$ , equation (3.26) simplifies to:

$$\begin{aligned} R_{in}(y = y_0) &= \frac{1}{2(G_1 \pm G_{12})} \cos^2 \left( \frac{\pi}{L} y_0 \right) \\ &= R_{in}(y = 0) \cos^2 \left( \frac{\pi}{L} y_0 \right) \end{aligned} \quad (3.27)$$

The inset feed creates a physical notch, hence introducing junction capacitance. The physical notch and its associated junction capacitance marginally affect the resonance frequency, which generally may fluctuate by approximately 1% (Rahman et al., 2020). The peak value is found at the boundary of the slot ( $y_0=0$ ), as the voltage reaches its highest point and the current is at its lowest. The lowest value happens at the center of the patch ( $y_0=L/2$ ) when the voltage gets zero and the current is at the highest level. When the inset feed source travels from the edge into the center of a patch, the resonant input impedance drops repeatedly reaching zero in the center. As the dimension of the inset feed point gets closer to the middle of the patch ( $y_0=L/2$ ), the  $\cos(2\pi y_0/L)$  curve exhibits rapid variation; thus, the input resistance similarly fluctuates dramatically with the location of the feed point (Singh & Bhargav, 2015).

### **3.3.3.2. Cavity model**

The cavity model is a widely used method for analyzing microchip antennas, especially rectangular patch antennas, by treating the patch as a cavity resonator. It assumes that the patch is a perfect electrical conductor (PEC), meaning that the transverse electric fields on its surface are zero and that the side walls are perfect magnetic conductors (PMC), where the transverse magnetic fields vanish. It considers the substrate as lossless and analyzes TM<sub>10</sub> as the only dominant mode of the cavity. The patch dimensions and substrate properties determine the resonant frequency. To account for fringing effects at the patch edges, the model uses effective dimensions slightly larger than the physical dimensions. The field distributions within the cavity provide insight into the antenna impedance, bandwidth, and radiation characteristics, with equivalent radiation apertures at the patch edges defining the radiation pattern. The cavity model is particularly useful for estimating the performance of patch antennas during the initial design phase, providing a satisfactory balance between simplicity and accuracy for thin substrates. It effectively predicts resonant frequencies, input impedance, and far-field radiation patterns. However, its assumptions limit its accuracy for antennas with thick substrates, complex geometries, or where surface wave effects are large. Despite these limitations, the cavity model remains a practical tool for understanding the fundamental behavior of thin-slice antennas and serves as the basis for more advanced analyses using full-wave methods.

### **3.3.4. Fundamental parameters of antennas**

Defining various parameters is essential for characterizing antenna performance. Not all parameters are required for a comprehensive description of antenna effectiveness (Balanis, 2015).

#### **3.3.4.1. Radiation pattern**

A radiation pattern delineates the distribution of power emitted by an antenna relative to the direction. The power change as a result of the incident angle is noticed in the antenna's far field. The radiative properties encompass energy, flux density, radiation intensity, electric field amplitude, directivity, and polarization. The primary focus of a radiation pattern is the two- or three-dimensional allocation of transmitted energy with respect to the observer's location on a surface or trajectory of constant radius. The amplitude field pattern represents the electric or magnetic field at a fixed radius, while

the amplitude power pattern graphically displays the spatial distribution of power density along a fixed radius bath (Balanis, 2015).

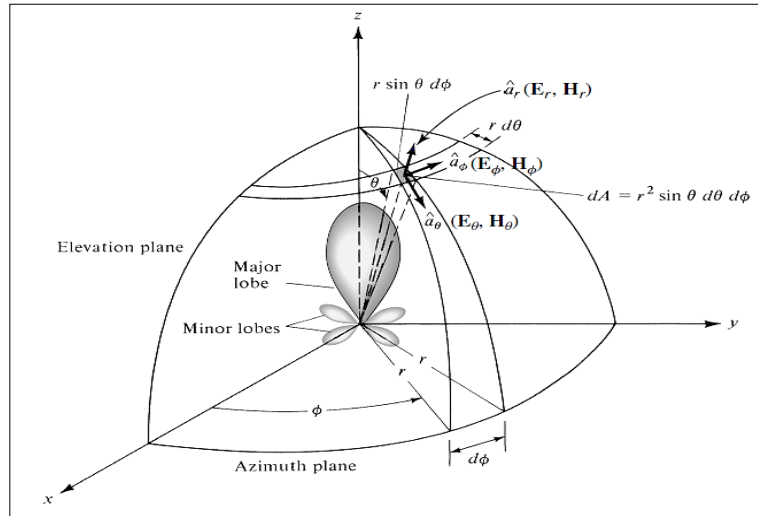


**Figure 3.10.** Antenna Coordinate system

### 3.3.4.2. Radiation power density

The measure of power related to an EM wave is the instantaneous Poynting vector, expressed as:

$$\mathcal{W} = \mathcal{E} \times \mathcal{H} \quad (3.28)$$

Where  $\mathcal{W}$  is the Poynting vector ( $\text{W/m}^2$ ),  $\mathcal{E}$  represents the electric field intensity ( $\text{V/m}$ ), and  $\mathcal{H}$  represents the magnetic-field intensity ( $\text{A/m}$ )

### 3.3.4.3. Radiation intensity

It is a crucial statistic that quantifies the power emitted by an antenna in a particular direction. The radiation intensity ( $U$ ) represents a far-field characteristic that is easily derived through the multiplication of the electromagnetic radiation density ( $P$ ) with the square of the radius ( $r$ ) (Balanis, 2015).

$$U = r^2 \cdot P(r, \theta, \phi) \quad (3.29)$$

Where  $P(r, \theta, \phi)$  is the radiated power density at a distance  $r$ .

**3.3.4.4. Beam width**

Beam width is a characteristic related to an antenna's radiation pattern. It can be described as the angular distance separating two similar spots located on opposing sides of the pattern peak. An antenna pattern comprises several beam widths. The Half-Power Beam Width (HPBW) is a commonly utilized measurement, defined by IEEE as the angle within a plane that encompasses the beam's maximum direction, delineating the two directions where the radiation intensity is reduced to half of its peak value. The angular gap between the initial nulls of the pattern is known as the First-Null Beam Width (FNBW), as shown in figure 3.10. Other beam widths refer to those where the pattern is  $-10$  dB from the peak or any alternative value. In practice, the word beam width, without further specification, typically denotes HPBW (Balanis, 2015).

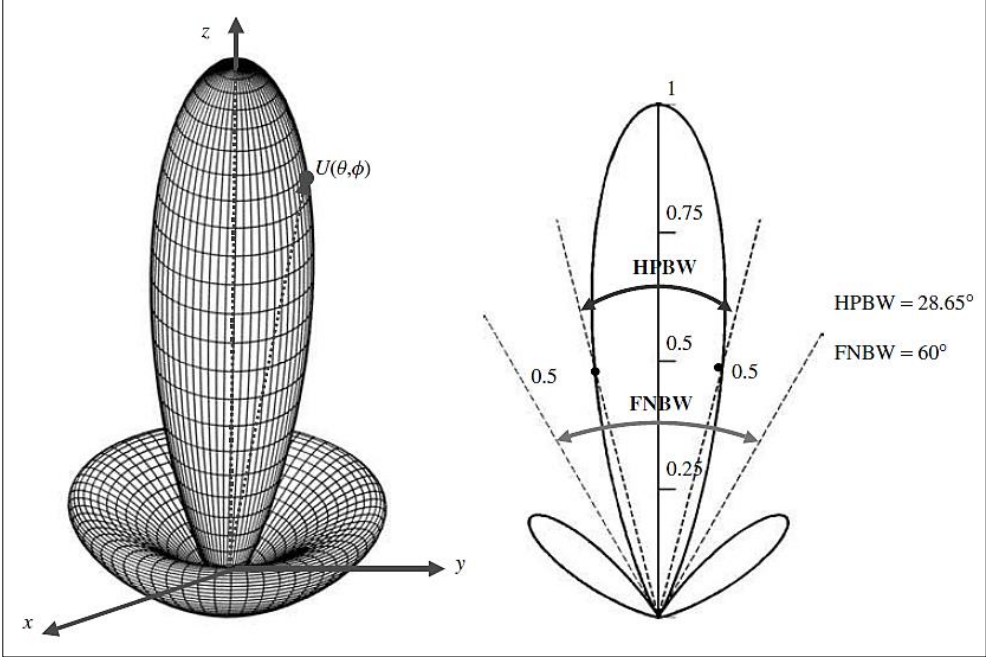


**Figure 3.11.** Three and two-dimensional power patterns.

**3.3.4.5. Directivity**

The directivity of an antenna ( $D$ ) is the proportion of the amount of radiation in a specific direction to the average radiation intensity across all directions. The mean radiation intensity equals the sum of the power emitted by the antenna divided by  $4\pi$ . The direction of the highest radiation intensity is inferred when the direction is unspecified (Balanis, 2015). Directivity can be given using equation (3.28).

$$D = \frac{4\pi U}{P_{rad}} \quad (3.30)$$

#### **3.3.4.6. Gain**

The gain of an antenna ( $G$  in dB) is intricately linked to its directivity; it quantifies both the efficiency and the directional properties of the antenna. The gain of an antenna in a specific direction is the ratio of its intensity in that direction to the amount of radiation that would arise from isotropic radiation of the power received by the antenna. The emitted radiation intensity for isotropically radiated power equals the power received by the antenna scaled by  $4\pi$  (Balanis, 2015). In general, the antenna gain can be given as:

$$G = \eta D \quad (3.31)$$

Where  $\eta$  represents the antenna efficiency

#### **3.3.4.7. Bandwidth**

Bandwidth (bw) refers to the range of frequencies throughout which the antenna's performance, concerning a particular attribute, meets defined criteria. It may additionally be described as the spectrum of frequencies, on either side of a central frequency, within which the antenna characteristics (including input impedance, pattern, beam width, polarization, side lobe level, gain, beam direction, and radiation efficiency) remain in a suitable level of those at the central frequency (Balanis, 2015).

#### **3.3.4.8. Polarization**

The polarization of an antenna in a specific direction can be described as the polarization of the wave emitted by the antenna. In the absence of a specified direction, polarization is assumed to align with the direction of the greatest gain. The polarization of the emitted energy fluctuates with the direction from the antenna's center, resulting in varying polarizations throughout different sections of the pattern (Balanis, 2015).

#### **3.3.4.9. Input impedance**

Input impedance can be described as the impedance exhibited by an antenna at its connection points. It is also characterized by the ratio of voltage to current at a pair of

endpoints or the proportion of the relevant components of the electric and magnetic fields at a certain location (Balanis, 2011).

#### **3.3.4.10. Return loss**

The return loss (RL) at the coaxial cable's input linked to the antenna is the disparity between forward and reflected power, measured in decibels (dB). The return loss is calculated as the ratio of the reflected power, PR, to the transmitted power, PT. The return loss must be minimized to optimize power transfer. This indicates that the ratio PR/PT should be minimized, or in decibels, the return loss should be maximized as a negative value. A return loss of -30dB is superior to one of -20dB (Patel & Chaudhari, 2015). It can be calculated using equation (3.32).

$$RL = -20\log_{10}(|\Gamma|) \quad (3.31)$$

Where  $\Gamma$  represents the magnitude of the reflection coefficient.

#### **3.3.4.11. Radiation efficiency**

Antenna efficiency is the ratio of the power supplied to the antenna to the power emitted by the antenna. An antenna that radiates the majority of the power supplied to its input is classified as a high-efficiency antenna. An antenna with low efficiency predominantly dissipates power as losses or reflects it owing to impedance mismatch. Antenna efficiency is defined as the ratio of radiated power to input power (Balanis, 2015).

Antenna efficiency, as a ratio, is a value ranging from 0 to 1. Antenna efficiency is typically expressed as a percentage; for instance, an efficiency of 0.5 equates to 50%. Antenna efficiency is commonly expressed in decibels (dB); an efficiency of 0.1 corresponds to 10% or -10 dB, while an efficiency of 0.5 or 50% equates to -3 dB.

### **3.3.5. Microstrip patch antennas bandwidth enhancing**

Microstrip patch antennas are extensively utilized in various systems because of their advantages, including low profile, lightweight, and ease of manufacture. However, one major drawback of traditional patch antennas is their limited bandwidth. To address this limitation, various techniques have been developed to enhance bandwidth.

1. Structural modifications

Structural modifications include changing the geometry or configuration of the patch and substrate to improve bandwidth.

- Slotted patch design: Introducing slots or slits into the patch changes the current distribution, which can generate additional resonant modes and improve impedance matching over a wider frequency range.
- Using a stacked patch configuration: This technique involves placing additional parasitic patches on top or below the main radiating patch. Coupling between spots creates multiple echoes, which combine to form a wider frequency band.
- Defective Ground Structures (DGS): Etching specific patterns into the ground plane can enhance bandwidth by modifying the electromagnetic properties of the antenna, such as inductance and capacitance.
- Broadband Shapes: Using non-traditional patch shapes, such as E-shaped, U-shaped, or H-shaped patches, can support multiple resonant frequencies, resulting in enhanced bandwidth.

## 2. Material Enhancements

Material properties fundamentally affect the bandwidth and performance of small antennas.

- Electromagnetic bandgap (EBG) structures: Embedding EBG structures into the substrate can prevent surface waves and improve bandwidth by enhancing radiation efficiency.
- Low Dielectric Constant Substrates: Using substrates with a low dielectric constant reduces the  $q$  factor of the resonator, resulting in a wider bandwidth. Examples include air-filled substrates.
- Thicker substrates: Increasing substrate thickness reduces effective permittivity and increases fringing fields, which can result in enhanced bandwidth. However, this may also lead to problems such as surface wave excitation and impedance mismatch.

## 3. Feeding Techniques

The choice of feeding method plays a crucial role in optimizing the impedance bandwidth.

- Aperture coupling: Using an aperture in the ground plane between the feed line and the patch creates a strong coupling, which enhances the bandwidth.
- Coaxial Probe Feed: Optimizing the position and size of the coaxial feed probe can result in better impedance matching across a wider frequency range.
- Proximity Coupling: this method involves laying the feedline near the radiated patch without direct contact, resulting in better impedance matching and wider bandwidth.
- Corporate Feed Networks: In arrays, it can lead to the use of broadband feeder networks with impedance circuits to greatly improve the fed bandwidth.

#### 4. Multilayer and Array Techniques

Combining multiple antenna elements or layers creates additional resonances that enhance bandwidth.

- Use of Metamaterials: Incorporating metamaterial-based structures can enable negative permittivity and permeability properties, which help in achieving broader bandwidth
- Array Approach: Coupling multiple patches or resonators operating at slightly different frequencies can create a composite resonance with a broader frequency range.

#### 5. Active Techniques

Active elements such as variables or PIN diodes can be combined to dynamically adjust the operating frequency and bandwidth.

- Reconfigurable Antennas: Using switches or other active components enables switching between different operating modes or frequencies, effectively broadening the bandwidth.
- Varactor-Tuned Patches: Adding varactor diodes to the patch allows real-time tuning of the resonance frequency and enhancement of the bandwidth.

A combination of structural modifications, material choices, advanced feeding techniques, and active tuning can be employed to achieve significant bandwidth improvements. The selection of the technique depends mainly on the application, design constraints, and required performance metrics.

### 3.3.6. Numerical methods for computational electromagnetics

Computational electromagnetics (CEM) involves the use of numerical methods to solve complex problems in electromagnetism, such as the behavior of electric and magnetic fields in different media and structures. From antenna design to waveguide analysis and electromagnetic compatibility (EMC), CEM has broad applications across many fields, including telecommunications, aerospace, and medical devices. These models are critical in predicting system behavior under various conditions and are used to guide design and decision-making processes. By utilizing numerical methods, these models provide approximate solutions to otherwise intractable problems.

Numerical simulations are designed to predict how physical systems respond to different types of stimuli or inputs. To achieve accurate simulations, mathematical models are created to represent the behavior of electromagnetic fields in the systems being studied. These models typically derive from fundamental laws of electromagnetism, most notably Maxwell's equations, which govern the relationships between electric and magnetic fields. Originally, Maxwell expressed these equations using potentials in Cartesian coordinates, which made them challenging to interpret and apply. Later, Heaviside and Hertz reformulated Maxwell's equations in terms of field quantities, simplifying their physical interpretation. Lorentz further contributed by introducing vector notation, which enhanced the equations' clarity and usability. These advancements culminated in the widely recognized first-order differential form of Maxwell's equations, expressed using vector and scalar quantities as shown in equations 3.32 to 3.35.

$$\nabla \times E = -\mu \frac{\partial H}{\partial t} \quad (\text{Faraday's law}) \quad (3.32)$$

$$\nabla \times H = \sigma E + \varepsilon \frac{\partial E}{\partial t} \quad (\text{Ampere's law}) \quad (3.33)$$

$$\nabla \cdot D = \rho \quad (\text{Gauss's law for electricity}) \quad (3.34)$$

$$\nabla \cdot B = 0 \quad (\text{Gauss's law for magnetism}) \quad (3.35)$$

Where  $E$  is the electric field in Newtons per Coulomb (N/C),  $H$  is the magnetic field in Amperes per meter (A/m),  $D$  is the electric flux density in Coulombs per square meter (C/m<sup>2</sup>),  $B$  is the magnetic flux density in Webers per square meter (Wb/m<sup>2</sup>),  $\epsilon$  is the permittivity of the dielectric medium in Farads per meter (F/m), and  $\mu$  is the permeability of the medium in Henries per meter (H/m) (Habash, 2007). The quantity  $\nabla$  ( $\rho$  is a vector operation,  $\sigma$  the conductivity of the medium, whose unit is Siemens per meter (S/m), and  $\rho$  the volume charge density in coulombs per cubic meter (C/m<sup>3</sup>). When  $\nabla$  is combined with  $\times$ , the result ( $\nabla \times$ ) is referred to as the curl of the vector quantity that follows. When  $\nabla$  is combined with dot, the result ( $\nabla \cdot$ ) is referred to as the divergence of the vector that follows (Habash, 2007).

Once mathematical models are established, numerical methods are employed to approximate solutions. These methods discretize continuous equations, converting them into forms that can be solved on a computational grid. The most widely used numerical techniques in CEM are:

- **Finite Element Method (FEM):** FEM is a highly effective numerical technique for solving complex mathematical problems. In FEM, the domain is subdivided into small elements, and a set of basis functions is defined for each element. These basis functions are non-zero only over a limited number of elements, allowing for localized approximations of the fields. FEM is particularly useful for problems involving complex geometries and is widely applied in frequency-domain simulations, such as antenna design and waveguide analysis.
- **Finite Difference Time Domain (FDTD):** FDTD is a time-domain numerical technique that discretizes Maxwell's equations in both space and time. It is especially effective for simulating transient phenomena, such as pulse propagation, and wideband systems. FDTD is commonly used for modeling systems where time-varying electromagnetic fields are of interest.
- **Finite Integration Technique (FIT):** FIT is another time-domain technique used to solve Maxwell's equations by discretizing them in an integral form. This method is particularly well-suited for handling problems with complex material properties and boundary conditions and is often employed in electromagnetic compatibility (EMC) simulations.

- Method of Moments (MoM): MoM is a technique used for solving integral equations that arise in electromagnetics. This method is commonly used for problems with open boundaries, such as antenna modeling and scattering problems. It works by converting the problem into a system of linear equations, which are then solved numerically.

These mathematical models are essential to computational electromagnetics, enabling the simulation and analysis of complex phenomena. Programs like CST Studio Suite, which employs techniques such as the Finite Integration Technique (FIT) and FEM, play a pivotal role in solving Maxwell's equations and modeling electromagnetic systems. These tools provide critical insights for applications such as antenna design, electromagnetic compatibility, and medical devices. Advances in computational power and modeling techniques continue to enhance CEM's ability to address complex challenges and drive innovation across diverse fields.

### **3.3.7. Microstrip Patch antennas for biomedical applications**

A microstrip patch antenna is a significant technological advancement utilized in various healthcare applications, including medical devices, remote monitoring, microwave examination, as well as additional on-body usage. In this context, M. Hag et al. (Haq & Khan, 2014), introduced a research on a Multiple Ring Slot Ultra-Wideband (MRS-UWB) patch antenna for medical use. By adjusting the feed's width and location concerning the partial ground structure's width, as well as the FR-4 substrate's dimensions, the suggested ring-slotted antenna was constructed and fed using a microstrip line. The feed line made use of stairs with rectangular slots, and the ground plane had its corners cut off. The antenna has an outstanding performance for the UWB approach based on the 10 dB bandwidth criterion, within the frequency range of 2-12 GHz. The maximum return loss (RL) is observed at frequencies of 4.3 GHz, 5 GHz, 8 GHz, and 11.6 GHz. The VSWR is less than 2 dB across the entire UWB range. This antenna was not subjected to actual testing; only simulation findings of the antenna were provided. A two-sleeve, small antenna working in the medical band was then proposed by Shikha Sukhija et al. (Sukhija & Sarin, 2017). The antenna was developed on an FR-4 substrate and tested in simulations by varying the ground plane length, as well as the first and second sleeves, at various times. In order to take measurements, materials that mimicked human tissue were used. The antenna's performance in the ISM band was significantly affected by the addition of two sleeves.

Microstrip patch antennas require being soft and comfortable to wear since they are employed in on-body applications. The problem of wearability or flexibility arises when FR-4 is used as a substrate. Kavitha et al. (Kavitha & Swaminathan, 2019) introduced a flexible textile antenna functioning at 2.4 GHz, utilizing FR4, denim cotton, and Teflon substrates. Their findings indicate that while the three substrates exhibit excellent performance features, the Teflon substrate is most appropriate for textile antenna designing. N.A. Ingale and colleagues (Ingale et al., 2008) proposed a structure for a textile antenna intended for on-body applications. Two antenna designs were created utilizing cotton and denim substrates, respectively. The textile substrate was attached to the copper sheet's ground plane using adhesive double-sided tape. Both antennas provide outstanding results for on-body applications. Enhancing the efficacy of a microstrip patch antenna is more effective with an array structure than with a single antenna element. Syahirah Shawalil et al. (Shawalil et al., 2019) proposed an antenna array for wearable applications. Researchers created and simulated an inset-fed microstrip patch antenna. The researchers utilized Shield IT as the patch material and jean cloth as the substrate. The next step was to create, manufacture, and conceal the designed two-element antenna array within the denim. The two-element microstrip patch antenna array outperforms the single-element antenna in terms of return loss, according to simulation and experimental results. Ameena Banu Mustafa et al. (Mustafa & Rajendran, 2019) introduced a dual flexible substrate antenna incorporating a defected ground structure (DGS) for use in medical observation systems. Initially, single-substrate antenna designs were created using Teflon and felt, both with and without DGS. Later, the same antenna designs were adapted to a dual-substrate configuration. Simulation results revealed that the dual-substrate antenna with DGS exhibited superior performance compared to other configurations in terms of return loss, voltage standing wave ratio (VSWR), and gain.

### **3.3.8. Microstrip patch antennas for breast cancer diagnosis**

An increasing number of microwave imaging applications are finding use for microstrip patch antennas, which can both send and receive backscattered signals. To acquire the best results, researchers are experimenting with various substrates, feeding strategies, and design methodologies for microstrip patch antennas. Rabia Caliskan et al. (Çalışkan et al., 2015) introduced an inset-fed antenna arrangement for breast cancer detection. This 2.45 GHz inset-fed rectangular patch antenna uses FR-4 as its substrate.

The simulation results are improved with some adjustments to the ground layer and slots on the radiating patch. Using a 3D breast model, they simulate five different antenna configurations. The simulation of the suggested antenna reveals a noticeable difference in the electric field, magnetic field, and current density parameters when comparing the breast model with and without the tumor. To test the antenna, they used a tumor radius of 20 mm. R. Karli et al.(Karli et al., 2016) introduced a compact planar ultra-wideband patch antenna for cancer identification operating at a frequency of 6 GHz. Researchers tested the antenna at several locations on the breast phantom and found that directly positioning the antenna on the skin may enhance the sensitivity of tumor identification by microwave imaging. The antenna showed the ability to identify tumors with a radius of 0.5 cm. The antenna's small dimensions, single-layer configuration, and extensive bandwidth make it an ideal choice for ultrawideband systems. A T-shaped slotted antenna was proposed for the early detection of breast cancer by Hemant Kumar Gupta et al.(Sharma & Thakre, 2017). Beams at 2.45 GHz are produced by the designed antenna. To enhance the antenna performance, a T-shaped slot was placed into the rectangular patch. They took two instances into account: the first is a breast phantom model with the tumor located in the middle of the patch antenna; the second is a similar model but with the tumor placed 50 mm distant from the patch. Their results showed that the current density and SAR of the breast phantoms with and without tumors were significantly different. J. J. Susila et al.developed a slot-loaded patch antenna. Tumor identification was conducted by analyzing fluctuations in the electric (E) and magnetic (H) fields, as well as current density, in both the existence and absence of a tumor. The proposed antenna exhibits a notable disparity among the previously mentioned characteristics. Suresh Subramanian et al.(Subramanian et al., 2018) designed an octagonal-shaped ultra-wideband (UWB) antenna using an FR-4 substrate for tumor diagnosis. The antenna operates within a frequency band of 3 GHz to 15 GHz, with tumor identification achieved through specific absorption rate (SAR) values. SAR simulations were conducted for different tumor sizes and locations, revealing significant differences between tumor-free and tumor-affected breast models. To improve impedance matching and bandwidth, a circular cut was introduced into the patch design. Additionally, T.V. Padmavathy et al.(Padmavathy et al., 2019) proposed an I-shaped antenna with dual C-shaped slots for breast cancer screening. This design operated within the 4 GHz to 10 GHz frequency range and utilized an FR-4 substrate with a

single-edge feedline. Tumor detection was achieved by evaluating SAR values, return loss, and gain.

### **3.3.9. Textile microstrip patch antennas**

The specificity of tumor identification is influenced by the distance of the antenna to the human breast phantom, with sensitivity improving as this distance decreases. Textile substrates are widely favored by researchers due to their ability to provide a smooth interface and enhanced comfort for patients. Fawzy Alsharif et al. (Alsharif & Kurnaz, 2018) proposed an innovative structure for a wearable patch antenna. The proposed antenna operates across a frequency band of 1.6 GHz to 11.2 GHz and utilizes 100% cotton as a substrate, with a dielectric constant of 1.6, to enhance its wearable properties, and copper as conductive material with an overall antenna size of  $70 \times 60 \text{ mm}^2$ . A staircase structure was incorporated into the design to achieve improved return loss performance. Srinivasan et al. (Srinivasan & Gopalakrishnan, 2019) introduced a wearable antenna designed for tumor detection, operating at 2.45 GHz. The antenna has an overall size of  $80 \times 80 \text{ mm}^2$  and uses denim fabric with a dielectric constant of 1.7 and a thickness of 1 mm as the substrate, ensuring both wearability and user comfort. The antenna employs a coaxial feeding technique, which enhances its performance. The evaluation of its performance was conducted using criteria including return loss, gain, radiation pattern, axial ratio, and voltage standing wave ratio (VSWR). Rexiline Sheeba et al. (Sheeba & Jayanthi, 2019) proposed the construction and analysis of patch antenna for identifying tumors in dermatological and breast tissues. The study introduced two antenna configurations functioning at roughly 2.4 GHz: one with a hexagonal patch without slots and another with a slotted hexagonal patch. Both designs utilized jean cotton as the substrate material and copper as patch and ground material. The two antenna structures were evaluated and contrasted based on parameters such as return loss, voltage standing wave ratio (VSWR), gain, and specific absorption rate (SAR). Additionally, simulations were performed to assess cancer identification capabilities in terms of current. Textile materials, characterized by significantly lower dielectric constants compared to non-textile materials, contribute to improved antenna bandwidth and reduced surface wave losses. However, these materials also lead to increased antenna diameters.

### 3.3.10. Antenna Array

An antenna array is a configuration of several interconnected antennas organized in a certain design that together function as a single unit to broadcast or receive radio waves, thus improving signal directionality, strength, and coverage. The antenna elements are often linked to a singular receiver or transmitter via feedlines that deliver power to the components in a designated phase. Arrays provide beamforming by regulating the phase and amplitude of signals at every element, enabling the signal beam's directional steering, mitigating interference, and enhancing gain relative to individual antennas. Common kinds are linear arrays, where antenna elements are organized in one dimension; planar arrays, which position elements in two-dimensional grids; and phased arrays, which electronically modify phases for dynamic beam steering. The history of antenna arrays goes back to the early 20th century when researchers began looking for ways to improve the performance of radar systems. During World War II, arrays gained significant importance for their use in military applications, allowing for accurate target detection and tracking. Advances in electronics in the 1950s made phased arrays possible and were widely used in defense and aerospace systems. In recent years, the development of digital signal processing and the miniaturization of electronics have expanded the use of antenna arrays in commercial applications such as wireless communications, such as 5G networks, and medical imaging. In addition to traditional applications, antenna arrays have played an important role in medical treatments such as hyperthermia cancer therapy.

Microwave antenna arrays are used to precisely focus energy on the tumor site while sparing surrounding healthy tissue. These arrays can focus heat with high precision by adjusting the phase and amplitude of the microwave signals. This approach has shown success in treating deep tumors, where conventional techniques struggle to deliver focused energy.

Element spacing is an important parameter in antenna array. The proper distance between adjacent elements in both the x and y direction is crucial to avoid grating lobes. For uniform spacing:

$$d_x = \frac{\lambda}{2}, d_y = \frac{\lambda}{2} \quad (3.36)$$

where  $\lambda$  is the wavelength of the operating frequency,  $dx$  and  $dy$  are the inter-element spacings along the x- and y-axes, respectively.

A beamformer modifies the phase and relative amplitude of the signal at each transmitter to alter the directionality of an array during transmission. This generates patterns of positive and negative interference in the waveform, influencing the signal's direction. Upon reception, the beamformer integrates inputs from several sensors to enhance the intended radiation pattern. Beamforming can be utilized for both signal transmission and reception, facilitating spatial selection to enhance performance. Figure 3.12 shows how to use beamforming and beam steering to control the phase and amplitude to steer a signal toward a specific direction.

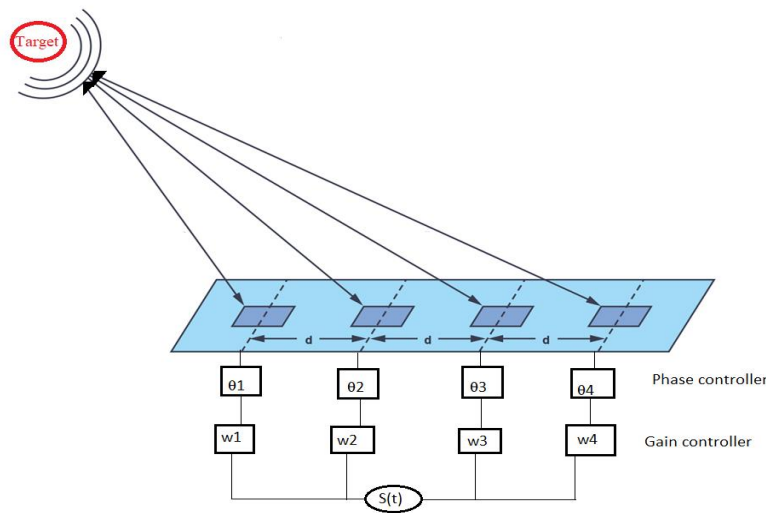


**Figure 3.12.** Using beamforming to control the phase and amplitude.

For an array steered towards a direction  $(\theta, \phi)$  in spherical coordinates, the phase shift is calculated by:

$$\psi_n = k(x_n \sin\theta \cos\phi + y_n \sin\theta \sin\phi) \quad (3.37)$$

Where  $k=2\pi/\lambda$  is the wave number,  $x_n$  and  $y_n$  are the coordinates of the n-th element,  $\theta$  is the elevation angle, and  $\phi$  is the azimuth angle.

The array factor (AF) can be expressed as:

$$AF(\theta, \phi) = \sum_{n=1}^N I_n e^{j\psi_n} \quad (3.38)$$

Where  $I_n$  is the amplitude of the  $n$ -th element.

For a uniform linear array with  $N$  elements and inter-element spacing  $d$ , the steering vector is:

$$w = [1, e^{jkdsin\theta}, e^{j2kdsin\theta}, \dots, e^{j(N-1)kdsin\theta}]^T \quad (3.39)$$

The output signal is:

$$y(t) = w^H s(t) \quad (3.40)$$

Where  $w$  is the beamforming weight vector,  $s(t)$  is the received signal, and  $H$  is the Hermitian transpose.

Antenna arrays provide high flexibility in shaping and steering beams using advanced techniques like beamforming and beam-steering. The choice of element spacing, phase shifts, and weighting significantly impacts the performance of the array, ensuring minimal interference and maximum gain in the desired direction.



## 4. RESEARCH METHODOLOGY

### 4.1. Methodology

Figure 4.1 shows the methodology flow chart, starting from the 3D breast model design, assigning material properties to the model, antenna design, and finally simulation and optimization of the antenna. Antenna radiation and its interaction with the breast tissues were simulated with Computer Simulation Technology CST software using the CST MICROWAVE STUDIO<sup>®</sup>. After testing the imaging system and its ability to detect tumors inside the breast, the same designed antenna is integrated into a 2x4 antenna array to be used in CST MPMYSICS<sup>®</sup> STUDIO to test its ability to generate the thermal heat needed for breast

hyperthermia that can damage tumors located in specific places inside the breast. Beamforming techniques are used to steer the radiation into the tumor's locations to increase its temperature up to 40°C – 45°C while keeping the temperature of the healthy tissues under 40°C.

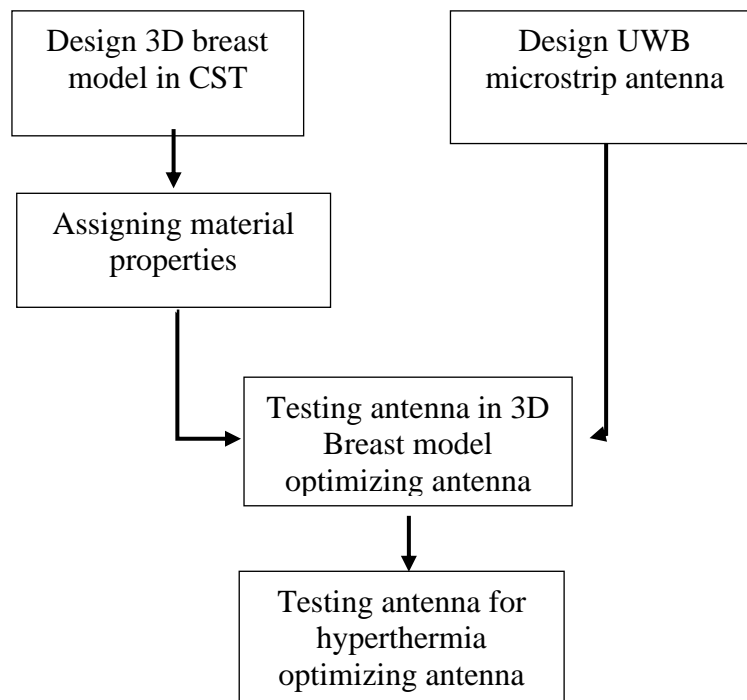


**Figure 4.1.** Methodology flow chart

## 4.2. Computer Simulation Technology CST

CST STUDIO SUITE® (CST, 2019) is a robust finite element method (FEM) modeling package designed for various electromagnetic issues and associated applications. The program offers an intuitive interface for managing numerous projects and views simultaneously, each potentially associated with a distinct module. The CST STUDIO SUITE® software package offers various simulation modules, two of which were utilized in this study: CST MICROWAVE STUDIO® and CST MPHYSICS® STUDIO.

CST MICROWAVE STUDIO® has been developed for rapid and precise 3D electromagnetic simulation of high-frequency issues. The module encompasses a range of distinct solvers functioning in both the time and frequency domains.

CST MPHYSICS® STUDIO is a tool for resolving thermal (Bioheat equation) and mechanical stress issues. This module is generally utilized alongside other modules to deal with connected simulation jobs. This study utilized CST STUDIO SUITE® version 2019 as a modeling and simulation tool. Figure 4.2 illustrates the CST user interface.

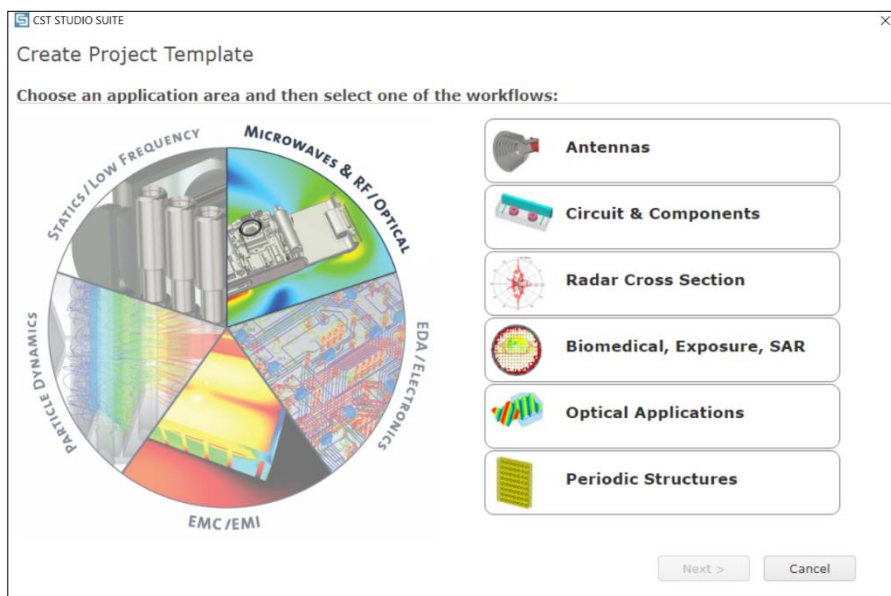


**Figure 4.2.** CST user interface



**Table 4.1.** Optimized Antenna Dimensions

Parameters	Dimensions (mm)
Patch Length	20
Patch Width	20
Substrate Length	31
Substrate Width	31
Substrate height	0.7
Partial Ground Length	10
Ground and patch height	0.11
Ground notch size 1	3.6*9
Ground notch size 2	7.6*1

### 4.3. Trust-Region Framework (TRF) for Ground Length Optimization

The Trust-Region Framework is a widely used optimization technique, particularly for solving nonlinear programming problems. It is an iterative approach that ensures robust and efficient convergence by restricting the step size within a predefined "trust region" around the current point. At each iteration, the method builds a local model of the objective function (or a subproblem) within a "trust region." The trust region is a neighborhood around the current iterate where the model is considered a reliable approximation of the objective function. A step is computed by solving this subproblem, and the size of the trust region is adjusted based on how well the model predicts the actual function.

When optimizing the partial ground length in the proposed antenna using CST, the Trust-Region Framework is applied as part of the software's parameter optimization tools. An objective function was defined (equation 4.1) to find the optimal partial ground length (GL) that maximizes bandwidth and minimizes reflection coefficients ( $|S_{11}| < -10$  dB) as a function of the ground length GL across the desired frequency range.

$$f(GL) = \sum_{i=1}^N \max\{S_{11}(GL, f_i) + 10, 0\}^2 \Delta f \quad (4.1)$$

Where  $f_i$  is the discrete frequency points as given by the simulation,  $N$  is the number of frequency points, and  $\Delta f = f_H - f_L / N$  is the frequency step size.

The term  $\max \{S_{11}(GL, f) + 10, 0\}$  penalizes values of  $S_{11}$  that exceed -10 dB. Squaring emphasizes larger deviations above -10 dB more heavily. By adding 10, the threshold shifts such that  $S_{11} + 10 = 0$  when  $S_{11} = -10$  Db. This ensures only  $S_{11}$  values above -10 dB (worse performance) contribute to the penalty.

#### 4.4. Breast Modeling and Assigning Material Properties

Different breast phantoms are designed to test the introduced antenna's feasibility for breast tumor detection or treatment. Dispersive dielectric properties can be incorporated using the Cole-Cole or the Debye model (Meaney et al., 2007). In our model, the dielectric properties of the skin, fat, and glandular tissues in the selected frequency spectrum are obtained from the IT'IS material parameters database (S. Gabriel et al., 1996), as illustrated in Table 4.2. Tumor characteristics are presumed based on existing literature (Halloran et al., 2016). Figure 4.4. shows the designed phantom with an overall 100 mm diameter. The thickness of the skin layer is 2 mm, the fat layer is 4 mm, and the glandular layer is 94 mm.

**Table 4.2.** Breast phantom tissue dielectric properties

Tissue	Electrical conductivity S/m	Permittivity	Density Kg/m <sup>3</sup>	Thermal Conductivity W/m/ °C	Heat Capacity J/Kg/ °C
Skin	2.34	34.1	1109	0.37	3391
Glandular	3.46	50	1041	0.33	2960
Breast Fat	0.35	4.46	911	0.21	2348
Tumor	4	54.9	1058	0.60	4200

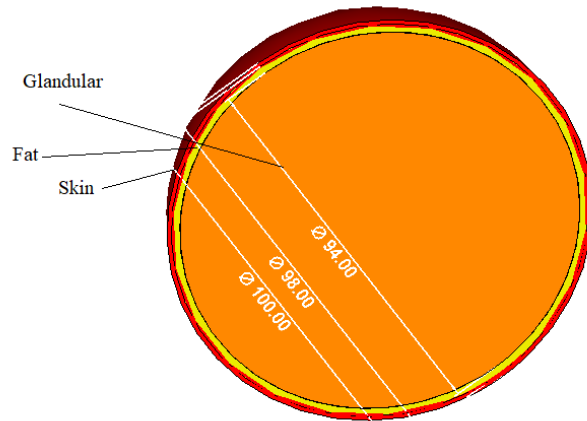


**Figure 4.4.** Proposed Breast Phantom

#### **4.5. Testing the Single Antenna in a 3D Breast Imaging Model**

The proposed antenna was tested in several models, first in a breast model without a tumor (Model A) and second with a tumor with a diameter of about 5 mm located at the (0, -10,12) of the phantom (Model B). The tumor shape was changed in model C to test the ability of the antenna to detect different tumor shapes. Then the location of the tumor in Model B was changed and a new 2mm radius tumor was inserted into the breast phantom to see the effects of these changes in the results (D). Figures 4.5 to 4.8 illustrate all simulation models, A, B, C, and D.

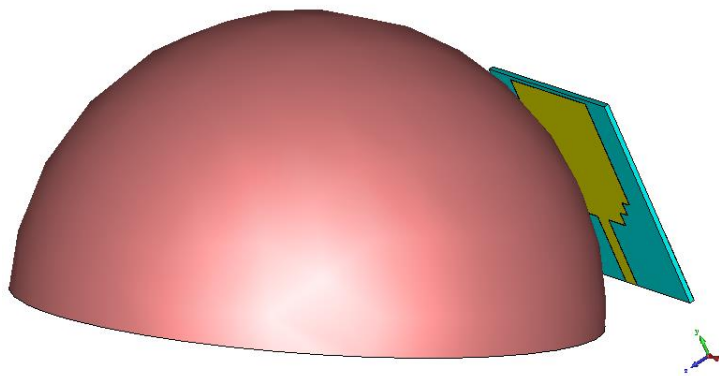


**Figure 4.5.** Single antenna with tumor-free breast (Model A)

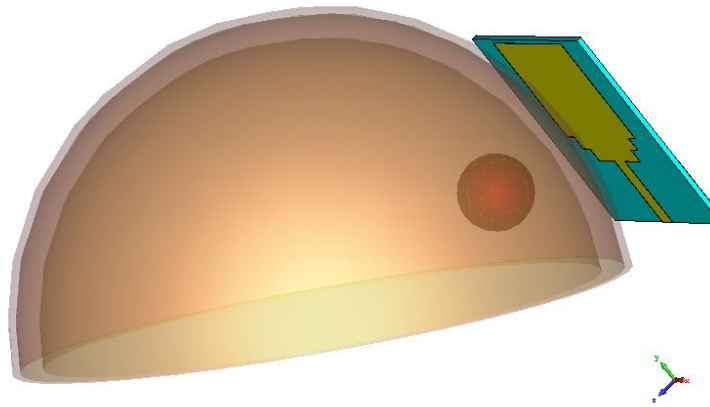


**Figure 4.6.** Single antenna with one spherical tumor breast model (Model B)

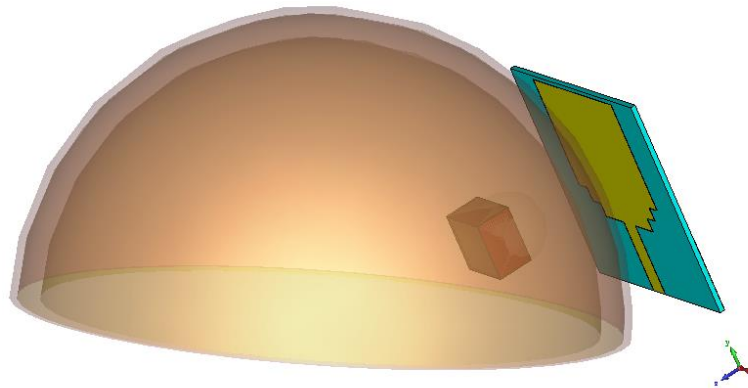


**Figure 4.7.** Single antenna with one cubic tumor breast model (Model C)

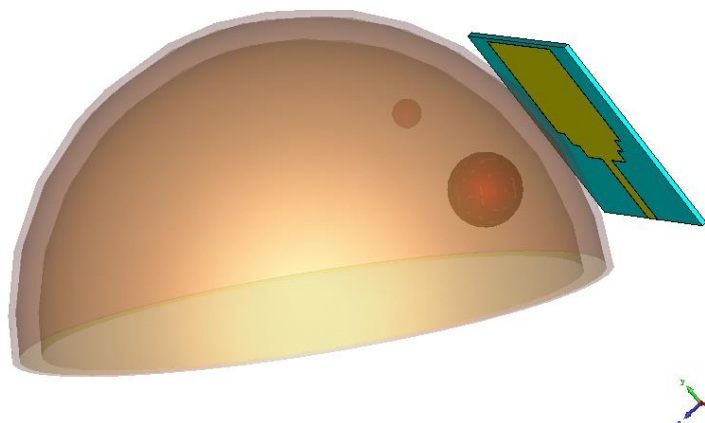


**Figure 4.8.** Single antenna with two tumors breast model (Model D)

#### 4.6. Pending Antenna For Flexibility Test

Figure 4.9 shows the proposed antenna after bending experiments to assess its flexibility. A 30 ° cylindrical bending has been applied to the main antenna.

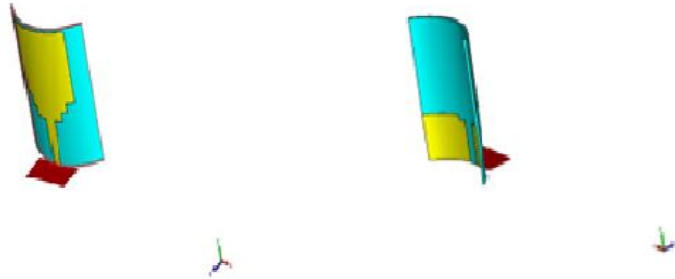


**Figure 4.9.** Antenna Bending

#### 4.7. Microstrip Patch Antenna Array Design For Hyperthermia

Antenna characteristics were tested and SAR values were calculated using the CST MICROWAVE STUDIO solver, to accurately determine tumor locations. To test the efficiency of the antenna in treating tumors using hyperthermia, the bioheat equation was solved using the thermal solver in CST MPHYSICS STUDIO, and then the resulting heat losses were converted into a real temperature distribution that takes into account the effects of living tissue.

The success of hyperthermia therapy depends primarily on the ability to precisely focus the heat, and this is where antenna arrays come in. Using multiple antennas reduces the power required by each antenna, helping to avoid hot spots on the skin. The ability of antenna arrays to focus energy reduces the risk of overheating non-target areas and potential side effects. The developed antenna is incorporated into a 2x4 antenna array, as illustrated in Figure 4.10, for utilization in CST MPHYSICS® STUDIO to evaluate its capacity to provide the thermal energy required for breast hyperthermia to target tumors situated in specific locations within the breast. Beamforming techniques are employed to direct radiation toward tumor sites, elevating their temperature to 40°C - 45°C, while maintaining the temperature of surrounding healthy tissues below 40°C.

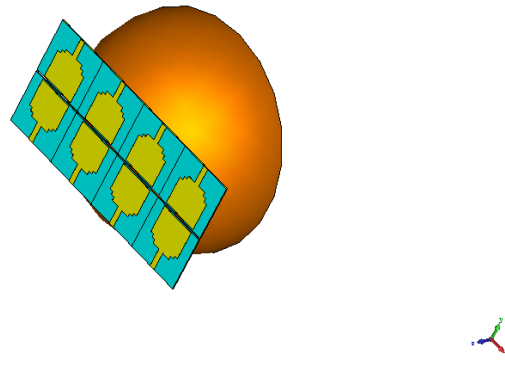


**Figure 4.10.** Proposed 2x4 antenna array for hyperthermia

#### 4.8. Testing the Array Antenna in 3D Breast Hyperthermia System

The proposed antenna was tested in several models, primarily, the antenna array was evaluated in a breast model with a tumor diameter of approximately 5 mm (Model E). Subsequently, the tumor location (Model F) was changed to show how the results were affected. A second tumor with a small size (2mm) was created in (Model G) to test the ability of the proposed antenna array to distribute temperature effectively in two different locations. Every model needed a different phase and amplitude adjustment for every element in the antenna to increase the temperature in a specified location. Inappropriate phase and amplitude are used again with model E to test its effect. Figures 4.11 to 4.13 illustrate all simulation models, E, F, and G.

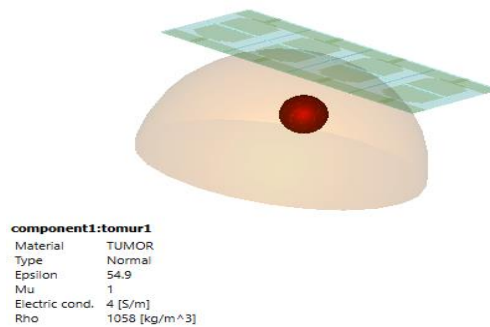


**Figure 4.11.** Antenna array with Model E including one tumor in the center

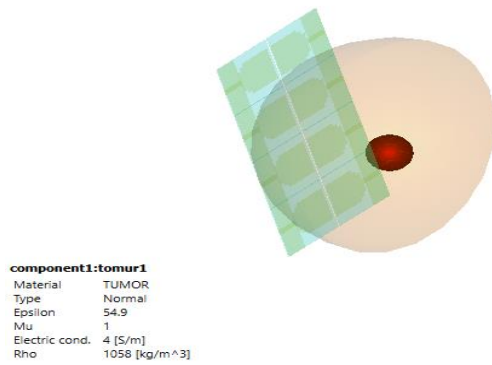


**Figure 4.12.** Antenna array with model F

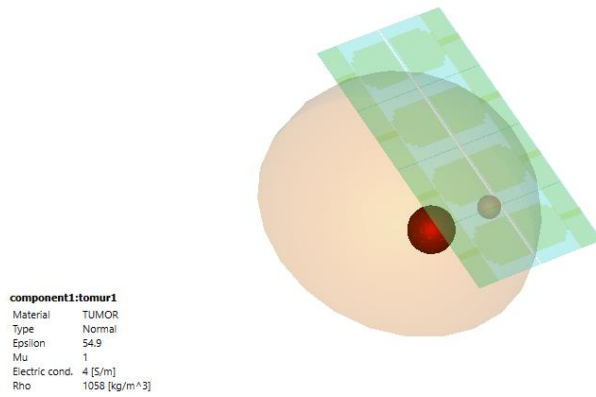


**Figure 4.13.** Antenna array with model G

#### 4.9. Testing the proposed antenna in a dynamic system

After testing the antenna's capability as a wearable device, its performance was further evaluated in a dynamic system to assess its suitability for unwearable imaging systems. Figure 4.14 illustrates the data collection setup, where the proposed antenna moves

horizontally along the x-axis from point 1 to point 112, with each step measuring 1mm to cover the entire breast area. At each position, the S-parameter signal is recorded.

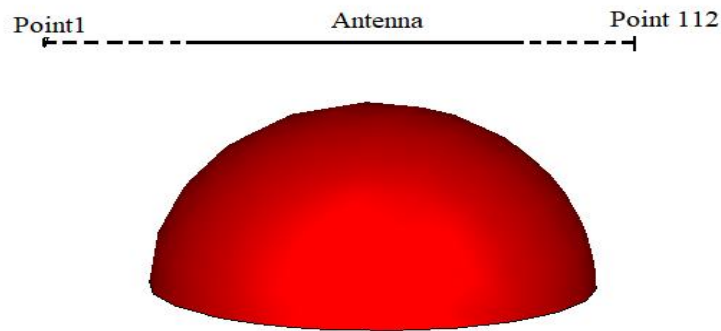


**Figure 4.14.** Signal collection from different 112 position

The collected signals are then exported to MATLAB and processed through multiple stages, as shown in Figure 4.15, to generate a 2D image.

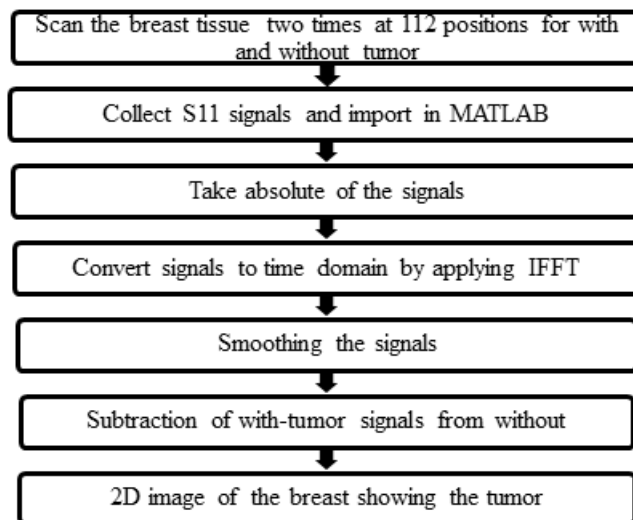


**Figure 4.15.**The procedure used to generate a 2D image

As illustrated in Figure 4.15, the collected signals are first imported into MATLAB for further analysis. The reflection coefficients are converted from decibels (dB) to absolute values within the frequency domain to facilitate subsequent processing. An inverse fast Fourier transform (IFFT) is then applied to transition these signals from the frequency domain to the time domain. To enhance the smoothness and continuity of the time-domain signals, a Savitzky-Golay filter is employed. Following this

preprocessing, the time-domain signal corresponding to a breast with a tumor is subtracted from the time-domain signal of a tumor-free breast. The resulting differential signal exhibits distinct peaks, which serve as indicators of the presence of a tumor. Finally, this processed signal is utilized to generate a two-dimensional (2D) image, providing a visual representation that aids in identifying tumor-affected regions.

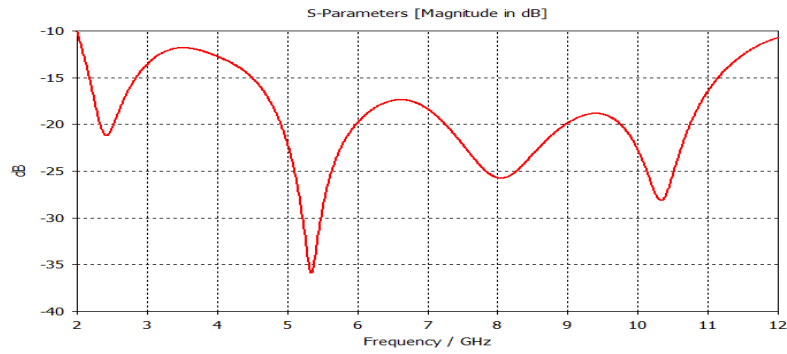
## **5. RESULTS AND DISCUSSIONS**

This chapter presents the results of the thesis that investigates the performance of an antenna designed for breast tumor detection and microwave hyperthermic therapy. The main performance parameters, such as gain, return loss, and voltage standing wave ratio, are evaluated. In addition, the specific absorption rate (SAR) and temperature distribution are explored in different simulation models in the context of their application for medical purposes. The SAR is evaluated to ensure safe electromagnetic exposure to tissues within the permissible range for medical applications and to exploit the absorption property of different tissues for radiation at different rates in breast cancer detection. In addition, the highest SAR values positions are examined to locate tumor centers or nearby areas, as tumors' dielectric properties cause them to absorb electromagnetic waves more effectively than surrounding breast tissues, thereby facilitating the identification of breast tumor locations compared to complex image processing techniques. Temperature distribution is also studied to exploit the resulting heat in microwave hyperthermic therapy for breast tumors.

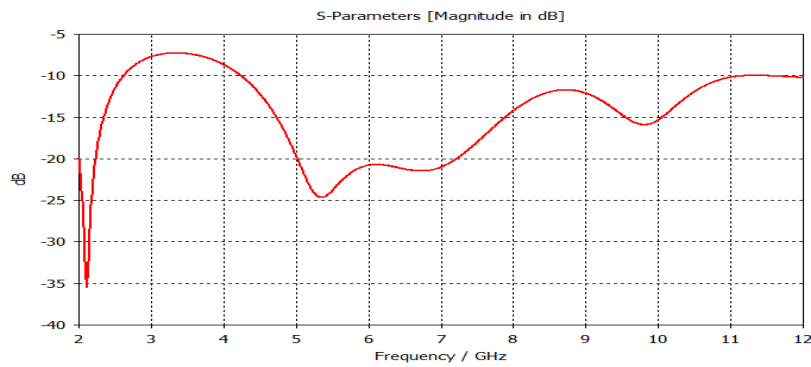
### **5.1. Simulation Results**

#### **5.1.1. Results of S-parameters**

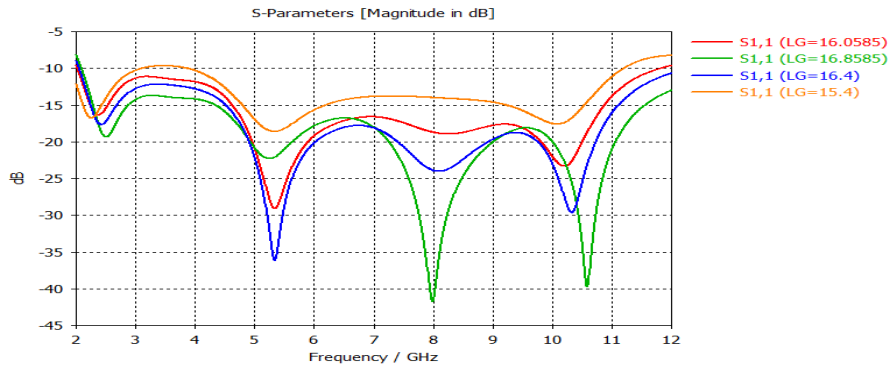
Figure 5.1 illustrates the return loss (S11) for the antenna in free space, while Figure 5.2 shows the effect of applying the antenna to the human breast. Figure 5.3 shows the effect of changing the partial ground length on the antenna's return loss (S11). On the other hand, figures 5.4 to 5.7 illustrate the return loss (S11) amplitude within the frequency range of 2–11.6 GHz for the antenna under various conditions of models A, B, C, and D. Figure 5.8. shows the bending effect on the antenna performance.



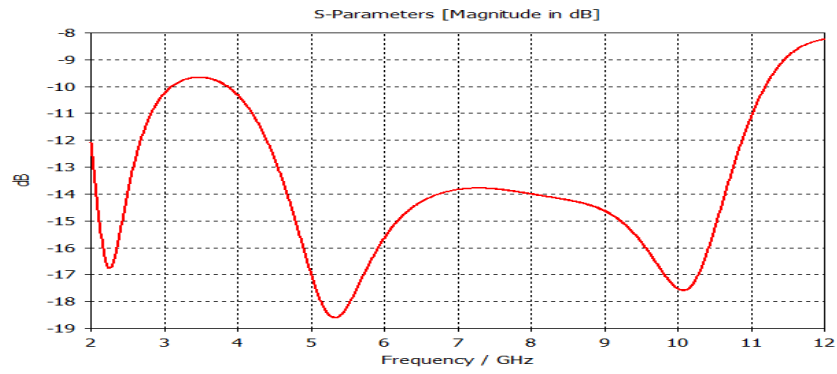
**Figure 5.1.** Antenna return loss (S11) in the free space.



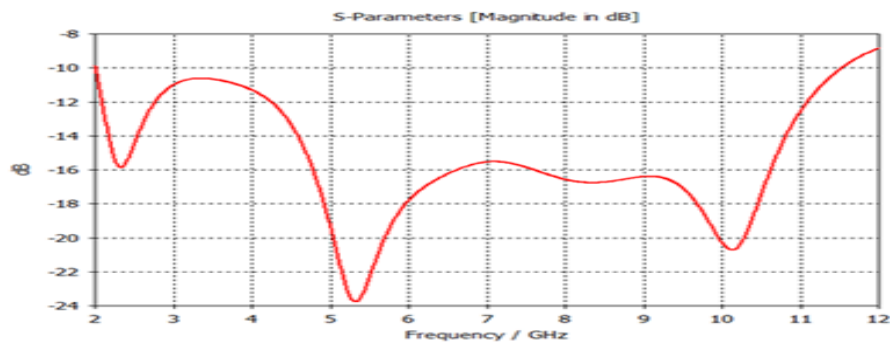
**Figure 5.2.** Antenna return loss (S11) in the presence of human breast before optimization.



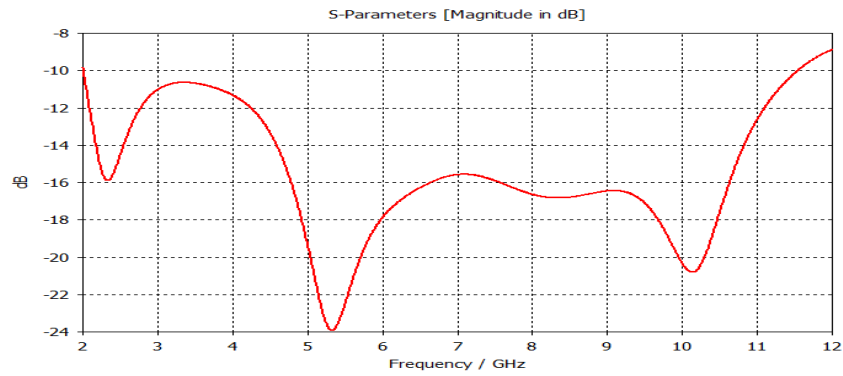
**Figure 5.3.** The effect of partial ground length and notches on the return loss



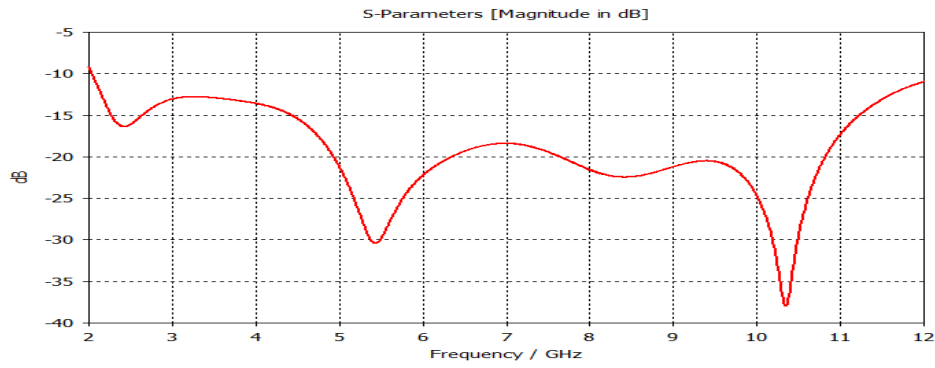
**Figure 5.4.** Antenna return loss (S11) in the presence of human breast after optimization (Model A)



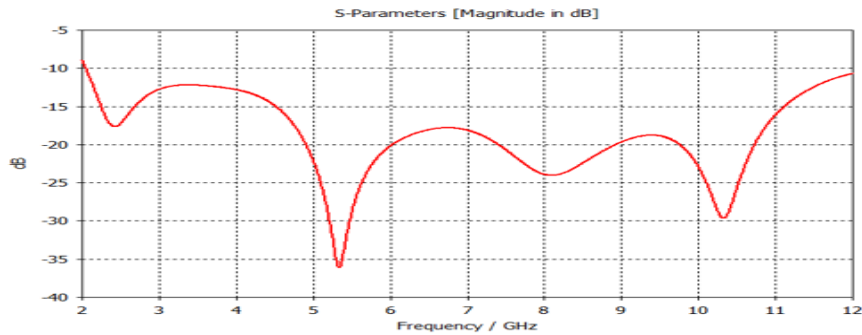
**Figure 5.5.** Antenna return loss (S11) in the presence of a 5 mm tumor (Model B)



**Figure 5.6.** Antenna return loss (S11) in the presence of a 5 mm tumor (Model C)



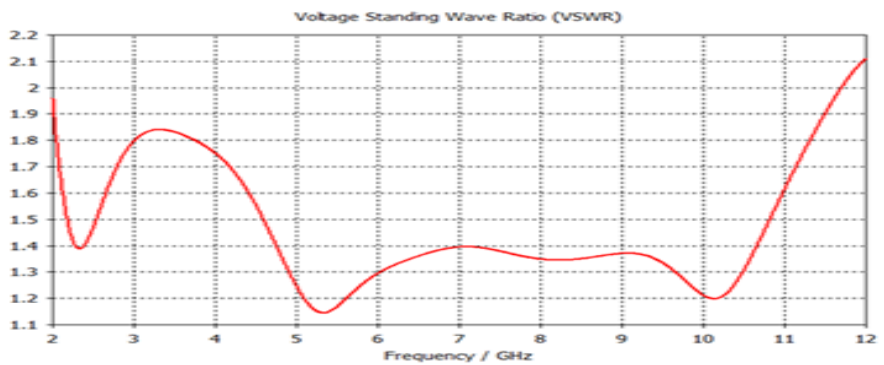
**Figure 5.7.** Antenna return loss (S11) in the presence of two tumors (Model D)



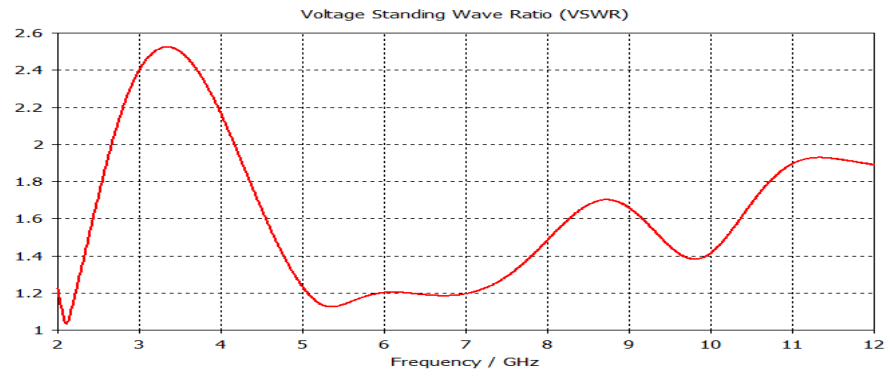
**Figure 5.8.** Antenna return loss (S11) after bending and optimization

### 5.1.2. VSWR Results

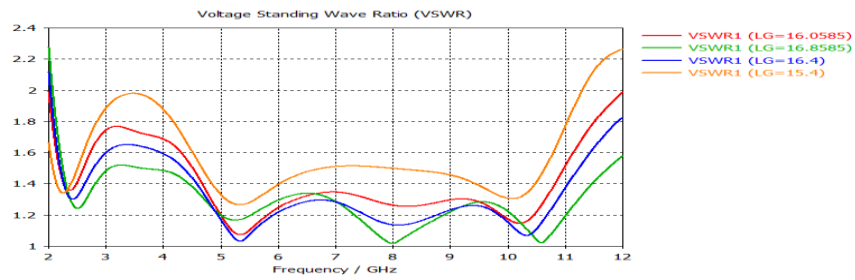
Figures 5.9 to 5.15 represent the voltage standing wave ratio (VSWR) results for the antenna under various conditions.



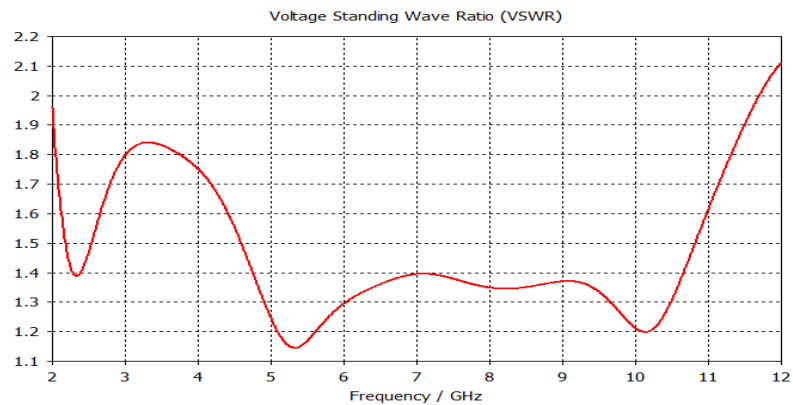
**Figure 5.9.** VSWR values for the proposed antenna in free space



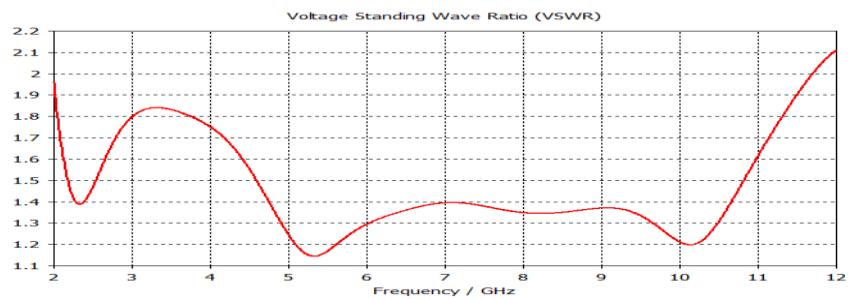
**Figure 5.10.** VSWR value in the presence of human breast before optimization.



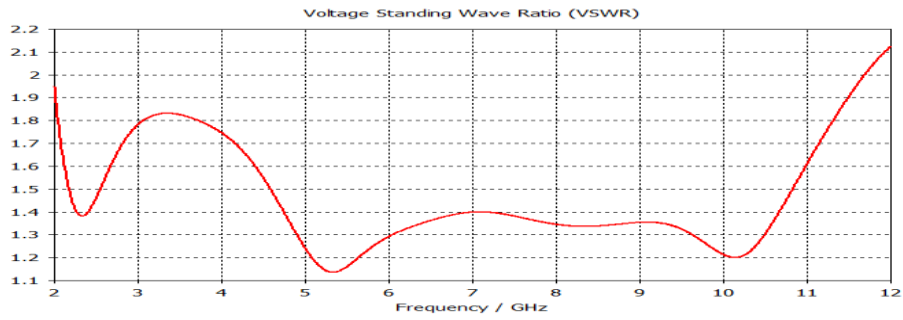
**Figure 5.11.** The effect of partial ground length on the VSWR



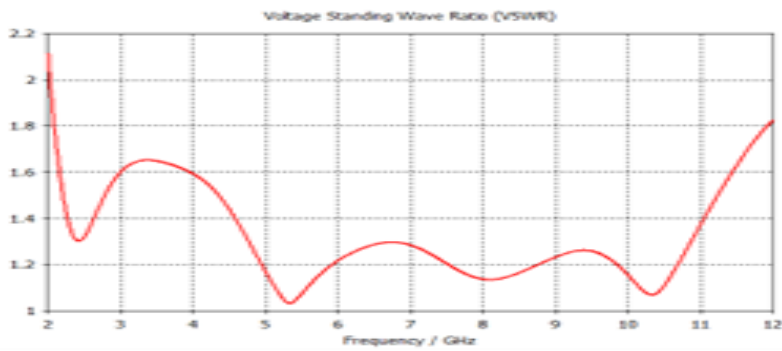
**Figure 5.12.** VSWR values for Model (A).



**Figure 5.13.** VSWR values for Model (B).



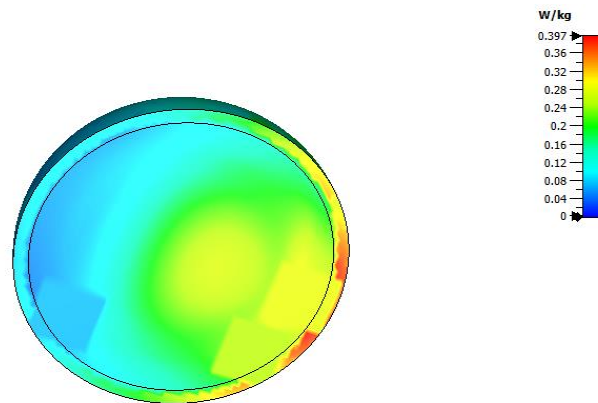
**Figure 5.14.**VSWR values for Model (C).



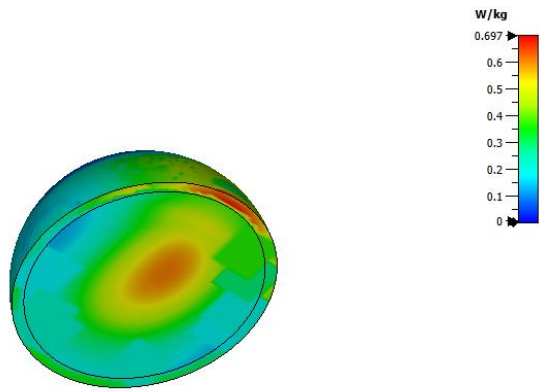
**Figure 5.15.**VSWR values for Model (D)

### 5.1.3. SAR Distribution

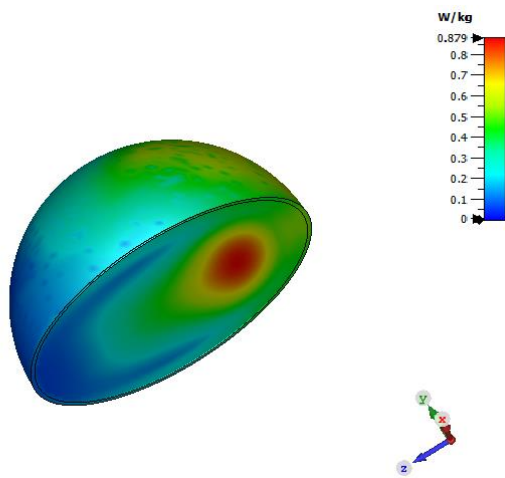
Figures 5.16 to 5.19 illustrate the specific absorption rate (SAR) in the tumor position and the surrounding tissues for the four models, A, B, C, and D, utilizing a single antenna element.



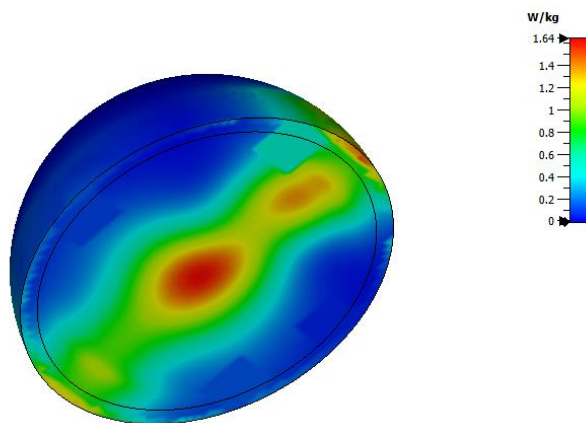
**Figure 5.16.** SAR distribution for Model (A).



**Figure 5.17.** SAR distribution for Model (B)



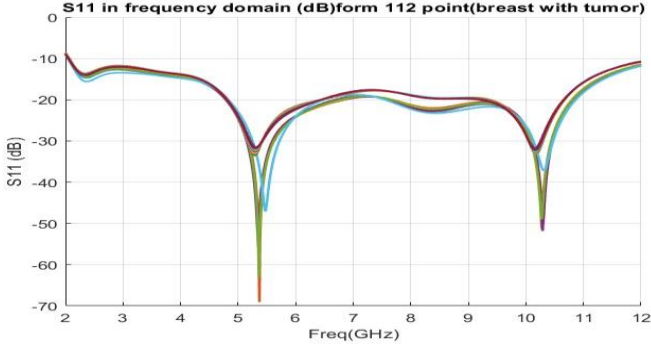
**Figure 5.18.** SAR distribution for Model (C)



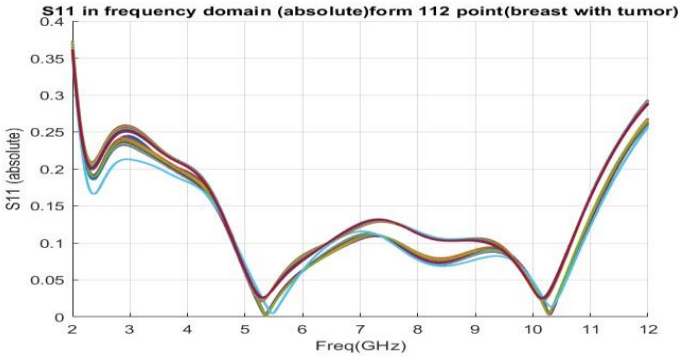
**Figure 5.19.** SAR distribution for Model (C)

**5.1.4. Results of a proposed antenna in a dynamic imaging system**

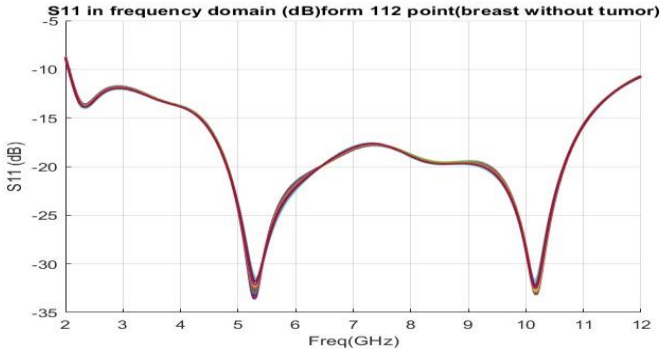
Figures 5.20 to 5.23 present the collected signals from 112 different points in the frequency domain, illustrating the results for scenarios with and without a tumor, represented in both dB and absolute values, respectively.



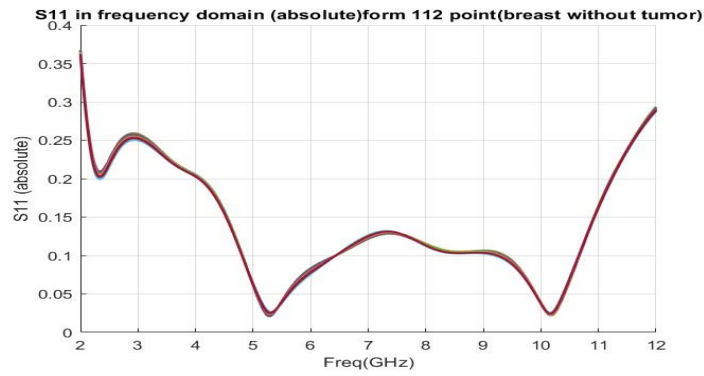
**Figure 5.20.**Collected signals in dB (Breast with tumor)



**Figure 5.21.** Collected signals in absolute (Breast with tumor)

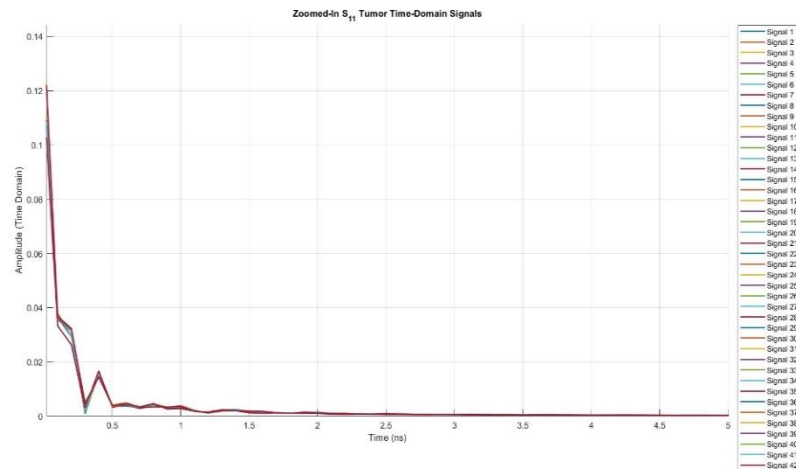


**Figure 5.22.**Collected signals in dB (Breast without tumor)

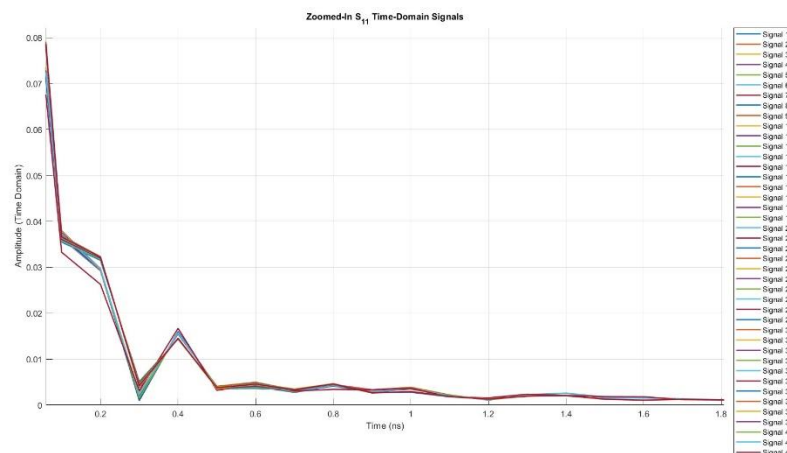


**Figure 5.23.** Collected signals in absolute (Breast without tumor)

Figures 5.24 and 5.25 display the time-domain signals after the application of the inverse fast Fourier transform (IFFT).



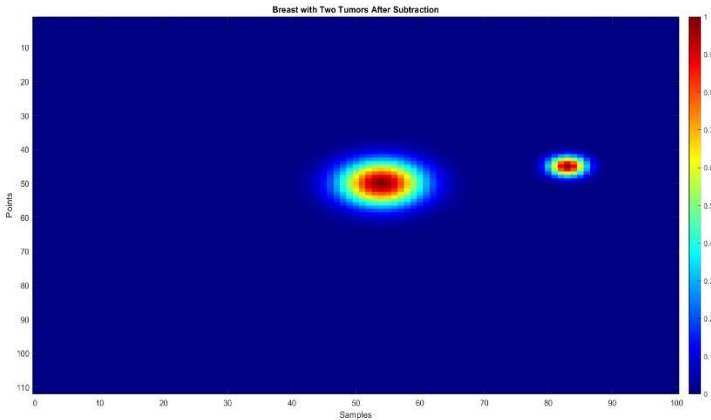
**Figure 5.24.** Zoomed time-domain signals (breast with tumors)



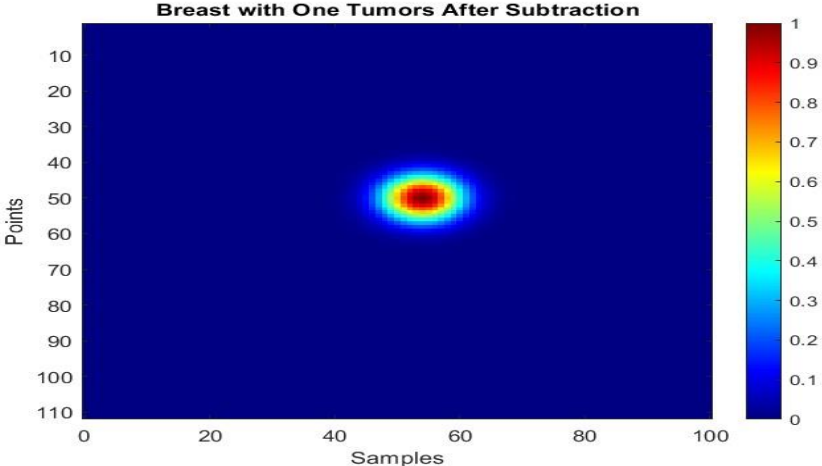
**Figure 5.25.** Zoomed time-domain signals (breast without tumor)

Figure 5.26 presents the resulting reconstructed image derived from the processed signals after the subtraction and smoothing processes, while Figure 5.27 shows the

reconstructed image after repeating all the processes with breast phantom involving one tumor with size 2mm.



**Figure 5.26.** Reconstructed image derived from breast phantom with two tumors



**Figure 5.27.** Reconstructed image derived from breast phantom with one tumor

**5.1.5. Temperature distribution**

Figures 5.28 to 5.31 present the cross-sectional temperature distribution within the tumor region and the surrounding background tissue for the three simulation models (E, F, and G) and the situation of using unsuitable phase or amplitude during array beamforming, obtained using the thermal solver of the CST MPHYSICS STUDIO.

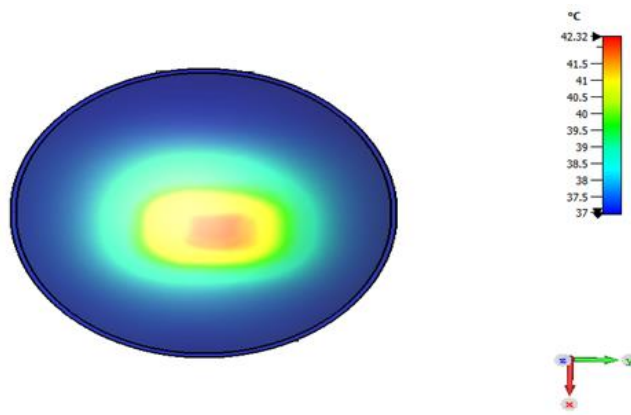


**Figure 5.28.** Temperature distribution for model E with one tumor (5 mm) radius in the center.

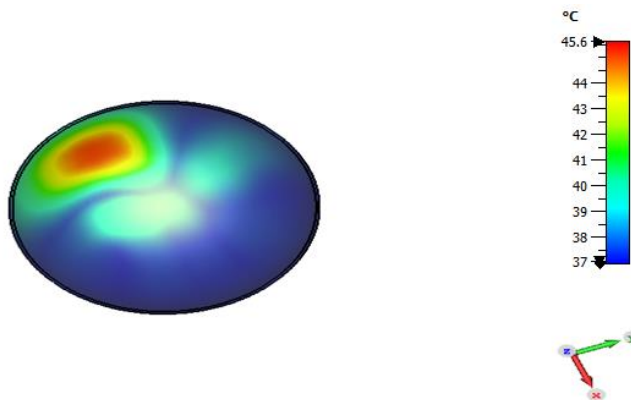


**Figure 5.29.** Temperature distribution for model H with one tumor (5 mm) radius.

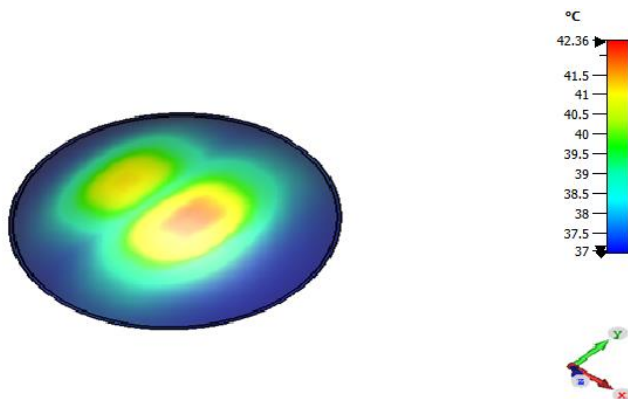


**Figure 5.30.** Temperature distribution for model G with two tumors (5 and 2 mm) radius.

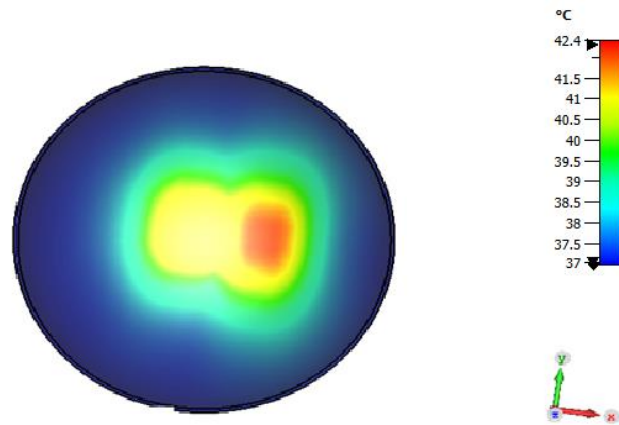


**Figure 5.31.**Temperature distribution when using unsuitable phase and power

## 5.2. Discussions

This study aimed to design a textile-based UWB microstrip patch antenna that can detect breast tumors in an early stage while simultaneously elevating the temperature of a targeted tumor site to the hyperthermia therapy range of 41 to 45 C, utilizing microwave theory and a 3D breast model. The system design consisted of a microstrip patch antenna and a breast model. The antenna element and the breast model are created via the CST software. The antenna was evaluated for early tumor detection applications using four numerical breast models with varying tumor sizes, shapes, and locations to assess its efficacy. The study's results indicated that the antenna was successful in identifying breast cancers.

The return loss of the antenna, specific absorption rate (SAR) values for radiation safety, voltage standing wave ratio, the effect of bending for antenna flexibility, and temperature distribution were analyzed and computed for each model to assess antenna performance and its capability to detect tumors and to heat tumor regions to a designated temperature degree.

The antenna was initially designed for operation in free space, and Figure 5.1 demonstrates an optimal return loss of around -38 dB. Figure 5.2 illustrates the fluctuation in antenna return loss resulting from applying it to the breast model. In general, the impedance mismatch arises from the dielectric characteristics of the body. The radiation pattern of an antenna situated on a human body changes due to the body's proximity, which results in shadowing and absorption. The gain decreases because of the body's energy absorption, while the efficiency declines due to dielectric losses

within the body. The frequency varies from the intended resonance frequency due to the influence of the body. Antennas are developed for free space; hence, antenna theory is not applicable to breast tissues, necessitating the optimization of antenna design for compatibility with human tissues. The return loss varied when the antenna was placed into a breast (a high-permittivity medium). Miniaturization techniques are employed to achieve the best return loss concerning the length of the antenna's partial ground. The antenna optimization procedure was conducted to attain the requisite bandwidth. The Trust Region Framework (TRF) technique was employed in the Electromagnetic Computer Simulation Technology (CST) software to optimize the ground plane length for the targeted bandwidth of 2-11.6 GHz. Figure 5.3 displays the impact of varying the partial ground length on the antennas' return loss. Figure 5.4 illustrates that the model free of a tumor exhibited a return loss of -18.5 dB. Figure 5.5 illustrates an increase in return loss from -18.5 dB to -24 dB attributable to the presence of a tumor with a radius of 5 mm. Figure 5.6 similarly illustrates an increase in S11 attributable to the presence of a cubic-shaped tumor, with an overall size approximately comparable to that of model B, indicating that tumors of equivalent sizes and locations displayed relatively identical increases in return losses, irrespective of their morphology. Despite the smaller dimensions of the secondary tumor in Model D, which comprises two tumors of varying sizes (5mm and 2mm) as shown in Figure 5.7, there was a significant elevation in the S11 value relative to Model A and an observable shifting in resonance frequency, suggesting that the number of reflective targets within the breast directly influenced the return loss.

The proposed antenna underwent bending experiments to assess its flexibility, considering that the human body is not flat. Figure 5.8 illustrates minor alterations in the resonance frequency due to cylindrical bending but remaining within the intended frequency range. This demonstrated that the antenna preserved its performance while bending, signifying its appropriateness for wearable applications. This is crucial as the antenna must conform to the body's contours for precise detection.

Figure 5.9 illustrates that the implementation of the designed antenna in a free space on the breast pattern produced substantial alterations in the VSWR values, with values in certain frequencies above the usual range. Conversely, Figure 5.10 illustrates the impact of varying the ground patch length on the VSWR values. Figures 5.11 to 5.15 demonstrate that the VSWR values for all four models, as well as for the antenna after

pending, fluctuated between 1 and 2 across the frequency range of 2–11.6 GHz, signifying an adequate impedance match between the antenna and the transmission line.

The specific absorption rate (SAR) measurements, which quantify the effects of electromagnetic field exposure, are maintained below the permissible limits for medical uses. The specific absorption rate (SAR) ranged from 0.397 to 1.64 W/g (10 g SAR) for the evaluated models, demonstrating that the antenna arrangement was appropriate for safe application in a breast cancer detection system. This conclusion is significant, as SAR values above the permissible range might adversely affect human tissues, which has been reported in several previous studies. Figures 5.16 to 5.19 illustrate the Specific Absorption Rate (SAR) values for a frequency of 5.4 GHz. The greatest SAR values are accurately obtained at tumor centers or their immediate surroundings, facilitating the identification of breast tumor locations without requiring further signal-processing operations.

After testing the antenna's capability as a wearable device, its performance was further evaluated in a dynamic system to assess its suitability for non-wearable imaging applications. Figures 5.26 and 5.27 illustrate the system's ability to detect tumors of various sizes and generate images by processing signals collected from 112 distinct points in the dynamic setup. The resulting images demonstrate the proposed antenna's effectiveness in detecting tumors, even in a dynamic imaging configuration. This underscores the antenna's versatility and adaptability for diverse imaging system applications.

As the specific absorption rate (SAR) permitted in medical imaging is restricted to 2 W/g (10 g SAR), which is inadequate for achieving the necessary temperature elevation in tumors for breast cancer treatment; therefore, an antenna array was developed to get the requisite thermal range. A 2x4 antenna array was employed to assess the antenna's effectiveness in producing the specified temperatures. Beamforming and steering techniques were employed to modify the phase of signals transmitted from specific antennas, ensuring optimal directionality of the electromagnetic wave towards the tumor, so enabling accurate targeting of malignant cells, even when situated deep into the breast. Proper phase changes provide constructive interference at the tumor location and destructive interference in other areas, reducing harm to adjacent healthy tissue. Due to the irregular shape and varying

position and depth of tumors, phase control facilitates adaptation to these variations, enhancing treatment success. The array showed successful performance in elevating the temperature up to 45 °C; however, it is observed that the peak temperature occurs at the center of the breast due to the uniform phase employed across all antennas. The phase of each antenna was modified to focus the radiation toward the tumor's center, as seen in Figures 5.28 to 5.30. Figure 5.28 shows that the antenna configuration is successful in increasing the temperature of the tumor located at the center of the breast model up to 42.3°C. When the tumor moved from the center to a point near the skin the temperature raised over 45°C (which is not preferable). Figure 5.30 shows the ability of our antenna to elevate two tumors at the same time to a temperature up to 42.36°C. Figure 5.31 illustrates the significance of calibrating power levels. As can be seen from Figure 5.31 sometimes the power can be insufficient to raise the tumor area above 41°C. Adjusting the power levels among the antenna elements facilitated precise calibration of energy deposition. Increased power is allocated to tumor areas necessitating enhanced heating, whereas less power is employed to prevent exposure. The heterogeneity of breast tissues, characterized by differing dielectric characteristics that influence energy absorption, necessitated power adjustments to ensure consistent tumor heating. Incorrect phase and power settings may result in "hot spots" within healthy tissue, leading to burns or discomfort.

The antenna's characteristics regarding return loss, VSWR, gain, SAR, temperature distribution, and flexibility satisfied the criteria for breast cancer diagnosis and hyperthermia.

A comparison was made between the current study and some previous studies to verify the validity of the results and the additions provided. The data in Table 5.1 indicates that while textile materials can attain a wide frequency range when utilized as substrates and conductors, as demonstrated in (Mahmood et al., 2021) and (Hossain et al., 2022), they consistently yield much larger antenna dimensions in comparison to antennas constructed using non-textile materials. A primary issue in the design of textile-based antennas arises from the dielectric characteristics of these materials. Antenna size is crucial for its compatibility with wearable imaging systems, particularly given the small dimensions of the human breast. The compact size of the antenna facilitates its incorporation into arrays. The primary accomplishment of the antenna developed in this study is its compact dimensions relative to previous

antennas. Conversely, as seen in Table 5.1, antennas of comparatively smaller size (Elsheikh & Eldamak, 2021; X. Lin et al., 2020) employ metal-based conductive materials for the patch and ground. This construction lacks adaptation to body shape, resulting in reduced comfort and potential safety concerns compared to fabric-based options. Furthermore, the antennas demonstrate a limited frequency band; this study is predicated on the successful creation of a compact and lightweight antenna that operates within the UWB frequency range using exclusively textile-based materials. It is noticeable that (Bahrami et al., 2014) successfully constructed a smaller antenna ( $20 \times 20 \text{ mm}^2$ ) than the antenna being examined, however it experienced a restricted frequency range. Most prior studies and the present study employed multi-layer breast models that simulate the anatomical structure of the actual breast. This work extends beyond previous research that successfully identified spherical cancers by evaluating the antenna's capability to detect tumors of various shapes and sizes. This novel technique addresses an important gap in the literature. This research reveals the capability to visualize cancers as small as 2 mm in diameter. The study demonstrated that the engineered textile-based UWB patch antenna was successful at identifying breast cancers of various sizes, forms, and locations. A textile-based substrate enhances wearer comfort, making it appropriate for wearable applications. It is essential to acknowledge that this study relied on digital breast models, necessitating more experimental validation to verify the antenna's efficiency in practical applications. The influence of additional variables, including diverse breast morphologies and distinct tissue properties, deserves examination.

**Table 5.1.** Comparison between the proposed antenna and four works from literature

Aspect	Proposed Work (abdulla & Demirkol, 2024)	Elsheikh et al.(Elsheikh & Eldamak, 2021)	Lin et al.(X. Lin et al., 2020)	Mahmood et al.(Mahmood et al., 2021)	Hossain et al.(Hossain et al., 2022)
Frequency range (GHz)	2–11.6	1.8–2.4 and 4–10	1.198–4.055	7-28	2.42–3.2 and 4–15
Substrate/conductive	Denim/fabric	Cotton/roger-fabric	Polyester/copper	Denim/fabric	Felt/fabric
Antenna size (mm <sup>2</sup> )	31 × 31	24 × 41	40 × 45	60 × 50	80 × 61
Breast phantom	Multilayer	Single layer	Multilayer	Multilayer	Multilayer
SAR value (W/Kg)	Less than 2	Less than 2	Less than 2	Less than 2	0.121
Max S11 value (-10dB)	-36	-30	-40	-50	-50
Tumor size (mm)	2 and 5	10 and 20	None	None	None

## **6. CONCLUSIONS AND RECOMMENDATIONS**

### **6.1. Conclusions**

This study aimed to create an innovative, cost-effective, comfortable, totally textile-based wearable UWB microstrip patch antenna that can detect early-stage breast cancer and treat cancer by elevating its temperature to the hyperthermia range (42°C-45°C). The antenna functioned within the 2–11.6 GHz frequency spectrum, enabling high-resolution capabilities at elevated frequencies and effective penetration at lower frequencies. The suggested antenna consisted of a denim substrate positioned between a patch layer and a ground plane constructed from a 100% polyamide-based fabric that had been metalized with copper, silver, and nickel. Obtaining such a wide bandwidth using textile materials is a major challenge. The integration of UWB microwave technology with textile-based antenna design provides a novel approach to addressing the limitations of conventional diagnostic and therapeutic methods. The designed single antenna was evaluated using four numerical breast models for the goal of early breast cancer diagnosis, with variations in tumor sizes, forms, and positions to assess the antenna's detection capability. The incorporation of tumors of various shapes addressed the majority of the deficiencies in prior studies, which regarded tumors as spherical. The specific absorption rate (SAR), return loss (S11), and voltage standing wave ratio (VSWR) were computed for each model to assess antenna performance. The simulated SAR values did not exceed 2 W/g (10 g SAR) (only 0.397 to 1.64), remaining below the acceptable limit for medical uses. The VSWR stayed within the permissible range of 1–2. The antenna's return loss ranged from –38 to –18.5 dB across the four models, exhibiting significant variations in response to alterations in tumor size or location. The bending impact was analyzed to evaluate the antenna's flexibility, demonstrating commendable performance post-bending. The proposed antenna did not necessitate an immersion medium. The effects of immersion-related imaging errors were eradicated, and the uncertainty in tumor localization was diminished. After testing the antenna's capability as a wearable device, its performance was further evaluated in a dynamic system to assess its suitability for non-wearable imaging

applications. The resulting images demonstrate the proposed antenna's effectiveness in detecting tumors, even in a dynamic imaging configuration. This underscores the antenna's versatility and adaptability for diverse imaging system applications.

On the other hand, a 2 by 4 antenna array was utilized to evaluate the antenna's efficiency in generating the required temperatures. Beamforming techniques were utilized to adjust the phase of signals emitted from designated antennas, assuring optimal directionality of the electromagnetic wave towards the tumor, hence facilitating precise targeting of malignant cells, even when located deep into the breast. This work demonstrates the feasibility of textile-based UWB antennas to elevate the temperature of breast cancers to adequate therapeutic levels. Our antenna shows the ability to increase tumor temperatures up to 42.3°C, 45.6°C, 43.3°C, and 42.4°C using different adjustments.

This study's results indicate that the suggested UWB textile-based microchip patch antenna is an efficient instrument for the early diagnosis of breast cancer and microwave hyperthermia treatment. Its dual utility in diagnostic and therapeutic domains, along with its wearability, renders it a valuable contribution to the field of biomedical engineering. This thesis advances the next generation of medical devices through the integration of UWB technology with textile-based antenna design. The results indicate the capability of wearable, flexible, multifunctional, and completely textile-based microwave antennas to revolutionize breast cancer care. The antenna requires experimental confirmation for application as a method in the diagnosis and treatment of breast cancer.

## **6.2. Recommendations and Future Works**

We recommend considering these additional points in future works to improve the proposed system:

- Perform research to verify antenna functionality among patients with varying breast sizes and tissue densities to guarantee generalizability and dependability.
- The proposed textile-based UWB microstrip patch antennas have shown promising results in simulations but need to be prototyped and their performance verified experimentally in real-world conditions. This includes

testing them on physical breast phantoms, followed by clinical trials to evaluate diagnostic and therapeutic efficacy in practical medical settings.

- Testing the proposed textile-based UWB antennas to diagnose and treat other medical conditions, such as lung, brain, skin, and liver cancer.
- Advanced imaging algorithms and machine learning approaches can be used to enhance tumor identification, localization, and discrimination between benign and malignant tissues.
- Utilize alternative textile materials with different dielectric properties to enhance antenna performance.



## REFERENCES

- Abdulla, F. A. A., & Demirkol, A. (2024). A novel textile-based UWB patch antenna for breast cancer imaging. *Physical and Engineering Sciences in Medicine*, 1–11.
- abdulla, F. A. ali, & Demirkol, A. (2024). A novel textile-based UWB patch antenna for breast cancer imaging. *Physical and Engineering Sciences in Medicine*. <https://doi.org/10.1007/s13246-024-01409-w>
- Akram, M., Iqbal, M., Daniyal, M., & Khan, A. U. (2017). Awareness and current knowledge of breast cancer. In *Biological Research* (Vol. 50, Issue 1). BioMed Central Ltd. <https://doi.org/10.1186/s40659-017-0140-9>
- Alex, A., Bhandary, E., & McGuire, K. P. (2020). Anatomy and Physiology of the Breast during Pregnancy and Lactation. *Diseases of the Breast during Pregnancy and Lactation*, 3–7.
- Alsharif, F., & Kurnaz, C. (2018). Wearable microstrip patch ultra wide band antenna for breast cancer detection. *2018 41st International Conference on Telecommunications and Signal Processing (TSP)*, 1–5.
- American Cancer Society. (2024). *Cancer Facts & Figures 2024*. Atlanta: American Cancer Society.
- Anand, P., Kunnumakara, A. B., Sundaram, C., Harikumar, K. B., Tharakan, S. T., Lai, O. S., Sung, B., & Aggarwal, B. B. (2008). Cancer is a preventable disease that requires major lifestyle changes. In *Pharmaceutical Research* (Vol. 25, Issue 9, pp. 2097–2116). Springer New York LLC. <https://doi.org/10.1007/s11095-008-9661-9>
- Bahrami, H., Porter, E., Santorelli, A., Gosselin, B., Popovic, M., & Rusch, L. A. (2014a). Flexible sixteen monopole antenna array for microwave breast cancer detection. *2014 36th Annual International Conference of the IEEE Engineering in Medicine and Biology Society, EMBC 2014*, 3775–3778. <https://doi.org/10.1109/EMBC.2014.6944445>
- Bahrami, H., Porter, E., Santorelli, A., Gosselin, B., Popovic, M., & Rusch, L. A. (2014b). Flexible sixteen monopole antenna array for microwave breast cancer detection. *2014 36th Annual International Conference of the IEEE Engineering in Medicine and Biology Society*, 3775–3778.
- Balanis, C. A. (2011). *Modern antenna handbook*. John Wiley & Sons.
- Balanis, C. A. (2012). *Advanced engineering electromagnetics*. John Wiley & Sons.
- Balanis, C. A. (2015). *Antenna theory: analysis and design*. John wiley & sons.
- Balanis, C. A. . (2005). *Antenna theory*. Wiley.

- Barnes, F. S., & Greenebaum, B. (n.d.). *Biological and Medical Aspects of Electromagnetic Fields HANDBOOK OF BIOLOGICAL EFFECTS OF ELECTROMAGNETIC FIELDS THIRD EDITION.*
- Bevacqua, M. T., Gaffoglio, R., Bellizzi, G. G., Righero, M., Giordanengo, G., Crocco, L., Vecchi, G., & Isernia, T. (2023). Field and Temperature Shaping for Microwave Hyperthermia: Recent Treatment Planning Tools to Enhance SAR-Based Procedures. *Cancers*, 15(5). <https://doi.org/10.3390/cancers15051560>
- Bond, E. J., Li, X., Hagness, S. C., & Van Veen, B. D. (2003). Microwave imaging via space-time beamforming for early detection of breast cancer. *IEEE Transactions on Antennas and Propagation*, 51(8), 1690–1705.
- Bond, E. J., Van Veen, B. D., & Hagness, S. C. (2006). Multiple window based ultrawideband microwave imaging for early-stage breast cancer detection. *Fourth IEEE Workshop on Sensor Array and Multichannel Processing, 2006.*, 127–131.
- Bourqui, J., Sill, J. M., & Fear, E. C. (2012). A prototype system for measuring microwave frequency reflections from the breast. *International Journal of Biomedical Imaging, 2012.* <https://doi.org/10.1155/2012/851234>
- Breast Cancer Grade.* (n.d.). <https://www.uptodate.com>.
- Çalışkan, R., Gültekin, S. S., Uzer, D., & Dündar, Ö. (2015). A Microstrip Patch Antenna Design for Breast Cancer Detection. *Procedia - Social and Behavioral Sciences*, 195, 2905–2911. <https://doi.org/10.1016/j.sbspro.2015.06.418>
- Camelia, G. (1996). Compilation of the Dielectric Properties of Body Tissues at RF and Microwave Frequencies. *Department of Physics, King's College London.*
- Carovac, A., Smajlovic, F., & Junuzovic, D. (2011). Application of Ultrasound in Medicine. *Acta Informatica Medica*, 19(3), 168. <https://doi.org/10.5455/aim.2011.19.168-171>
- Carr, J. J. (2001). *Practical Antenna Handbook*, MacGraw-Hill. *United States of America.*
- Carver, K., & Mink, J. (1981). Microstrip antenna technology. *IEEE Transactions on Antennas and Propagation*, 29(1), 2–24.
- Chandraprasad, M. S., Dey, A., & Swamy, M. K. (2022). Introduction to cancer and treatment approaches. In *Paclitaxel* (pp. 1–27). Elsevier.
- Chaudhary, S. S., Mishra, R. K., Swarup, A., & Thomas, J. M. (1984). Dielectric properties of normal & malignant human breast tissues at radiowave & microwave frequencies. *Indian Journal of Biochemistry & Biophysics*, 21(1), 76–79.
- Cheng, Y., & Fu, M. (2018). Dielectric properties for non-invasive detection of normal, benign, and malignant breast tissues using microwave theories. *Thoracic Cancer*, 9(4), 459–465. <https://doi.org/10.1111/1759-7714.12605>
- Chu, K. F., & Dupuy, D. E. (2014). Thermal ablation of tumours: biological mechanisms and advances in therapy. *Nature Reviews Cancer*, 14(3), 199–208.

- Coleman BM BCh, M. P., Rachet, B., Maringe, C., Coleman, M. P., Forman, D., Bryant, H., & Butler, J. (2011). Cancer survival in Australia, Canada, Denmark, Norway, Sweden, and the UK, 1995–2007 (the International Cancer Benchmarking Partnership): an analysis of population-based cancer registry data. *Lancet*, 377. <https://doi.org/10.1016/S0140>
- Coleman, C. (2017). Early Detection and Screening for Breast Cancer. In *Seminars in Oncology Nursing* (Vol. 33, Issue 2, pp. 141–155). W.B. Saunders. <https://doi.org/10.1016/j.soncn.2017.02.009>
- Conceição, R. C., Mohr, J. J., & O'Halloran, M. (2016). *An introduction to microwave imaging for breast cancer detection*.
- Cong, L., Liu, Q., Zhang, R., Cui, M., Zhang, X., Gao, X., Guo, J., Dai, M., Zhang, T., Liao, Q., & Zhao, Y. (2018). Tumor size classification of the 8th edition of TNM staging system is superior to that of the 7th edition in predicting the survival outcome of pancreatic cancer patients after radical resection and adjuvant chemotherapy. *Scientific Reports*, 8(1). <https://doi.org/10.1038/s41598-018-28193-4>
- Cruciani, S., Santis, V. D., Feliziani, M., & Maradei, F. (2012). Cole-Cole vs Debye models for the assessment of electromagnetic fields inside biological tissues produced by wideband EMF sources. *2012 Asia-Pacific Symposium on Electromagnetic Compatibility*, 685–688. <https://doi.org/10.1109/APEMC.2012.6237915>
- Derneryd, A. (1978). A theoretical investigation of the rectangular microstrip antenna element. *IEEE Transactions on Antennas and Propagation*, 26(4), 532–535.
- Deschamps, G. A. (1953). Microstrip microwave antennas. *Proceedings of the Third Symposium on the USAF Antenna Research and Development Program, Oct*, 18–22.
- Duck, F. A. (2008). Hazards, risks and safety of diagnostic ultrasound. In *Medical Engineering and Physics* (Vol. 30, Issue 10, pp. 1338–1348). <https://doi.org/10.1016/j.medengphy.2008.06.002>
- Edge, S. B. . (2010). *AJCC cancer staging manual*. Springer.
- EGAN, R. L. (1966). MAMMOGRAPHY. *AJN The American Journal of Nursing*, 66(1). <https://journals.lww.com/ajnonline/fulltext/1966/01000/mammography.29.aspx>
- El Dein, A. Z., & Amr, A. (2010). Specific absorption rate (SAR) induced in human heads of various sizes when using a mobile phone. *2010 7th International Multi-Conference on Systems, Signals and Devices*, 1–6.
- Elsheakh, D. M., Alsherif, S. A., & Eldamak, A. R. (2023). Textile monopole sensors for breast cancer detection. *Telecommunication Systems*, 82(3), 363–379.
- Elsheikh, D., & Eldamak, A. R. (2021). Microwave textile sensors for breast cancer detection. *2021 38th National Radio Science Conference (NRSC)*, 1, 288–294.
- Epstein, N. R., Meaney, P. M., & Paulsen, K. D. (2014). 3D parallel-detection microwave tomography for clinical breast imaging. *Review of Scientific Instruments*, 85(12). <https://doi.org/10.1063/1.4901936>

- Fear, E. C., Li, X., Hagness, S. C., & Stuchly, M. A. (2002). Confocal microwave imaging for breast cancer detection: localization of tumors in three dimensions. *IEEE Transactions on Biomedical Engineering*, 49(8), 812–822. <https://doi.org/10.1109/TBME.2002.800759>
- Feng, Y., Spezia, M., Huang, S., Yuan, C., Zeng, Z., Zhang, L., Ji, X., Liu, W., Huang, B., Luo, W., Liu, B., Lei, Y., Du, S., Vuppalapati, A., Luu, H. H., Haydon, R. C., He, T. C., & Ren, G. (2018). Breast cancer development and progression: Risk factors, cancer stem cells, signaling pathways, genomics, and molecular pathogenesis. In *Genes and Diseases* (Vol. 5, Issue 2, pp. 77–106). Chongqing University. <https://doi.org/10.1016/j.gendis.2018.05.001>
- Flanagan, F. L., Dehdashti, F., & Siegel, B. A. (1998). PET in breast cancer. *Seminars in Nuclear Medicine*, 28(4), 290–302.
- Fornes-Leal, A., Garcia-Pardo, C., Frasson, M., Pons Beltrán, V., & Cardona, N. (2016). Dielectric characterization of healthy and malignant colon tissues in the 0.5–18 GHz frequency band. *Physics in Medicine & Biology*, 61(20), 7334. <https://doi.org/10.1088/0031-9155/61/20/7334>
- Gabriel, C., Gabriel, S. M., & Corthout, E. (1996). The dielectric properties of biological tissues: I. Literature survey. *Physics in Medicine and Biology*, 41 11, 2231–2249. <https://api.semanticscholar.org/CorpusID:11664493>
- Gabriel, S., Lau, R. W., & Gabriel, C. (1996). The dielectric properties of biological tissues: III. Parametric models for the dielectric spectrum of tissues. In *Phys. Med. Biol* (Vol. 41). <http://iopscience.iop.org/0031-9155/41/11/003>
- Gao, Y., Reig, B., Heacock, L., Bennett, D. L., Heller, S. L., & Moy, L. (2021). Magnetic Resonance Imaging in Screening of Breast Cancer. In *Radiologic Clinics of North America* (Vol. 59, Issue 1, pp. 85–98). W.B. Saunders. <https://doi.org/10.1016/j.rcl.2020.09.004>
- Gerami, R., Sadeghi Joni, S., Akhondi, N., Etemadi, A., Fosouli, M., Foroughi Eghbal, A., & Souri, Z. (2022). Review Article A literature review on the imaging methods for breast cancer. In *Int J Physiol Pathophysiol Pharmacol* (Vol. 14, Issue 3). [www.ijppp.org](http://www.ijppp.org)
- Giftsy, A. L. S., Kommuri, U. K., & Dwivedi, R. P. (2023). Flexible and Wearable antenna for Biomedical Application: Progress and Opportunity. *IEEE Access*.
- Groumpas, E. I., Koutsoupidou, M., & Karanasiou, I. S. (2022). Biomedical Passive Microwave Imaging and Sensing: Current and future trends. *IEEE Antennas and Propagation Magazine*, 64(6), 84–111. <https://doi.org/10.1109/MAP.2022.3210860>
- Grzegorzcyk, T. M., Meaney, P. M., Kaufman, P. A., Diflorio-Alexander, R. M., & Paulsen, K. D. (2012). Fast 3-D tomographic microwave imaging for breast cancer detection. *IEEE Transactions on Medical Imaging*, 31(8), 1584–1592. <https://doi.org/10.1109/TMI.2012.2197218>
- Guan, Y.-S. (2015). Microwave coagulation therapy of hepatocellular carcinoma. *Hepatoma Research*, 1, 159–164.
- Habash, R. (2007). *Bioeffects and therapeutic applications of electromagnetic energy*. CRC press.

- Habash, R. W. Y., Bansal, R., Krewski, D., & Alhafid, H. T. (2007). Thermal therapy, Part III: ablation techniques. *Critical Reviews<sup>TM</sup> in Biomedical Engineering*, 35(1–2).
- Hadadi, I., Rae, W., Clarke, J., McEntee, M., & Ekpo, E. (2021). Diagnostic Performance of Adjunctive Imaging Modalities Compared to Mammography Alone in Women with Non-Dense and Dense Breasts: A Systematic Review and Meta-Analysis. In *Clinical Breast Cancer* (Vol. 21, Issue 4, pp. 278–291). Elsevier Inc. <https://doi.org/10.1016/j.clbc.2021.03.006>
- Hagness, S. C., Taflove, A., & Bridges, J. E. (1997). *FDTD ANALYSIS OF A PULSED MICROWAVE CONFOCAL SYSTEM FOR BREAST CANCER DETECTION*.
- Hagness, S. C., Taflove, A., & Bridges, J. E. (1998). Two-Dimensional FDTD Analysis of a Pulsed Microwave Confocal System for Breast Cancer Detection: Fixed-Focus and Antenna-Array Sensors. In *IEEE TRANSACTIONS ON BIOMEDICAL ENGINEERING* (Vol. 45, Issue 12).
- Hagness, S. C., Taflove, A., & Bridges, J. E. (1999). Three-Dimensional FDTD Analysis of a Pulsed Microwave Confocal System for Breast Cancer Detection: Design of an Antenna-Array Element. In *IEEE TRANSACTIONS ON ANTENNAS AND PROPAGATION* (Vol. 47, Issue 5).
- Hamza, M. N., Islam, M. T., & Koziel, S. (2024). Advanced sensor for non-invasive breast cancer and brain cancer diagnosis using antenna array with metamaterial-based AMC. *Engineering Science and Technology, an International Journal*, 56, 101779.
- Hesabgar, S. M., Sadeghi-Naini, A., Czarnota, G., & Samani, A. (2017). Dielectric properties of the normal and malignant breast tissues in xenograft mice at low frequencies (100Hz–1MHz). *Measurement*, 105, 56–65. <https://doi.org/https://doi.org/10.1016/j.measurement.2017.04.004>
- Heywang-Köbrunner, S. H., Viehweg, P., Heinig, A., & Kiichler, C. (1997). Contrast-enhanced MRI of the breast: accuracy, value, controversies, solutions. In *European Journal of Radiology* (Vol. 24). ELSEVIER.
- Heywang-Köbrunner, S. H., Hacker, A., & Sedlacek, S. (2011). Advantages and disadvantages of mammography screening. In *Breast Care* (Vol. 6, Issue 3, pp. 199–207). <https://doi.org/10.1159/000329005>
- Hipwell, J. H., Vavourakis, V., Han, L., Mertzaniidou, T., Eiben, B., & Hawkes, D. J. (2016). A review of biomechanically informed breast image registration. In *Physics in Medicine and Biology* (Vol. 61, Issue 2, pp. R1–R31). Institute of Physics Publishing. <https://doi.org/10.1088/0031-9155/61/2/R1>
- Hoheisel, M. (2006). Review of medical imaging with emphasis on X-ray detectors. *Nuclear Instruments and Methods in Physics Research, Section A: Accelerators, Spectrometers, Detectors and Associated Equipment*, 563(1), 215–224. <https://doi.org/10.1016/j.nima.2006.01.123>
- Holland, K., Sechopoulos, I., Mann, R. M., den Heeten, G. J., van Gils, C. H., & Karssemeijer, N. (2017). Influence of breast compression pressure on the performance of population-based mammography screening. *Breast Cancer Research*, 19(1). <https://doi.org/10.1186/s13058-017-0917-3>

- Hossain, Ananda Sanagavarapu Mohan, & Mohammed Jainul Abedin. (2013). Beamspace Time Reversal Microwave Imaging for Breast Cancer Detection. *IEEE*.
- Hossain, K., Sabapathy, T., Jusoh, M., Lee, S.-H., Rahman, K. S. A., & Kamarudin, M. R. (2022). Negative index metamaterial-based frequency-reconfigurable textile CPW antenna for microwave imaging of breast cancer. *Sensors*, 22(4), 1626.
- Ingale, N. R., Bhirud, R., Jadhav, S., & Salunkhe, S. (2008). Designing of Textile Antenna for on Body Communication. *International Research Journal of Engineering and Technology*, 2308. www.irjet.net
- Islam, M. T., Mahmud, M. Z., Islam, M. T., Kibria, S., & Samsuzzaman, M. (2019). A Low Cost and Portable Microwave Imaging System for Breast Tumor Detection Using UWB Directional Antenna array. *Scientific Reports*, 9(1), 15491. <https://doi.org/10.1038/s41598-019-51620-z>
- Kalimuthu, R., Yegiyants, S. S., & Brenzek, C. (2015). Anatomy of the breast, axilla, and chest wall. *Breast Disease: Comprehensive Management*, 1–22.
- Kang, K., Chu, X., Dilmaghani, R., & Ghavami, M. (2007). Low-complexity Cole-Cole expression for modelling human biological tissues in (FD)2TD method. *Electronics Letters*, 43(3), 143–144. <https://doi.org/10.1049/el:20073644>
- Karanasiou, I. S., Uzunoglu, N. K., & Garetsos, A. (2004). Electromagnetic analysis of a non-invasive 3D passive microwave imaging system. *Journal of Electromagnetic Waves and Applications*, 18(3), 379–380. <https://doi.org/10.1163/156939304323085793>
- Karli, R., Ammor, H., Shubair, R. M., AlHajri, M. I., Alkurd, R., & Hakam, A. (2016). Miniature planar ultra-wide-band microstrip antenna for breast cancer detection. *2016 16th Mediterranean Microwave Symposium (MMS)*, 1–4.
- Kavitha, A., & Swaminathan, J. N. (2019). Design of flexible textile antenna using FR4, jeans cotton and teflon substrates. *Microsystem Technologies*, 25(4), 1311–1320. <https://doi.org/10.1007/s00542-018-4068-y>
- Klemm, M., Craddock, I., Leendertz, J., Preece, A., & Benjamin, R. (2008). Experimental and clinical results of breast cancer detection using UWB microwave radar. *2008 IEEE International Symposium on Antennas and Propagation and USNC/URSI National Radio Science Meeting, APSURSI*. <https://doi.org/10.1109/APS.2008.4619673>
- Koundal, D., Kadyan, V., Dutta, P., Anand, V., Aggarwal, S., & Gupta, S. (2020). 1 - Computational techniques in biomedical image analysis: overview. In D. Koundal & S. Gupta (Eds.), *Advances in Computational Techniques for Biomedical Image Analysis* (pp. 3–31). Academic Press. <https://doi.org/https://doi.org/10.1016/B978-0-12-820024-7.00001-3>
- Ku, G., & Wang, L. V. (2000). Scanning thermoacoustic tomography in biological tissue. *Medical Physics*, 27(5), 1195–1202.
- Kwon, S., & Lee, S. (2013). Instantaneous microwave imaging with time-domain measurements for breast cancer detection. *Electronics Letters*, 49(10), 653–654. <https://doi.org/10.1049/el.2013.0248>

- Kwon, S., & Lee, S. (2016). *Recent Advances in Microwave Imaging for Breast Cancer Detection*. 2016.
- Lazebnik, M., McCartney, L., Popovic, D., Watkins, C. B., Lindstrom, M. J., Harter, J., Sewall, S., Magliocco, A., Booske, J. H., Okoniewski, M., & Hagness, S. C. (2007). A large-scale study of the ultrawideband microwave dielectric properties of normal breast tissue obtained from reduction surgeries. *Physics in Medicine and Biology*, 52(10). <https://doi.org/10.1088/0031-9155/52/10/001>
- Lazebnik, M., Okoniewski, M., Booske, J. H., & Hagness, S. C. (2007). Highly accurate debye models for normal and malignant breast tissue dielectric properties at microwave frequencies. *IEEE Microwave and Wireless Components Letters*, 17(12), 822–824. <https://doi.org/10.1109/LMWC.2007.910465>
- Lazebnik, M., Popovic, D., McCartney, L., Watkins, C. B., Lindstrom, M. J., Harter, J., Sewall, S., Ogilvie, T., Magliocco, A., Breslin, T. M., Temple, W., Mew, D., Booske, J. H., Okoniewski, M., & Hagness, S. C. (2007). A large-scale study of the ultrawideband microwave dielectric properties of normal, benign and malignant breast tissues obtained from cancer surgeries. *Physics in Medicine and Biology*, 52(20), 6093–6115. <https://doi.org/10.1088/0031-9155/52/20/002>
- Li, X., Bond, E. J., Van Veen, B. D., & Hagness, S. C. (2005). An overview of ultrawideband microwave imaging via space-time beamforming for early-stage breast-cancer detection. *IEEE Antennas and Propagation Magazine*, 47(1), 19–34.
- Lima, Z. S., Ebadi, M. R., Amjad, G., & Younesi, L. (2019). Application of imaging technologies in breast cancer detection: A review article. In *Open Access Macedonian Journal of Medical Sciences* (Vol. 7, Issue 5, pp. 838–848). Open Access Macedonian Journal of Medical Sciences. <https://doi.org/10.3889/oamjms.2019.171>
- Lin, J. (2012). *Electromagnetic interaction with biological systems*. Springer Science & Business Media.
- Lin, X., Chen, Y., Gong, Z., Seet, B.-C., Huang, L., & Lu, Y. (2020). Ultrawideband textile antenna for wearable microwave medical imaging applications. *IEEE Transactions on Antennas and Propagation*, 68(6), 4238–4249.
- Lo, Y. T., & Lee, S. W. (2013). *Antenna Handbook: theory, applications, and design*. Springer Science & Business Media.
- Lui, H. S., Fhager, A., & Persson, M. (2012). On the forward scattering of microwave breast imaging. *International Journal of Biomedical Imaging*, 2012. <https://doi.org/10.1155/2012/582037>
- Mahmood, S. N., Ishak, A. J., Saeidi, T., Soh, A. C., Jalal, A., Imran, M. A., & Abbasi, Q. H. (2021). Full ground ultra-wideband wearable textile antenna for breast cancer and wireless body area network applications. *Micromachines*, 12(3), 322.
- Margaret Campbell, A., & John, M. (1990). *Measurements and Analysis of the Microwave Dielectric Properties of Tissues*.

- Matloubian, Mehran., Ponti, Elmira., & Choudhury, Debabani. (1999). *1999 IEEE MTT-S International Microwave Symposium digest: June 13-19, 1999, Anaheim Convention Center, Anaheim, California*. Institute of Electrical and Electronics Engineers ; IEEE Service Center.
- Meaney, P. M., Fanning, M. W., Li, D., Poplack, S. P., & Paulsen, K. D. (2000). *A Clinical Prototype for Active Microwave Imaging of the Breast*. *48*(11), 1841–1853.
- Moore, A. (2010). The practice of breast ultrasound: techniques, findings, differential diagnosis. *Ultrasound in Medicine and Biology*, *36*(2), 358.
- Morrow, M., Waters, J., & Morris, E. (2011). MRI for breast cancer screening, diagnosis, and treatment. *The Lancet*, *378*(9805), 1804–1811.
- Munson, R. (1974). Conformal microstrip antennas and microstrip phased arrays. *IEEE Transactions on Antennas and Propagation*, *22*(1), 74–78.
- Mustafa, A. B., & Rajendran, T. (2019). An Effective Design of Wearable Antenna with Double Flexible Substrates and Defected Ground Structure for Healthcare Monitoring System. *Journal of Medical Systems*, *43*(7). <https://doi.org/10.1007/s10916-019-1306-5>
- Nathanson, S. D., Detmar, M., Padera, T. P., Yates, L. R., Welch, D. R., Beadnell, T. C., Scheid, A. D., Wrenn, E. D., & Cheung, K. (2022). Mechanisms of breast cancer metastasis. In *Clinical and Experimental Metastasis* (Vol. 39, Issue 1, pp. 117–137). Springer Science and Business Media B.V. <https://doi.org/10.1007/s10585-021-10090-2>
- Nathanson, S. D., Krag, D., Kuerer, H. M., Newman, L. A., Brown, M., Kerjaschki, D., Pereira, E. R., & Padera, T. P. (2018). Breast cancer metastasis through the lympho-vascular system. *Clinical and Experimental Metastasis*, *35*(5–6), 443–454. <https://doi.org/10.1007/s10585-018-9902-1>
- Nicosia, L., Gnocchi, G., Gorini, I., Venturini, M., Fontana, F., Pesapane, F., Abiuso, I., Bozzini, A. C., Pizzamiglio, M., Latronico, A., Abbate, F., Meneghetti, L., Battaglia, O., Pellegrino, G., & Cassano, E. (2023a). History of Mammography: Analysis of Breast Imaging Diagnostic Achievements over the Last Century. In *Healthcare (Switzerland)* (Vol. 11, Issue 11). MDPI. <https://doi.org/10.3390/healthcare11111596>
- Nicosia, L., Gnocchi, G., Gorini, I., Venturini, M., Fontana, F., Pesapane, F., Abiuso, I., Bozzini, A. C., Pizzamiglio, M., Latronico, A., Abbate, F., Meneghetti, L., Battaglia, O., Pellegrino, G., & Cassano, E. (2023b). History of Mammography: Analysis of Breast Imaging Diagnostic Achievements over the Last Century. In *Healthcare (Switzerland)* (Vol. 11, Issue 11). MDPI. <https://doi.org/10.3390/healthcare11111596>
- Nikolova, N. K. (2011). Microwave Imaging for Breast Cancer. *IEEE Microwave Magazine*, *12*(7), 78–94. <https://doi.org/10.1109/MMM.2011.942702>
- O’Hara, B. M., Counsel, O., Jarrett, C. D., & Slattery, K. M. (2002). *Federal Communications Commission*.

- Padmavathy, T. V., Venkatesh, P., Bhargava, D., & Sivakumar, N. (2019). Design of I-shaped dual C-slotted rectangular microstrip patch antenna (I-DCSRMPA) for breast cancer tumor detection. *Cluster Computing*, 22, 13985–13993. <https://doi.org/10.1007/s10586-018-2161-8>
- Pang, C. L. K. (2015). *Hyperthermia in oncology*. CRC Press.
- Patel, J. R., & Chaudhari, J. B. (2015). Optimization and Return loss Reduction Of Micro strip Patch Antenna. *International Journal of Innovative Research in Computer and Communication Engineering*, 3(6), 4996–5003.
- Pennes, H. H. (1948). Analysis of tissue and arterial blood temperatures in the resting human forearm. *Journal of Applied Physiology*, 1(2), 93–122.
- Pfannenstiel, A. (2020). *Applicators and methods to achieve precise spatial control of the treatment zone during microwave ablation*. Kansas State University.
- Philadelpho, F., Calas, M. J. G., Carneiro, G. D. A. C., Silveira, I. C., Vaz, A. B. R., Nogueira, A. M. C., Bergmann, A., & Lopes, F. P. P. L. (2021). Comparison of Automated Breast Ultrasound and Hand-Held Breast Ultrasound in the Screening of Dense Breasts. *Revista Brasileira de Ginecologia e Obstetricia*, 43(3), 190–199. <https://doi.org/10.1055/s-0040-1722156>
- Pollacco, D. A., Farina, L., Wismayer, P. S., Farrugia, L., & Sammut, C. V. (2018). Characterization of the dielectric properties of biological tissues and their correlation to tissue hydration. *IEEE Transactions on Dielectrics and Electrical Insulation*, 25(6), 2191–2197. <https://doi.org/10.1109/TDEI.2018.007346>
- Porter, E., Bahrami, H., Santorelli, A., Gosselin, B., Rusch, L. A., & Popovic, M. (2016). A Wearable Microwave Antenna Array for Time-Domain Breast Tumor Screening. *IEEE Transactions on Medical Imaging*, 35(6), 1501–1509. <https://doi.org/10.1109/TMI.2016.2518489>
- Pulumati, A., Pulumati, A., Dwarakanath, B. S., Verma, A., & Papineni, R. V. L. (2023). Technological advancements in cancer diagnostics: Improvements and limitations. In *Cancer Reports* (Vol. 6, Issue 2). John Wiley and Sons Inc. <https://doi.org/10.1002/cnr2.1764>
- Rahman, M. Z., Nath, K. C. D., & Mynuddin, M. (2020). Performance analysis of an inset-fed circular microstrip patch antenna using different substrates by varying notch width for wireless communications. *International Journal of Electromagnetics and Applications*, 10(1), 19–29.
- Redig, A. J., & Mcallister, S. S. (2013). Breast cancer as a systemic disease: A view of metastasis. In *Journal of Internal Medicine* (Vol. 274, Issue 2, pp. 113–126). <https://doi.org/10.1111/joim.12084>
- Ronckers, C. M., Erdmann, C. A., & Land, C. E. (2005). Radiation and breast cancer: A review of current evidence. In *Breast Cancer Research* (Vol. 7, Issue 1, pp. 21–32). <https://doi.org/10.1186/bcr970>
- Rosen, A., Rosen, H. D., Hsi, R. A., Rosen, D., Happawana, G., Evans, G., Fathy, A., & Stern, L. (2004). Advances in RF-microwave and light sources for applications in therapeutic medicine. *15th International Conference on Microwaves, Radar and Wireless Communications (IEEE Cat. No. 04EX824)*, 2, 461–466.

- Russo, J. (2021). The Future of Prevention and Treatment of Breast Cancer. In *The Future of Prevention and Treatment of Breast Cancer*. Springer International Publishing. <https://doi.org/10.1007/978-3-030-72815-1>
- S Gabriel, R W Lau, & C Gabriel. (1996). The dielectric properties of biological tissues: III. Parametric models for the dielectric spectrum of tissues. *Physics in Medicine & Biology*, 41(11), 2271. <https://doi.org/10.1088/0031-9155/41/11/003>
- Sabouni, A., Hahn, C., Noghianian, S., Sauter, E., & Weiland, T. (2013). Study of the Effects of Changing Physiological Conditions on Dielectric Properties of Breast Tissues. *ISRN Biomedical Imaging*, 2013, 1–5. <https://doi.org/10.1155/2013/894153>
- Sardari, D., & Verga, N. (2011). *Cancer treatment with hyperthermia*. Citeseer.
- Semenov, S. (2009). Microwave tomography: Review of the progress towards clinical applications. In *Philosophical Transactions of the Royal Society A: Mathematical, Physical and Engineering Sciences* (Vol. 367, Issue 1900, pp. 3021–3042). Royal Society. <https://doi.org/10.1098/rsta.2009.0092>
- Sha, L., Ward, E. R., & Stroy, B. (2002). A review of dielectric properties of normal and malignant breast tissue. *Proceedings IEEE SoutheastCon 2002 (Cat. No.02CH37283)*, 457–462. <https://doi.org/10.1109/SECON.2002.995639>
- Sharma, H. K. G. R., & Thakre, V. V. (2017). Breast cancer detection by T-shaped slotted planner antenna. *Indian Journal of Science and Technology*, 10, 8.
- Shawalil, S., Abdul Rani, K. N., & Rahim, H. A. (2019). 2.45 GHZ wearable rectenna array design for microwave energy harvesting. *Indonesian Journal of Electrical Engineering and Computer Science*, 14(2), 677–687. <https://doi.org/10.11591/ijeecs.v14.i2.pp677-687>
- Sheeba, I. R., & Jayanthi, T. (2019). Design and analysis of a flexible softwear antenna for tumor detection in skin and breast model. *Wireless Personal Communications*, 107, 887–905.
- Siegel, R. L., Miller, K. D., Wagle, N. S., & Jemal, A. (2023). Cancer statistics, 2023. *CA: A Cancer Journal for Clinicians*, 73(1), 17–48. <https://doi.org/10.3322/caac.21763>
- Sill, J. M., & Fear, E. C. (2005). Tissue sensing adaptive radar for breast cancer detection—Experimental investigation of simple tumor models. *IEEE Transactions on Microwave Theory and Techniques*, 53(11), 3312–3319.
- Singh, S. V., & Bhargav, A. (2015). A Survey on Patch Antenna Bandwidth Enhancement through Feed Techniques and Novel Proximity Slot Coupling Approach. *International Journal of Advanced Research in Electrical, Electronics and Instrumentation Engineering*, 04(01), 254–263. <https://doi.org/10.15662/ijareeie.2015.0401038>
- Smith, D., Yurduseven, O., Livingstone, B., & Schejbal, V. (2014). Microwave imaging using indirect holographic techniques. *IEEE Antennas and Propagation Magazine*, 56(1), 104–117.

- Son, S. H., Simonov, N., Kim, H. J., Lee, J. M., & Jeon, S. I. (2010). Preclinical prototype development of a microwave tomography system for breast cancer detection. *ETRI Journal*, 32(6), 901–910. <https://doi.org/10.4218/etrij.10.0109.0626>
- Srinivasan, D., & Gopalakrishnan, M. (2019a). Breast cancer detection using adaptable textile antenna design. *Journal of Medical Systems*, 43(6), 177.
- Srinivasan, D., & Gopalakrishnan, M. (2019b). Breast cancer detection using adaptable textile antenna design. *Journal of Medical Systems*, 43(6), 177.
- Subramanian, S., Sundarambal, B., & Nirmal, D. (2018). Investigation on simulation-based specific absorption rate in ultra-wideband antenna for breast cancer detection. *IEEE Sensors Journal*, 18(24), 10002–10009.
- Sukhija, S., & Sarin, R. K. (2017). Design and performance of two-sleeve low profile antenna for bio-medical applications. *Journal of Electrical Systems and Information Technology*, 4(1), 49–61. <https://doi.org/10.1016/j.jesit.2016.10.013>
- Suleman, M., & Riaz, S. (2020). 3D in silico study of magnetic fluid hyperthermia of breast tumor using Fe<sub>3</sub>O<sub>4</sub> magnetic nanoparticles. *Journal of Thermal Biology*, 91. <https://doi.org/10.1016/j.jtherbio.2020.102635>
- Sung, H., Ferlay, J., Siegel, R. L., Laversanne, M., Soerjomataram, I., Jemal, A., & Bray, F. (2021). Global Cancer Statistics 2020: GLOBOCAN Estimates of Incidence and Mortality Worldwide for 36 Cancers in 185 Countries. *CA: A Cancer Journal for Clinicians*, 71(3), 209–249. <https://doi.org/10.3322/caac.21660>
- Surowiec, A. J., Stuchly, S. S., Barr, J. R., & Swarup, A. (1988). Dielectric Properties of Breast Carcinoma and the Surrounding Tissues. *IEEE Transactions on Biomedical Engineering*, 35(4), 257–263. <https://doi.org/10.1109/10.1374>
- Talseth-Palmer, B. A., & Scott, R. J. (2011). Genetic Variation and its Role in Malignancy. In *Int J Biomed Sci* (Vol. 7, Issue 3). [www.ijbs.org](http://www.ijbs.org)
- Timmerman, R. D., Bizekis, C. S., Pass, H. I., Fong, Y., Dupuy, D. E., Dawson, L. A., & Lu, D. (2009). Local surgical, ablative, and radiation treatment of metastases. *CA: A Cancer Journal for Clinicians*, 59(3), 145–170.
- Vander Vorst, A., Rosen, A., & Kotsuka, Y. (2006). *RF/microwave interaction with biological tissues*. John Wiley & Sons.
- Vorherr, H. (2012). *The breast: morphology, physiology, and lactation*. Elsevier.
- Wang, L. (2023). Microwave Imaging and Sensing Techniques for Breast Cancer Detection. In *Micromachines* (Vol. 14, Issue 7). Multidisciplinary Digital Publishing Institute (MDPI). <https://doi.org/10.3390/mi14071462>
- White, E., Velentgas, P., Mandelson, M. T., Lehman, C. D., Elmore, J. G., Porter, P., Yasui, Y., & Taplin, S. H. (1998). Variation in Mammographic Breast Density by Time in Menstrual Cycle Among Women Aged 40–49 Years. *JNCI: Journal of the National Cancer Institute*, 90(12), 906–910. <https://doi.org/10.1093/jnci/90.12.906>

- World Health Organization. (2024, March 13). *Breast cancer*.  
<https://www.who.int/news-room/fact-sheets/detail/breast-cancer>
- WT Joines, Y Zhang, C Li, & RL Jirtle. (1994). *The measured electrical properties of normal and malignant human tissues from 50 to 900 MHz*.
- Xu, Y., Xu, M., & Wang, L. V. (2002). Exact frequency-domain reconstruction for thermoacoustic tomography. II. Cylindrical geometry. *IEEE Transactions on Medical Imaging*, 21(7), 829–833.

## **CURRICULUM VITAE**

Name Surname : Fawzia ABDIEN ALI ABDULLA :

### **EDUCATION:**

- **B.Sc.** : 2011, University of Gezira, Faculty of Engineering and Technology, Electronics Engineering
- **M.Sc.** : 2016, Sakarya University, Electrical and Electronics Engineering, Electronics
- **PhD** : 2024, Sakarya University, Electrical and Electronics Engineering, Electronics

### **PROFESSIONAL EXPERIENCE :**

- She work as teaching assistant at the University of Gezira's Department of Electronics Engineering, Sudan Between 2012 to 2016.
- She work as a lecturer at the University of Gezira's Department of Electronics Engineering, Sudan from 2016 till now.

### **PUBLICATIONS, PRESENTATIONS AND PATENTS ON THE THESIS:**

- Abdulla, F. A. A., & Demirkol, A. (2024). A novel textile-based UWB patch antenna for breast cancer imaging. *Physical and Engineering Sciences in Medicine*, 1-11.

### **OTHER PUBLICATIONS, PRESENTATIONS AND PATENTS:**

- Abdulla, F. A. A., & Demirkol, A. (2016, October). Multi-targets tracking using parallel Kalman filter. *In 2016 CIE International Conference on Radar (RADAR) IEEE* , pp. 1-4.
- Fadel, I. A., Alsanabani, H., Öz, C., Kamal, T., Iskefiyeli, M., & Abdien, F. (2021). Hybrid fuzzy-genetic algorithm to automated discovery of prediction rules. *Journal of Intelligent & Fuzzy Systems*, 40(1), 43-52.

- Gidom, M., Abdulla, F. A., & Uygun, Ö. (2018, August). Efficiency Analysis of Lighting Bulbs Using Fuzzy Data Envelopment Analysis. *In 2018 International Conference on Computer, Control, Electrical, and Electronics Engineering (ICCCEE)* (pp. 1-4). IEEE.